WILSON, GREGORY T., M.S. Investigation into the Mechanism of Catalysis for the Kinetic Resolution of α,α-Disubstituted γ-Hydroxy Esters. (2018)
Directed by Dr. Kimberly S. Petersen 109 pp

The synthesis of enantioenriched, biologically active compounds is a vital area of interest for synthetic chemists. The lactone motif is found in several biologically important molecules, and the development of kinetic resolutions capable of producing enantioenriched lactones is important for the total synthesis of these types of compounds. The chiral Brønsted-acid catalyst, *R*-TRIP, has proven to be effective in producing enantioenriched α,α-disubstituted lactones with up to 94% ee. A study of the effects of varying electronic substituents on the kinetic resolution of α,α-disubstituted-γ-hydroxy esters to produce enantioenriched γ-lactones is the focus of this study. The introduction of varying electron-withdrawing and electron-donating substituents in the para position of an α-Ph group is hypothesized to cause a change in the selectivity and rate of reaction through resonance, induction, hydrogen bonding and pi-stacking. This project seeks to broaden the scope and understanding of the catalyst-substrate interaction to improve upon this synthetic methodology.

INVESTIGATION INTO THE MECHANISM OF CATALYSIS FOR THE KINETIC RESOLUTION OF α,α-DISUBSTITUTED γ-HYDROXY ESTERS

by

Gregory T. Wilson

A Thesis Submitted to
the Faculty of The Graduate School at
The University of North Carolina at Greensboro
in Partial Fulfillment
of the Requirements for the Degree
Master of Science

Greensboro
2018

Approved by

_____
Committee Chair

APPROVAL PAGE

This thesis written by Gregory T. Wilson has been approved by the following committee of the Faculty of The Graduate School at the University of North Carolina at Greensboro.

Committee Chair _____

Committee Members _____

_____

_____
Date of Acceptance by Committee

_____
Date of Final Oral Examination

ACKNOWLEDGMENTS

Dr. Mitchell Croatt, Dr. Jerry Walsh, and Dr. Jason Reddick, for supporting me as my committee members. Dr. Franklin Moy for all the work done to keep our NMRs running around the clock. Dr. Daniel Todd, for assistance with our mass spectrometry needs. Dr. Ghassan Qabaja for my laboratory training and advice. Dr. Petersen, for taking a chance on me, and giving me the opportunity to study under your advisement.

TABLE OF CONTENTS

Page

LIST OF TABLES

Page

LIST OF FIGURES

Page

CHAPTER I

INTRODUCTION

1.1 Chirality

Most biologically active compounds contain one or more chiral centers. A chiral center is defined as any atom in a molecule that is bonded to four or more different substituents and is nonsuperimposable. In a molecule with only one chiral center, there exists the possibility for two stereoisomers which are nonsuperimposable mirror images. These mirror images (enantiomers) have the same physical properties except for their optical activity, meaning the enantiomers will rotate plane-polarized light in opposite directions. Often in biologically active compounds, only one of the two possible enantiomers is the active compound, while the other is sometimes inactive or possibly toxic. This is a result of the geometric shape of the two individual enantiomers. One enantiomer has a specific three-dimensional geometry that allows it to interact favorably with a target, while the other enantiomer does not, or can interact with a different target. This is seen in the Parkinson's drug, dihydroxy-3,4 phenylalanine (Dopa). L-Dopa **1** is the active isomer that is marketed in the treatment of Parkinson's disease. The inactive enantiomer, D-Dopa **2**, has been shown to cause agranulocytosis which is a condition in which a patient's white

blood cell counts, specifically the neutrophils, are lowered. This can result in the inability of the patient to fight off infections.[1]

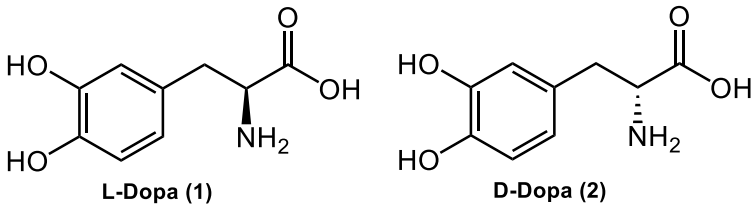

Figure 1. (L)- and (D)-Dopa

Due to this, and many other drugs that have similar issues with the activity of optical isomers, there exists a need to either separate enantiomers or to synthesize molecules in an enantiopure fashion. In chiral support chromatography, two enantiomers are passed through a column packed with chiral material, usually a polymer carbohydrate, that allows for their separation. This method, while effective, is both expensive and wasteful due to large amounts of solvents necessary to achieve separation and chiral columns on the preparatory scale are very expensive. Another, synthetic option is to avoid producing the undesired enantiomer altogether. This can be done through several methods, but in this project, it is achieved through a kinetic resolution.

1.2 Kinetic Resolutions

Kinetic resolutions have long been used to produce enantioenriched materials and have the potential of producing products with up to 50% yield and up to 100% ee.

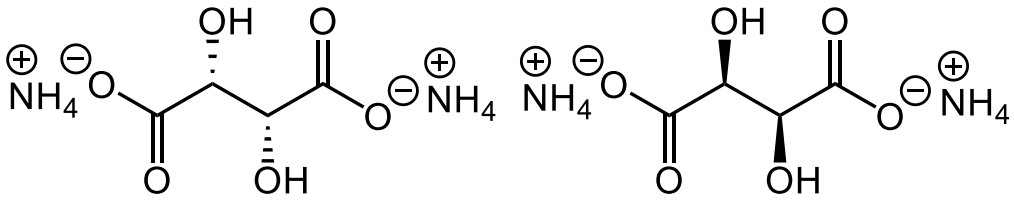

Figure 2. Ammonium (L)- and (D)-Tartrate

Louis Pasteur was the first to observe a kinetic resolution in 1858 when he reacted racemic ammonium tartrate with *Penicillium glaucum*. The resulting isolated product was shown to be ammonium L-tartrate (**3**). The mold converted ammonium D-tartrate (**4**) leaving behind the opposite enantiomer.[2]

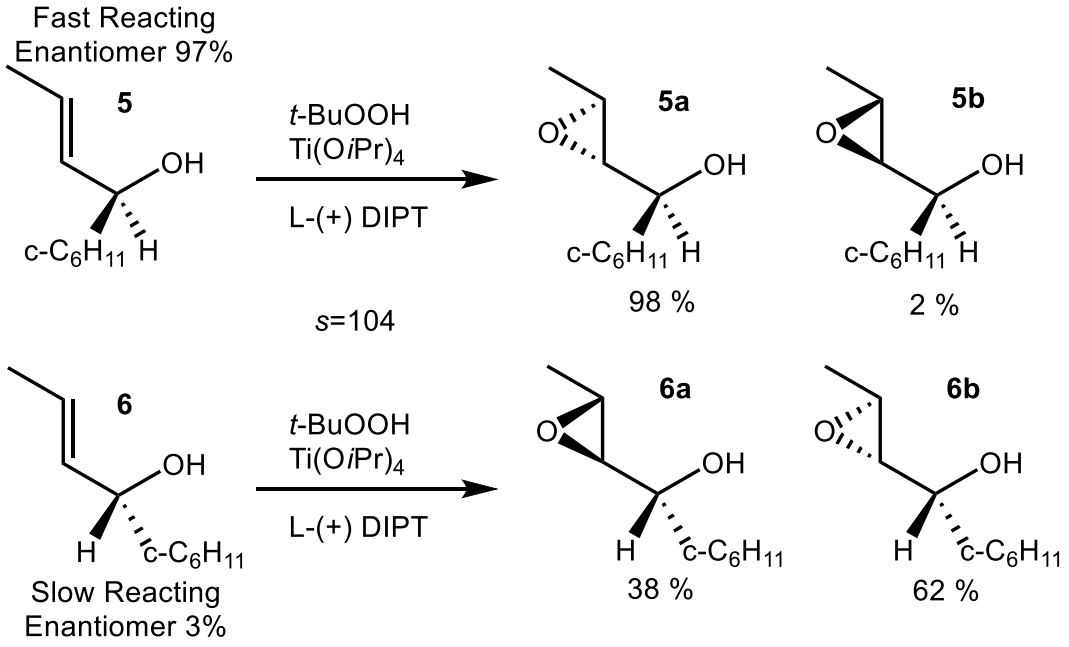

Figure 3. Sharpless Epoxidation

In 1981, Sharpless published a paper on the kinetic resolution of allylic alcohols catalyzed by diisopropyl tartrate and titanium tetra(isopropoxide) in the presence of *tert*-butylperoxide (Figure 3). The resolution of allylic alcohols allowed for the production of enantioenriched epoxides with high selectivities. The titanium tetra(isopropoxide) and enantioenriched diisopropyl tartrate form a complex that allows for the selective addition of oxygen to either the *re* or *si*, top or bottom, face of the alkene.[3] This opened the door for nonenzymatic kinetic resolutions to become a useful synthetic technique.

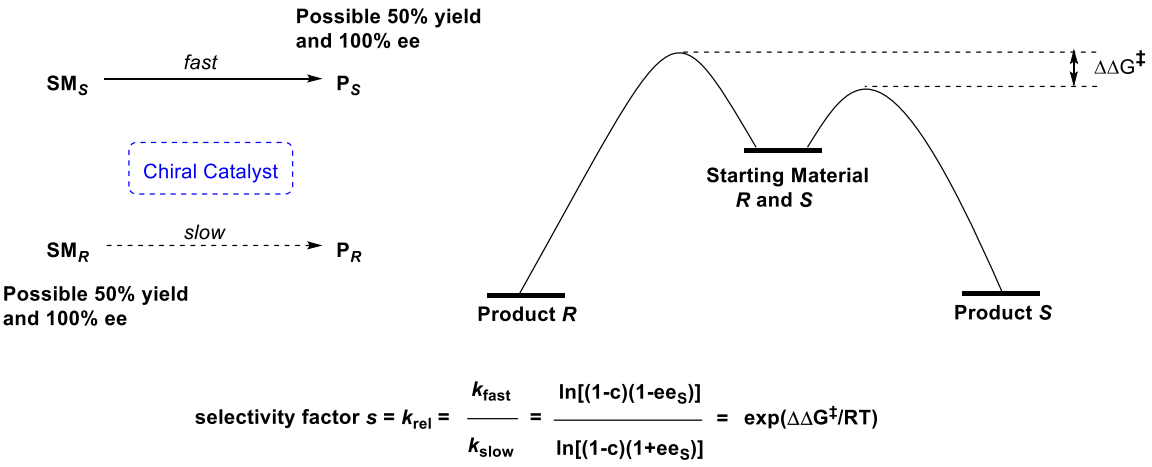

Figure 4. General Scheme for Kinetic Resolutions

Kinetic resolutions take advantage of chiral catalysts that produce enantioenriched materials by forming a more favorable complex with one enantiomer as opposed to the opposite enantiomer. Therefore, the rate of formation for one enantiomer increases causing it to react faster due to a decrease in the activation energy for that enantiomer. The other enantiomer

forms a less favorable complex with the chiral catalyst, causing the rate of reaction to decrease, resulting in less product formation for that enantiomer, Figure 4. The ratio of the rates of these two reactions is equal to the selectivity factor (s):

$$s = \frac{k_{fast}}{k_{slow}} = \frac{\ln[(1-c)(1-ee_s)]}{\ln[(1-c)(1+ee_s)]} = \exp(\frac{\Delta G^{\ddagger}}{RT}).^{4}$$

This is calculated in the Petersen lab by measuring the conversion (*c*) via NMR and the enantiomeric excess (*ee*) via chiral HPLC. A perfect kinetic resolution would have an infinite selectivity factor, giving rise to product for only one enantiomer, while leaving the opposite enantiomer completely unreacted. If using a kinetic resolution for the synthesis of enantioenriched building blocks, usually the unreacted, enantioenriched starting materials that are left as a result of the chiral catalysis are isolated.

Table 1. Selectivity Table for Respective *ee*[5]

	% Conversion Required for given *ee*		
Selectivity	**90% *ee***	**95% *ee***	**99% *ee***
2	**97.2**	**98.6**	**99.7**
5	**74.7**	**79.4**	**86.6**
10	**62.0**	**65.8**	**72.0**
25	**53.4**	**55.9**	**59.6**
50	**50.4**	**52.4**	**54.8**

Over the course of a kinetic resolution, as conversion increases, the enantiomeric excess of the starting material will continually rise, while the product being formed will start at a peak enantiomeric excess point and then the *ee* will begin to decrease as more of the unfavored enantiomer is converted to product. In order for a kinetic resolution to be considered synthetically useful, it is generally accepted that a resolution with selectivities at or above 10 could provide enough enantioenriched starting materials without having too high of a conversion. A chart of the ee's achievable at varying conversion levels is shown in Table 1.[5] To achieve an enantiomeric excess (*ee*) of 95% with a selectivity factor of 10 would require a conversion of 65.8%. This would result in 34.2% (100% - 65.8%) of enantioenriched product with 95% *ee*.[5] Anything lower than this level is considered by most chemists to sacrifice too much material in achieving high enantiopurity. Conversion rates required to achieve ee's of 90, 95, and 99% at varying selectivities are also listed in Table 1.

NMR is a powerful analytical tool that can be used for the identification and quantification of organic molecules. Internal standards can be used in NMR analysis to allow for the determination of the amount of a substance that is present. This is done by preparing a solution of known concentration of the internal standard and relating the integration of the proton peaks of the standard versus that of the compound of interest through the equation: $C_x = [C_{std}*(I_x/N_x)]/(I_{std}/N_{std})$, where C is concentration, I is integration, and N is the number of nuclei.[6] Using this equation, the concentration of starting materials in a

kinetic resolution can be determined by taking a NMR spectrum at time zero and again at the time of interest. The change in concentrations can then be used to determine percent conversion. Chiral HPLC analysis is then carried out with both racemic starting materials and the enantioenriched starting materials from the reaction. This allows for the determination of the enantiomeric excess (*ee*) by taking the difference in the area of the major enantiomer and the minor enantiomer. Together with the conversion collected from NMR data, selectivity can be determined through the use of the formula discussed previously.

1.3 Chiral Brønsted Acid Catalysis

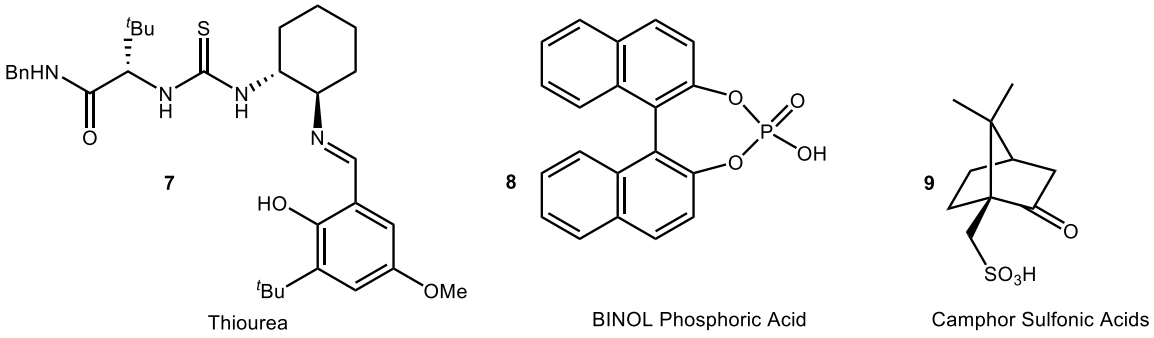

Figure 5. Chiral Brønsted Acid Catalysts

Brønsted acid catalysis is a popular area of concentration for asymmetric chemists. Chiral Brønsted acid organocatalysts give organic chemists a convenient route to producing enantioenriched materials. Organocatalysts are less difficult to handle and store than transition metal catalysts, as well as less susceptible to moisture and oxygen.[7] They have also been shown to be useful in a wide variety of stereoselective reactions.[7] There are many types of Brønsted

acid catalysts readily available for asymmetric use. These include, but are not limited to: thiourea compounds **7**, binol phosphoric acids **8**, and camphorsulfonic acids **9** (Figure 5).[8]

Activation of substrates via Brønsted acid catalysis occurs through hydrogen bonding and sometimes full proton transfer.[9] The Petersen group has utilized the Brønsted phosphoric acid catalyst, *R*-TRIP **57**, for the kinetic resolution of α-substituted γ-hydroxy esters in their transition to γ-lactones. In Figure 6, the backbone of *R*-TRIP is represented by the arch between the oxygens of the phosphoric acid in compound **11**. This kinetic resolution is thought to be activated via hydrogen bonding coordination of the hydroxy and carbonyl functional groups of the hydroxy ester **12** (Figure 6).[10]

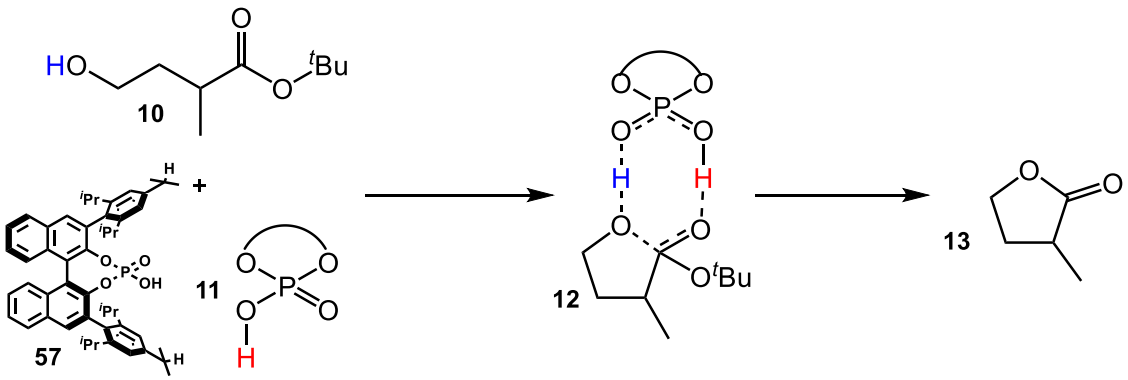

Figure 6. Activation of Substrate through Hydrogen Bonding.

The source of enantioselectivity with Brønsted acid organocatalysts is proposed to arise through the chiral environment provided by the enantioenriched catalyst. Specifically, for the kinetic resolution of α-substituted γ-hydroxy esters, the enantioselectivity is thought to be produced from the steric clash between the bulky 2,4,6-triisopropbylphenyl substituents on the catalyst **57** and the methyl group of the hydroxy ester. The enantiomer of starting material that has the methyl group facing the bulky phenyl substituent of the catalyst will be unfavored **15**, whereas the opposite enantiomer **14** will form a more favorable complex with the methyl group facing away from the catalyst (Figure 7).[10]

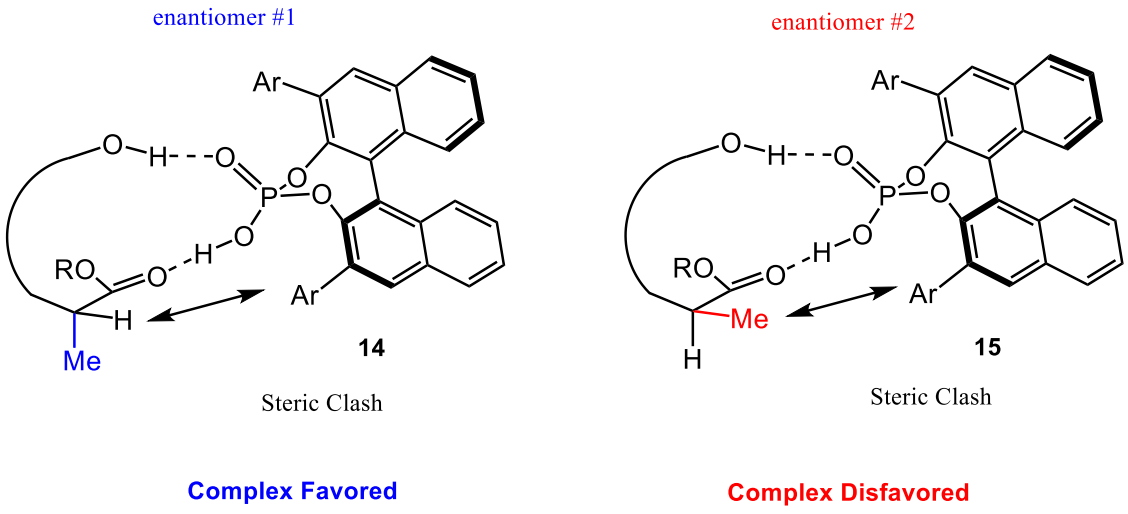

Figure 7. Binding of Catalyst and Proposed Source of Enantioselectivity

1.4 Hammett Studies

Hammett studies are a useful technique in determining the effects that electronics have on the rate and selectivity of a kinetic resolution. Hammett parameters (σ) are calculated from the difference in the log of the equilibrium constants (Ka) of a given benzoic acid derivative versus that of benzoic acid itself ($\sigma = \log K_X - \log K_H$).[11] If a linear correlation exists, it is indicative of a constant reaction mechanism over all substrates. The slope/sensitivity of this plot (ρ) will indicate how significant electronics are for the rate and selectivity. A large slope for the plot of rate versus Hammett parameters (σ) will indicate how sensitive lactonization is to the introduction of electron-donating and electron-withdrawing groups. A positive slope will mean that there is a decrease in positive charge for the transition state and vice versa.[11] This can be further broken down into the effects both resonance and induction have on the kinetic resolution through the use of the Swain-Lupton approach.[12] In this method, the individual contributions that both induction (*f*) and resonance (*r*) have on the overall electronic effect (σ) are calculated and used to plot against the selectivity or rate of the substrates in a given kinetic resolution.[12,13] Using field and resonance parameters for the substituents, determined by Hansch, a plot will be made with these values against rate or selectivity to determine the sensitivity constants f and r. If these values are similar, then there will be equal contribution from resonance and induction and vice versa.[11,13]

1.5 Conclusion

In this project, the kinetic resolution of α,α-disubstituted γ-hydroxy esters via chiral Brønsted phosphoric acid was studied using both Hammett plots and qualitative analysis of differing intermolecular interactions. The goal of this study was to broaden the understanding of this kinetic resolution in the hopes that the efficiency of this methodology could be improved upon for its future utilization in the synthesis of complex, biologically active compounds with all-carbon quaternary centers.

CHAPTER II

SYNTHESIS OF α,α-DISUBSTITUTED γ-HYDROXY ESTERS

2.1 Introduction

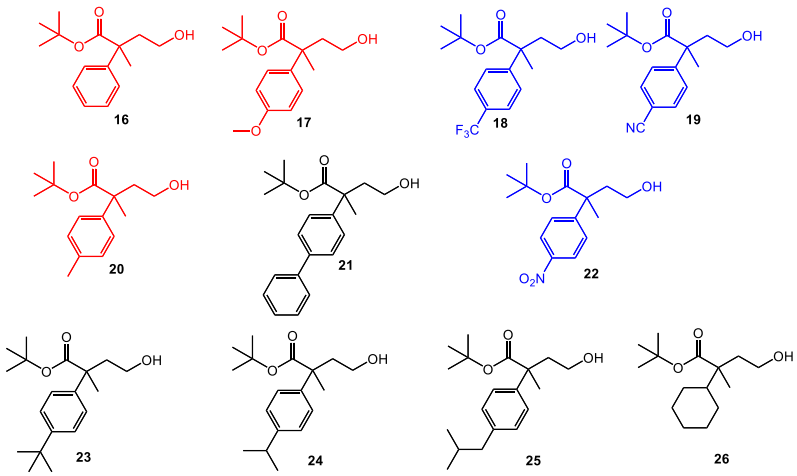

Figure 8. Esters to be Synthesized

To carry out a Hammett study for the kinetic resolution of α,α-disubstituted γ-hydroxy esters, a series of α,α-disubstituted γ-hydroxy esters were to be synthesized. The substrates proposed for this study are shown in Figure 8. These substrates were chosen for their electronic and steric properties. Those in red were chosen for their electron donating capabilities, blue for their electron withdrawing, and black for mostly steric reasons. Compound **26** was chosen to probe the effects that π-stacking could have on the catalyst-substrate interaction.

2.2 Synthesis of Substrates for Study

A general synthetic scheme for the synthesis of these substrates is shown in Figure 9. This scheme was not capable of producing product for all of the proposed substrates as will be discussed later.

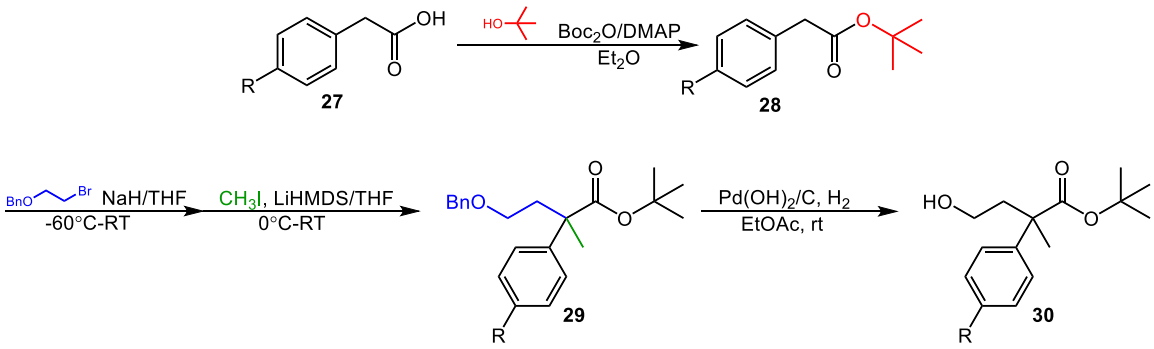

Figure 9. General Synthetic Scheme

The synthesis of all substrates started from their respective phenyl acetic acids **27**. These acids were all converted to *tert*-butyl esters **28** via di-*tert*-butyl dicarbonate coupled esterification. Following esterification, two alkylations were used to produce a protected hydroxy ester **29**. The benzyl protecting group was removed via hydrogenolysis, catalyzed by $Pd(OH)_2/C$ in excess hydrogen gas, to produce the desired hydroxy ester **30**. This synthesis worked well for the majority of substrates; however, a few substrates were more difficult to obtain.

2.2.1 Problems in Synthesis

Initially, it was proposed to use DCC coupling in the first esterification step of the synthetic scheme. This procedure yielded no product formation for the *para*-CH_3. This led to the use of an alternative esterification method using di-*tert*-

butyl dicarbonate as a coupling reagent. This method worked very well giving high yields for all of the substrates in this study.

The synthesis of the *para*-nitro **22** and *para*-cyano compounds **19** proceeded normally through the general synthetic scheme until the final step of hydrogenolysis. It was unpredicted, but not surprising, that the hydrogenolysis would reduce both the *para*-nitro and *para*-cyano substituents to their respective amines.

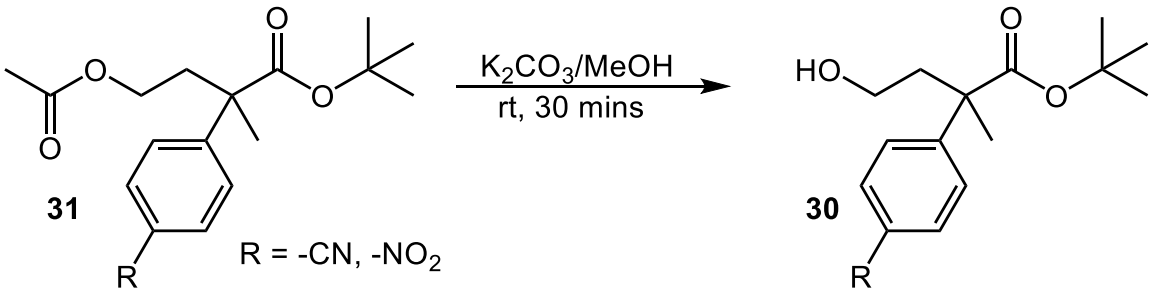

Figure 10. Acetate Deprotection of -CN and -NO_2

These substrates were again synthesized with an acetate protecting group in instead of the former benzyl protecting group (Figure 10). This new substrate design allowed for deprotection via hydrolysis with potassium carbonate. This reaction can be monitored by TLC such that it allows the removal of the acetate group without affecting the *tert*-butyl esters of the substrate itself. If left to react long enough, the *tert*-butyl esters could be converted to carboxylic acids, but at a slower rate. This method of synthesis proved successful for these substrates.

The *para*-chloro compound **18** was one substrate that also proved difficult to synthesize. The problem with this substrate arose during the second alkylation.

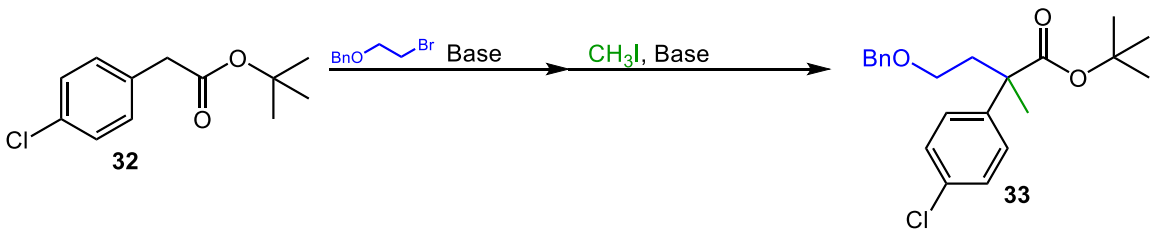

Figure 11. Alkylations of *para*-Chloro

The first alkylation of this substrate using sodium hydride as the base worked reasonably well, albeit with relatively low yields around 30-40%. The second alkylation using lithium bis(trimethylsilyl)amide was initially unsuccessful. Both potassium and sodium bis(trimethylsilyl)amides were used as a base as well, both unsuccessfully. Sodium hydride was used and the methylation appeared to be successful. Flash chromatography was not effective in separating the starting material from the product. Due to this, a HPLC preparative column was used to separate the two compounds. The separation was successful, but due to a leak in the HPLC system, the majority of material was lost. This led to the decision to remove this substrate from the study to focus on the synthesis of the remaining compounds.

2.2.2 Synthesis through α-Arylation

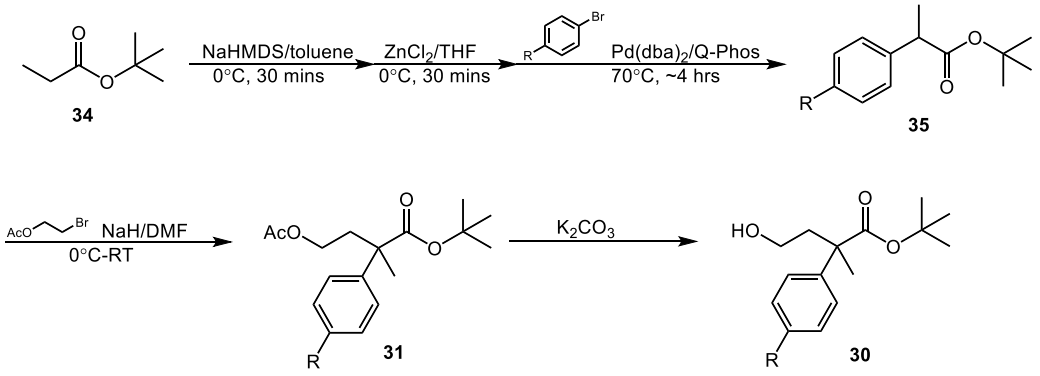

Figure 12. Synthesis via Negishi Coupling

Due to the issues that arose during the synthesis of previously discussed substrates, a new plan of synthesis was devised (Figure 12). The direct α-arylation of propionate **34** through Negishi coupling (Figure 12) would have shortened the synthesis by one step and prevented any problems there were with esterifications.[14] By using propionate, only one alkylation would be needed followed directly by the deprotection step. This Negishi coupling reaction was reported exactly in literature with both *para*-cyano and *para*-nitro bromo benzenes. The Negishi coupling reaction takes place through the generation of a zinc enolate that is then added through oxidative addition to an aryl halide followed by reductive elimination to form the arylated product. This reaction initially worked well giving yields up to 40% for the *para*-cyano **19** and 67% for the *para*-nitro **22** substrates. These yields were not as high as reported in literature. This issue was resolved by bubbling argon through the dried solvents

before use, helping to remove any dissolved oxygen that may be present in the solvent that allows for the oxidation of the palladium catalyst. After using this updated procedure, a yield of 93% was achieved for the *para*-cyano substituent **19**, but it was discovered that this reaction only worked well with fresh catalyst and future iterations resulted in drastically reduced or zero percent yield. Due to the instability of the catalyst, it was decided to revert to the original mode of synthesis.

The initial problems with the alkylations of the *para*-chloro substrate **18** as described above led to the attempt of another α-arylation via Hartwig-Buchwald coupling (Figure 13).[15] The use of this procedure would have allowed for the synthesis of large amounts of starting materials to produce compound **38** and then, in theory, add any aryl halide that was desired and readily available.

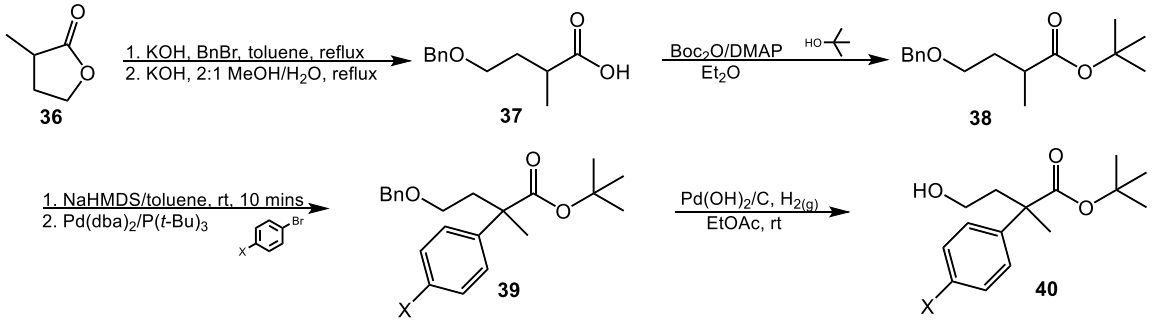

Figure 13. Synthesis via Hartwig-Buchwald Coupling.

The addition of aryl halides to a tertiary alpha position had been reported in literature using bis(dibenzylideneacetone)palladium(0) and tri-*tert*-butyl phosphine with high yields.[15] This reaction was attempted as shown in Figure 14

with conversion of **38** to **39** above, but no desired product was obtained. A new product was formed but NMR did not show any aromatic peaks. Mass spectrometry analysis suggested the presence of a chlorine at the alpha position of the ester. Upon receiving these results, the original plan of synthesis was determined to be the best method.

2.2.3 Synthesis of α-Cyclohexyl Substrate

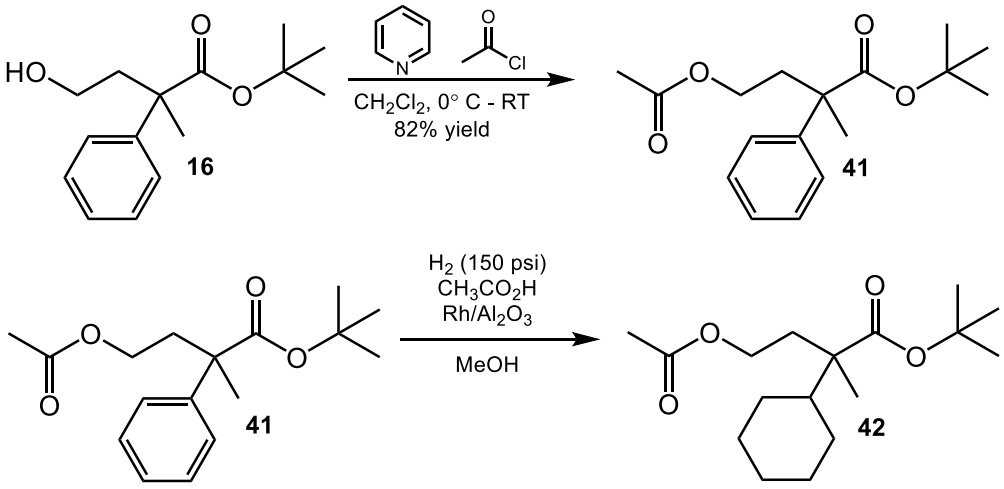

Figure 14. Synthesis of Cyclohexyl Substrate

The last substrate that was tested was the α-cyclohexyl substrate **26**. This substrate was synthesized from the reference compound **16** via hydrogenation of the phenyl ring (Figure 14).[16] This reaction was originally attempted at 55 psi in a Parr shaker without first protecting the alcohol. This resulted in formation of lactone; however, NMR showed that the hydrogenation was successful. As a result, the alcohol was protected with an acetate protecting group prior to

hydrogenation. Once protected, hydrogenation of the benzene ring was unsuccessful at 55 psi. A bomb reactor was obtained that allowed for the hydrogenation at a pressure of 150 psi and the desired product **42** was obtained.

2.3 Future Work

There are three substrates left to synthesize: -isopropyl, -nitro, and the cyclohexyl substrate. The cyclohexyl substrate needs to be scaled up to produce a usable amount of material. After the synthesis of these substrates, the resulting hydroxy esters will be ready for their kinetic resolutions. Also, the methoxy, cyano, and nitro products will be synthesized in large scale to prepare them for large scale kinetic resolutions.

2.4 Conclusion

The synthesis of *para*-substituted α-phenyl compounds for the study of the *R*-TRIP catalyzed lactonization of α,α-disubstituted γ-hydroxy esters has been completed for the reference, cyano, methoxy, tolyl, biaryl, *tert*-butyl, and trifluoromethyl groups. Planned synthesis of nitro, isopropyl, and cyclohexyl substrates is in progress. These substrates have been employed in the kinetic resolution and the results of their effects will be discussed in Chapter three.

CHAPTER III

STUDY OF BRØNSTED ACID CATALYZED KINETIC RESOLUTION

3.1 Introduction

3.1.1 Previous Work in the Petersen Group

The kinetic resolution of α-substituted γ-hydroxy esters has been previously studied by the Petersen group.[10] The substrate scope is shown in Table 2 below.

Table 2. Substrate Scope of α-Substituted Hydroxy Esters

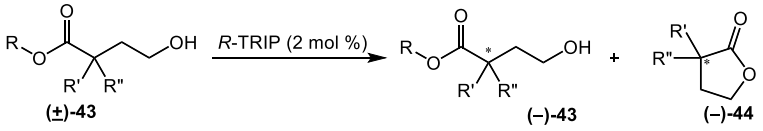

R = $C(CH_3)_3$, R' = Me, R" = H (**43a**)
R = $CH(CH_3)_2$, R' = Me, R" = H (**43b**)
R = $CH(CH(CH_3)_2)_2$, R' = Me, R" = H (**43c**)
R = $C(CH_3)_3$, R' = $CH(CH_3)_2$, R" = H (**43d**)
R = $C(CH_3)_3$, R' = phenyl, R" = H (**43e**)
R = $C(CH_3)_3$, R' = CH_2CH_3, R" = H (**43f**)
R = $C(CH_3)_3$, R' = allyl, R" = H (**43g**)
R = $C(CH_3)_3$, R' = Ph, R" = Me (**43h**)

entry	substrate	solvent	temp (°C)	time (h)	% conv	ee % 35	ee % 36	s
1	**43a**	CH_2Cl_2	5	24	40	58	31	25
2	**43b**	CH_2Cl_2	5	8	68	21	24	1.4
3	**43c**	CH_2Cl_2	35	144	50	14	27	1.5
4	**43d**	hexanes	5	72	56	52	37	3.9
5	**43e**	toluene	5	40	71	50	26	2.3
6	**43f**	CH_2Cl_2	rt	24	67	85	n/a	6.1
7	**43g**	CH_2Cl_2	5	72	63	86	50	7.9
8	**43h**	CH_2Cl_2	5-rt	232	53	83	66	16.7

Selectivities as high as 25 for compound **43a** were observed, displaying the capability of this resolution to produce enantioenriched, all-carbon quaternary centers in γ-lactones.[10] Compound **43h** has a methyl and phenyl substituent at

the alpha position and had a selectivity of 16.7.[10] The presence of this phenyl group allows for the substitution of various electron donating and withdrawing substituents at positions around the phenyl ring. It was proposed that the introduction of these types of groups at the *para* position would allow for a linear free energy relationship (LFER) study of the effects of those groups on the cyclization of the hydroxy ester. If the introduction of these groups resulted in a significant change in the rate and selectivity of the kinetic resolution, the role electronics are playing in this cyclization could be identified.

3.1.2 Origin of Kinetic Resolution

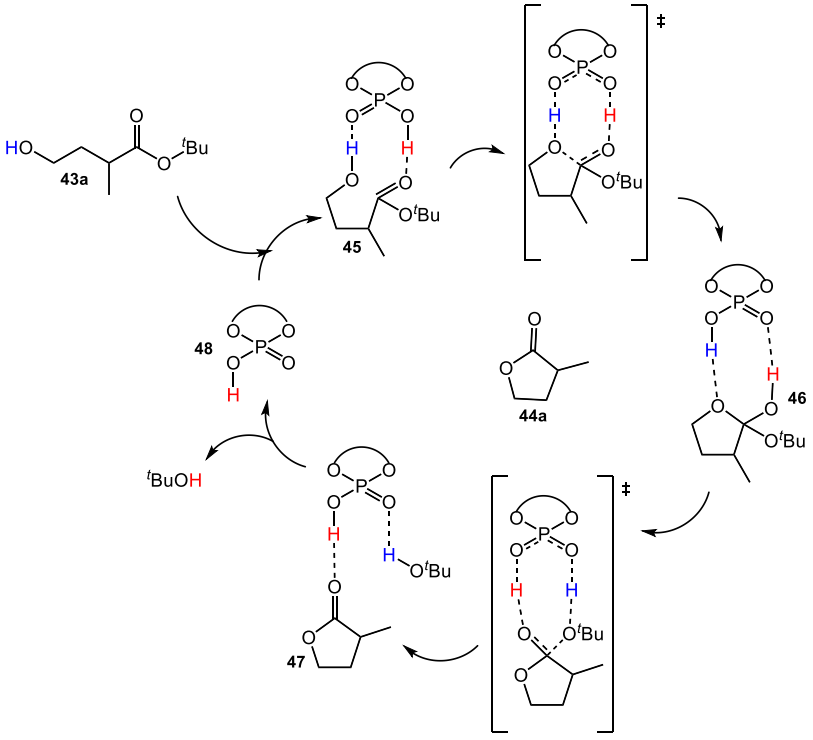

Figure 15. Step-wise Catalysis of Hydroxy Esters via *S*-TRIP

The mechanism for the kinetic resolution of α-substituted γ-hydroxy esters was investigated by Changotra et. Al.[17] Two mechanisms were proposed for the cyclization of hydroxy esters by *S*-TRIP. One mechanism was a concerted pathway in which hydrogen bonding between the acidic proton of the phosphoric acid from the catalyst and the oxygen atom of the *tert*-butyl group allows for the nucleophilic attack from the hydroxy oxygen to the carbonyl and subsequent release of the *tert*-butyl group. This pathway is expected to be of higher energy and thus the step-wise pathway shown in Figure 15 is the more likely mechanism of catalysis. This mechanism proceeds through a hydrogen bonding event between the carbonyl of the substrate **43a** and the acidic proton of the catalyst **48**, while the hydrogen of the hydroxy group from the substrate hydrogen bonds with the free oxygen of the catalyst. This creates a stronger electrophile at the carbonyl carbon and a stronger nucleophile at the oxygen of the hydroxy group. C-O bond formation occurs with full proton transfer of the acidic proton from the catalyst to the carbonyl forming the tetrahedral intermediate **46**. The proton from the hydroxy group is transferred to the other oxygen of the catalyst. The hydrogen bond then moves to the oxygen of the *tert*-butyl group creating a better leaving group at the carbonyl. The carbon oxygen double bond reforms kicking off the *tert*-butyl group and forming the lactone **47** which then dissociates from the regenerated catalyst to yield the final lactone **44a**.

The lactonization transition state **[45-46]** was evaluated to determine the lowest energy conformation of lactone that leads to stereo-control. This was done by evaluating the different conformers of isopropyl groups at the *para* position of the aryl rings on the catalyst. The dihedral angles between the hydrogen of the middle carbon on the isopropyl group, the carbon that hydrogen is attached to and the carbon-carbon bond of the phenyl rings were evaluated, Φ_1 and Φ_2. The lowest energy conformation for this angle was the *S*_si_syn **50** conformer of the lactone. This means that the *S* enantiomer is favored with addition to the *si* face of the lactone and *syn* addition shown in Figure 16. The activation barrier for the stepwise pathway was confirmed to be 10.8 kcal/mol less than the concerted pathway indicating that that the stepwise mechanism is the most likely.

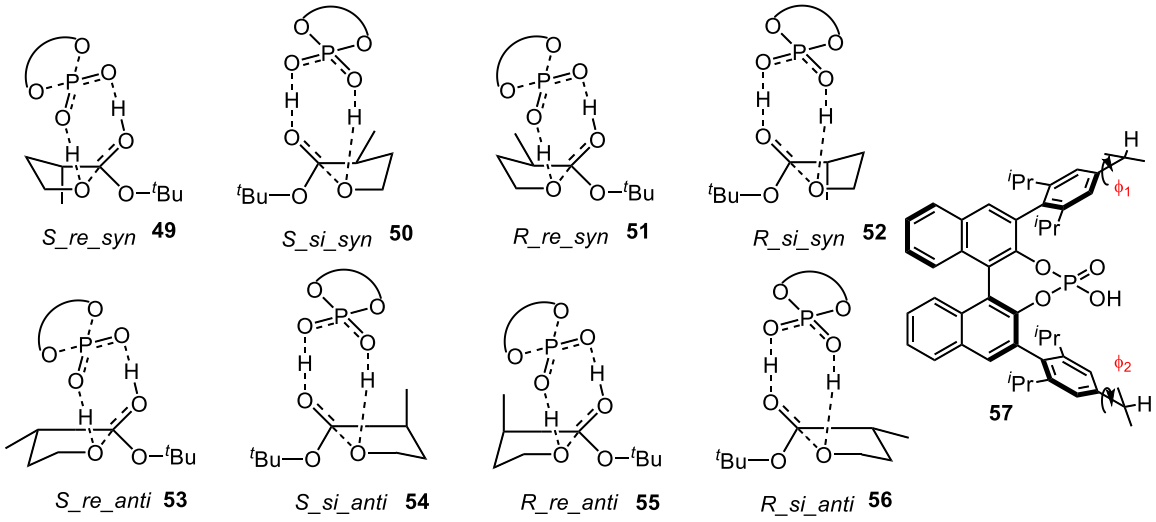

Figure 16. Conformational Energy Differences with Dihedral Angles

The transition state for the *S_si_syn* **50** is 0.9 kcal/mol lower than *R_si_anti*. **56**; therefore, they have come to the conclusion that the C-O bond forming step is the stereo-controlling step and the mechanism proceeds through a step-wise pathway.[17]

3.1.3 LFER and Kinetic Study of Silylation-Based Kinetic Resolution

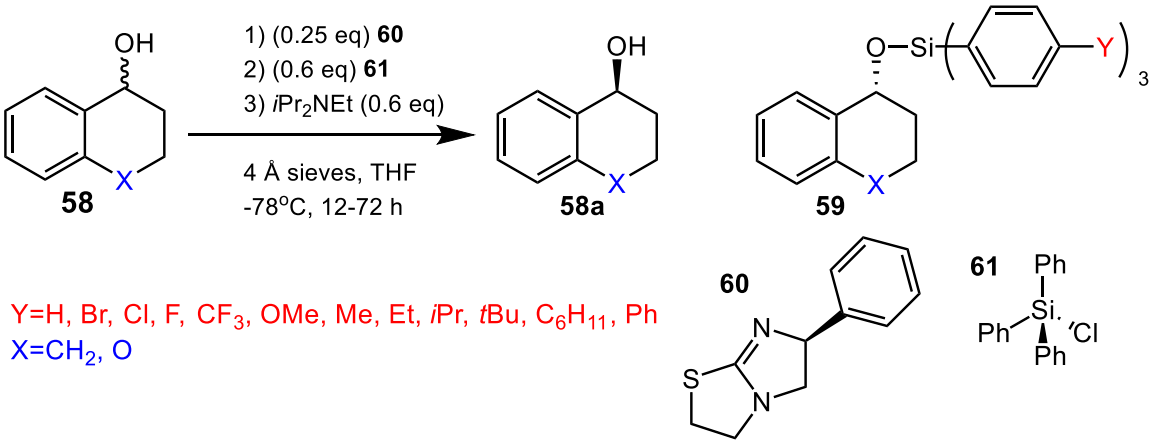

Figure 17. Silylation-Based Kinetic Resolution

In a paper by Alkhani et. Al., a Linear Free Energy Relationship (LFER) study was performed on the tetramisole **60** catalyzed, silylation-based kinetic resolution of secondary alcohols **58**.[13] The effects of electronics were evaluated via Hammett plots by measuring the rate and selectivity for the kinetic resolution when a variety of electron withdrawing and electron donating substituents were placed at the *para* position of the three phenyl rings of the triphenylsilyl chloride **61** (Figure 17). The rates of the fast reacting enantiomers were measured with ReactIR and plotted against Hammett parameters (σ) recalculated by Hansch.[11]

The resulting least squares regression revealed a correlation between electronics and reaction rate. Electron donating substituents caused a decrease in reaction rates by up to two orders of magnitude, while electron withdrawing groups caused an increase in reaction rates of up to five orders of magnitude compared to the rate of the compound with only a hydrogen at the *para* position (Figure 18). This linear correlation confirms that the reaction mechanism for all substrates is consistent and that there is a significant sensitivity of the reaction to the introduction of different electronic effects at the *para* position.

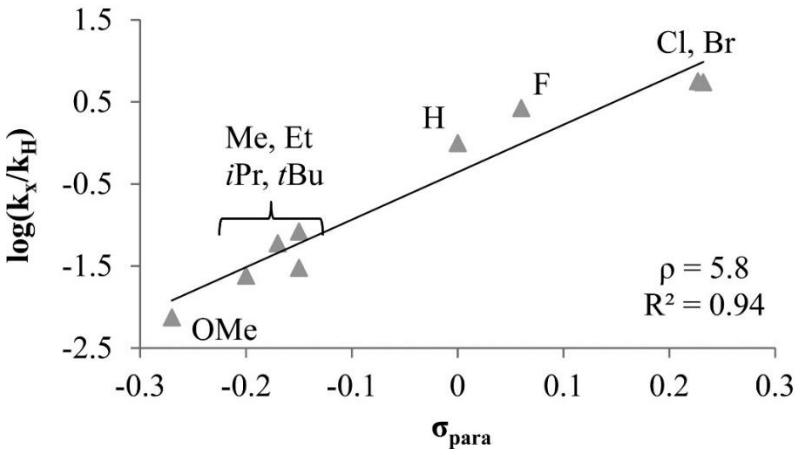

Substituent	Hammett Value σ_p
H	0.00
Br	0.23
Cl	0.22
F	0.06
OMe	-0.27
Me	-0.17
Et	-0.15
*i*Pr	-0.15
*t*Bu	-0.20

Figure 18. Hammett Plot for Silylation-Based Kinetic Resolution

When electron donating groups are introduced, electron density is added to the silicon atom resulting in a lower electrophilicity, while the removal of electron density by electron withdrawing groups results in higher electrophilicity by removing electron density from the silicon atom. This is consistent with the proposed mechanism and transition state shown in Figure 19.

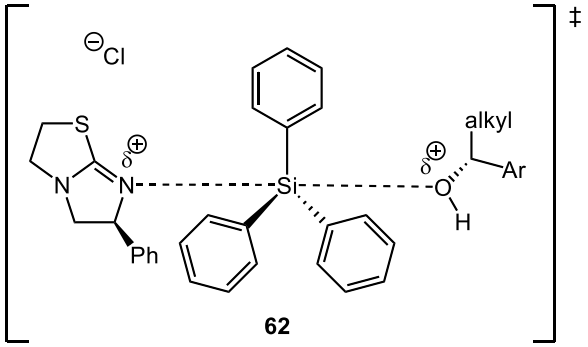

62

Proposed Transition State

Figure 19. Transition State of Silylation-Based Kinetic Resolution

The electron withdrawing substituents result in a more product-like transition state by giving the catalyst more time to distinguish between the enantiomers resulting in a larger energy difference between those enantiomers.[13]

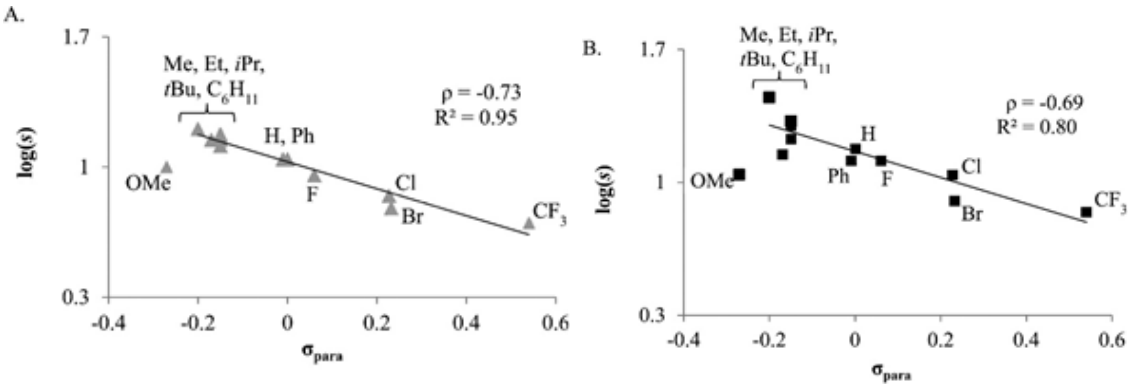

Figure 20. Silylation-Based Hammett Plot for Selectivity

A plot of selectivity versus the Hammett parameters was also carried out. This is made possible due to the fact that selectivity factors are a ratio of reaction rates. This plot, shown in Figure 20 reveals a negative linear correlation between the selectivity and the electronic parameter meaning that the introduction of

electron withdrawing groups results in lowered selectivity and vice versa for electron donating groups to an extent. The strongest electron donating group, methoxy, did not follow this trend and resulted in a lower selectivity respective to the plot. When this substituent was removed from the plot, a linear correlation was observed.[13] This type of plot was the intended focus of this project; however, measuring the reaction rate of the pure enantiomers of starting materials was not possible due to the lack of a chiral preparatory column. Therefore, only the Hammett versus selectivity plot to determine if there is a sensitivity to the electronics in selectivity was utilized.

3.2 Results and Discussion

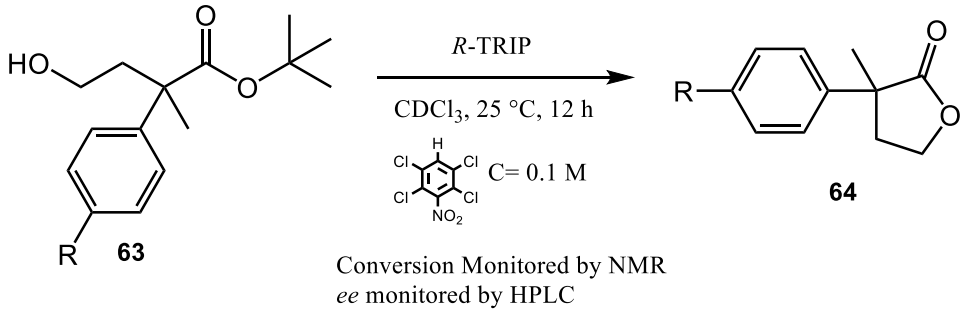

Figure 21. Kinetic Resolution of α,α-Disubstituted γ-Hydroxy Esters

A series of α,α-disubstituted γ-hydroxy esters were synthesized as discussed in Chapter 2 and subjected to the *R*-TRIP catalyzed kinetic resolution shown in Figure 21 above. The effects that varying electronic substituents had at the *para* position of the phenyl ring were evaluated through a Hammett plot of selectivity versus Hammett parameters (σ), calculated by Hansch.[11], as well as

qualitative observations made with consideration to the intermolecular forces that are present. The substrate scope is shown in Table 3 below. Electron donating substituents are shown in red and withdrawing substituents shown in blue. If a direct correlation were present between electronics and selectivity, a change in selectivity as the substrate is converted from electron donating to electron withdrawing would be expected.

Table 3. Substrate Scope for Kinetic Resolution

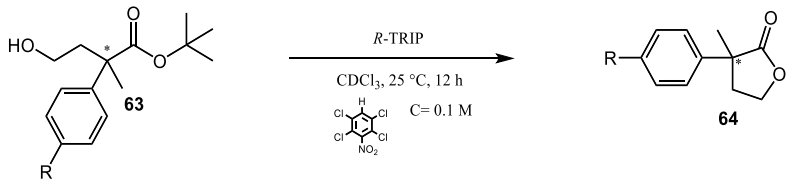

Entry	R	Time	Conv.	EE	S	Rate
1	-H	18 hrs	22%	22%	9.9	-2.5×10^{-5}
2	-OMe	48 hrs	22%	26%	27	-2.9×10^{-5}
3	$-C_6H_5$	18 hrs	18%	10%	3.2	-7.2×10^{-6}
4	-CN	18 hrs	22%	25%	26	-1.4×10^{-5}
5	$-CH_3$	48 hrs	15%	7.7%	2.8	-7.5×10^{-6}
6	$-CF_3$	18 hrs	18%	11%	3.6	-1.2×10^{-5}
7	-*t*-butyl	12 hrs	12%	9.1%	5.7	N/A

When the strongly electron donating substituent (-OMe) was introduced, a relatively high selectivity of 27 was observed. If the prediction that electronics are playing a direct role in the mechanism of catalysis at the *para* position of the phenyl ring hold true, then a reduction in selectivity when the strong electron withdrawing group (-CN) is introduced would be expected. However, a similar

selectivity of 26 was observed for this substituent. This suggests that since the carbon alpha to the carbonyl was effectively an sp^3 block between the aromatic system in the ring and the active portion of the molecule (the carbonyl), that resonance was contributing very little to the electronics introduced at the *para* position of the phenyl ring. Considering methoxy substituents act as electron donating contributors entirely through resonance, it was hypothesized that induction could be responsible for the increased selectivity that was observed.

The oxygen of the methoxy substituent is strongly electron withdrawing which would allow it to inductively act upon the carbonyl portion of the substrate. To test this hypothesis, a trifluoromethyl substituent at the *para* position was employed. Logically, if induction is solely responsible for the increased selectivity that is observed, then the strong induction introduced by a trifluoro group would result in high selectivities. A reduced selectivity of 3.6 was observed when this trifluoromethyl group was introduced. This observation led to the conclusion that electronics between the *para* position of the alpha phenyl ring and the carbonyl were playing a minor role in the selectivities observed between the groups.

Since the substituents that have shown increased selectivities have hydrogen bonding capabilities, it is proposed that a hydrogen bonding interaction between those *para* substituents and the catalyst are responsible for the observed increase in selectivity. While fluorine is a known hydrogen bond acceptor, it has been shown that organic carbon-fluorine bonds are very poor hydrogen bond acceptors, and often do not participate in hydrogen bonding at

all.[18] If hydrogen bonding is the reason for the increased selectivity observed in the kinetic resolution, then this would explain why the trifluoromethyl substituent did not enjoy the increased selectivity gained by that of the cyano and methoxy substituents.

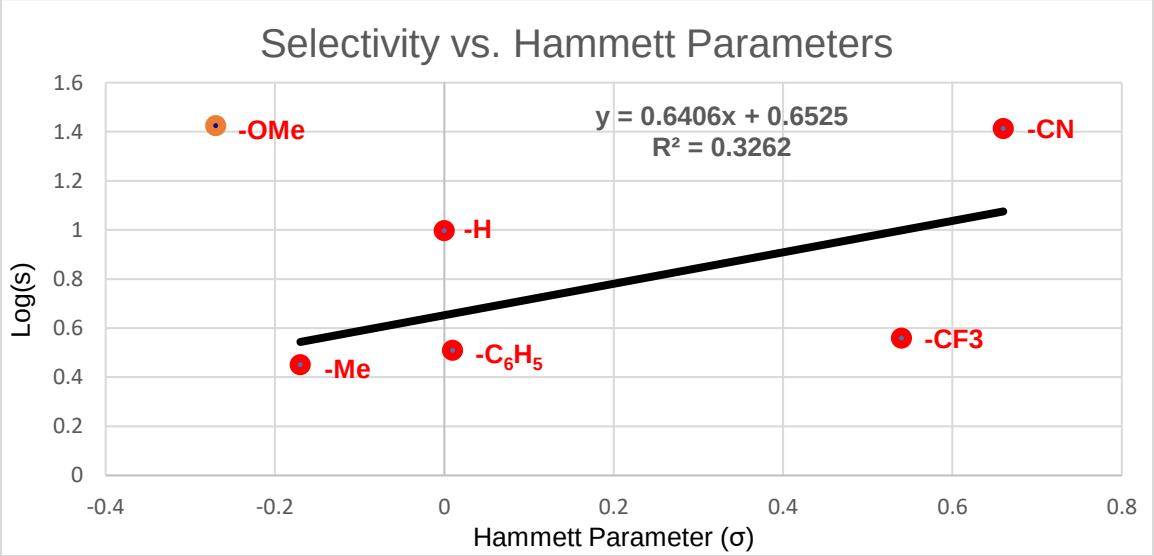

Figure 22. Hammett Plot of Selectivity vs. Hammett Parameters

A Hammett plot of selectivity versus Hammett parameters was employed, as shown in Figure 22. This also supports the assumptions made from Table 3 above. There is very little correlation between the selectivity and the Hammett parameters, indicating that selectivity is not sensitive to electronics at the *para* position. Due to the inability to measure the rates of reaction for individual enantiomers in the kinetic resolution, it is difficult to determine, definitively, that the mechanism of action for each substrate is the same or different. However, it is interesting to note that the overall reaction rates for the high selectivity

substituents were measured to be about one order of magnitude faster than the substituents with lower selectivities. This suggests a lowered overall activation energy for these substituents.

To gain a better understanding as to why an increase in selectivity was being observed for the hydrogen bonding capable substituents, collaborators at the Indian Institute of Technology in Mumbai were asked to do Density Functional Theory (DFT) tests on the substrates. The cyano substituent was compared with the reference compound to generate the energy diagram in Figure 22 below. The compound numbers in Figure 22 do not relate to compound numbers throughout the document. Compounds 1 and 2 in Figure 22 are equivalent to 16 and 19 in Figure 8. The transition state **[3-4]**, which is the stereoselective C-O bond forming transition state, for the cyano substrate had a slightly lower activation energy barrier (9.8 kcal/mol) versus that of the reference (9.7 kcal/mol). This could at least partly be the cause of the moderately higher selectivity that was observed experimentally between the cyano and the reference substrate.

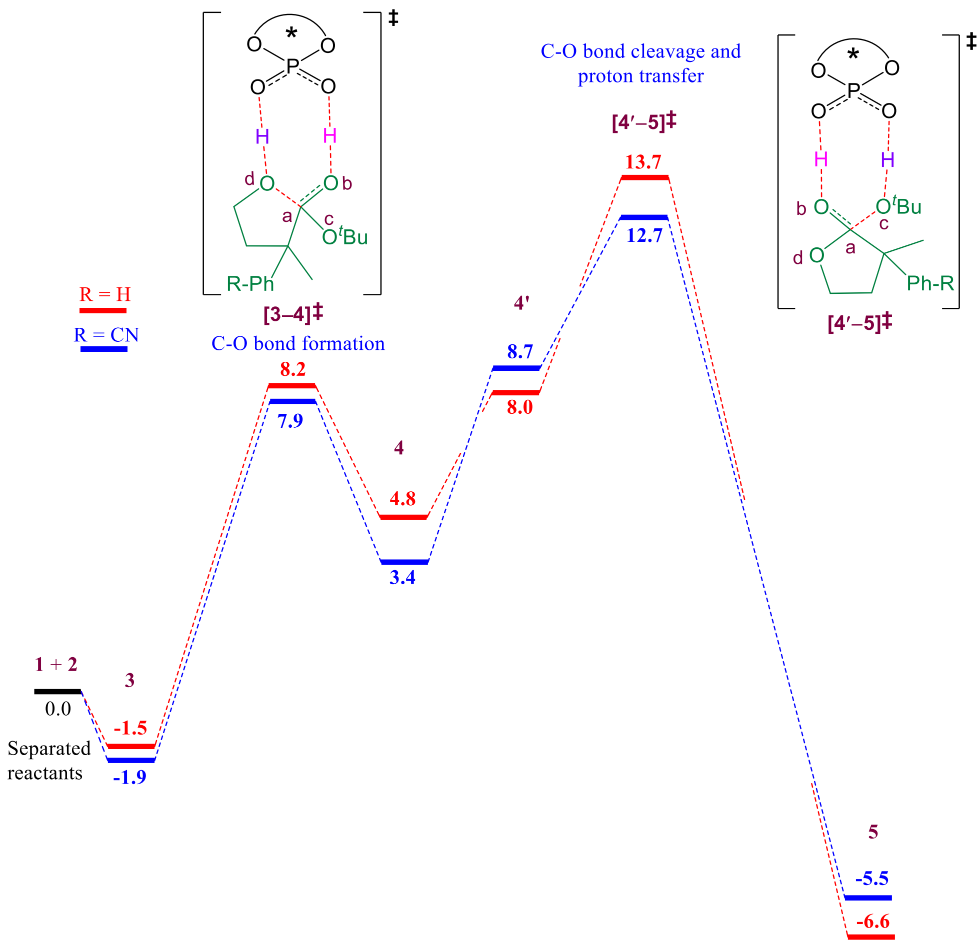

Figure 23. Energy Diagram of Cyano and Reference Compounds

It was also noted that the overall activation energy barrier for the cyano was 14.6 kcal/mol from **3** to **[4’-5]** transition state, while the reference was 15.2 kcal/mol. The overall reaction rate for the cyano was slightly higher and this difference in activation energy barrier supports that experimental observation. Further studies with more in depth experiments evaluating individual enantiomer energy differences will hopefully give more insight into these observations.

3.3 Future Work

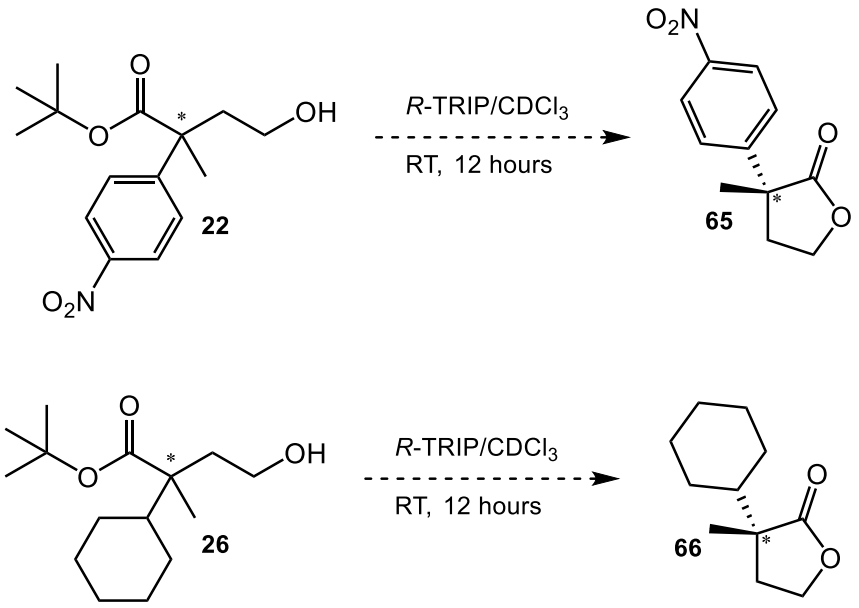

Figure 24. Future Substrates for Kinetic Resolution

There is still more support needed for the hypothesis that hydrogen bonding between catalyst and the hydrogen bond acceptors of the *para* substituents, methoxy and cyano, are responsible for the observed increase in selectivity. Another hydrogen bond accepting group, nitro **22**, is being synthesized and is expected to have the same increased selectivities for this substituent as were seen in the cyano **19** and methoxy **17**. It is also planned to finish the synthesis of an α-cyclohexyl substrate **26** to evaluate if the aromatic system at the alpha position is participating in pi-stacking that facilitates the selectivity of the kinetic resolution.

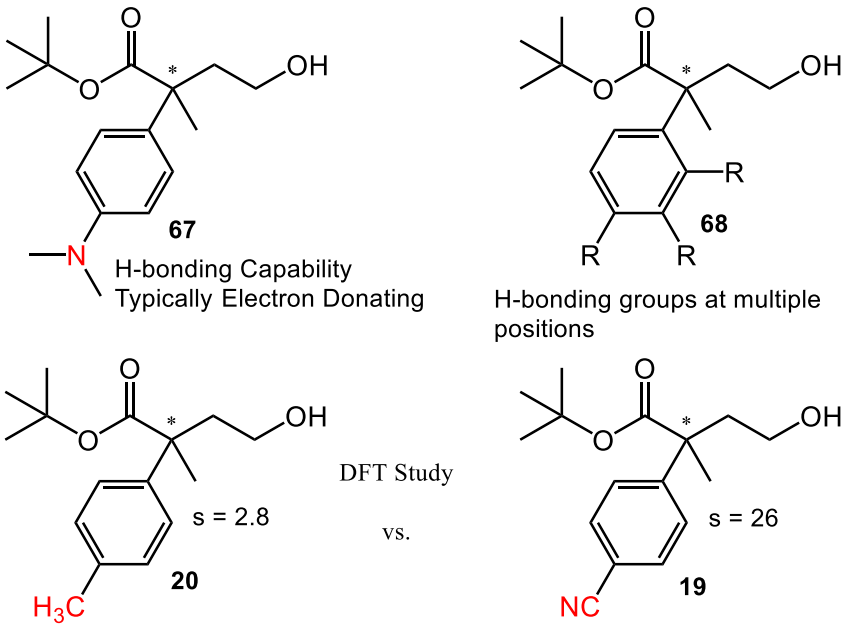

Figure 25. Future Directions

More DFT studies are to be done comparing one of the substrates with much lower selectivity (tolyl) **20** and one of the higher selectivity substrates (cyano) **19**. This along with an individual enantiomer analysis could prove more useful in determining if there is a significant change in the activation energies of the stereoselective transition state resulting in the observed selectivity differences. Another potentially useful substrate would be a *para* dimethyl amine substituent **67**. This substrate would typically be electron donating, much like the methoxy, but also having hydrogen bonding capability. The employment of this substrate could support the hypothesis that hydrogen bonding at this position is causing the observed increase in selectivities. Evaluating hydrogen bonding effects at other positions around the phenyl ring **68** to determine if the change in

position results in increased or decreased selectivities could also provide useful insights.

3.4 Conclusion

In conclusion, it has been observed that the placement of hydrogen bonding capable substituents at the *para* position of the α-phenyl ring on α,α-disubstituted γ-hydroxy esters results in a significant increase in the kinetic resolution. It is proposed that there is a hydrogen bonding interaction taking place between these substituents and the Brønsted acid catalyst *R*-TRIP that results in a greater reduction in activation energy for the fast reacting enantiomer. Electronic effects at the *para* position seem to have little effect on the selectivity of the reaction as is suggested by a lack of correlation in the Hammett plot. More DFT studies along with a broader substrate scope are planned to evaluate the efficacy of this hypothesis.

CHAPTER IV

EXPERIMENTAL

4.1 General Information

All solvents and reagents were purchased from commercial sources and used without purification. Anhydrous solvents were dried under standard procedures. ^{1}H and ^{13}C nuclear magnetic resonance (NMR) spectra were collected utilizing either a 400 or 500 MHz spectrometer with $CDCl_3$ as a solvent at room temperature. The NMR chemical shifts (δ) are reported in ppm. Abbreviations for ^{1}H NMR: s = singlet, d = doublet, t = triplet, q = quartet, sept = septet, m = multiplet. All reactions were monitored via TLC using silica G F_{254} precoated glass plates. Flash column chromatography was done using flash grade silica gel (particle size: 40-63 μ 230 x 400 mesh). Enantiomeric excess (ee) was measured by HPLC analysis on Chiralcel OJ-H and OD-H columns.

4.2 Esterification of Phenylacetic Acids

4.2.1 Esterification of 4-Nitrophenylacetic Acid

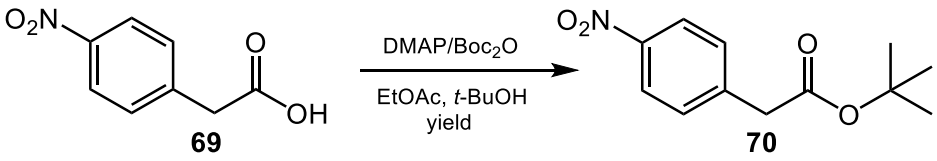

Figure 26. Esterification of 4-Nitrophenylacetic Acid **69**

4-Nitrophenylacetic acid **69** (181 mg, 1.00 mmol) was dissolved in ethyl acetate (1.00 mL) and *tert*-butanol (1.00 mL). 4-Dimethylaminopyridine (12.2 mg, 0.10 mmol) was added and the solution was stirred at room temperature for 15 min. Di-*tert*-butyl dicarbonate (241 mg, 1.10 mmol) was warmed to rt and added via syringe to the reaction which was stirred at rt for 23 h. The reaction mixture was extracted with diethyl ether and washed twice with 1 M HCl (2 $\times$ 10 mL), then twice with saturated sodium bicarbonate (2 $\times$ 10 mL). Finally, the organic layer was washed with brine (20 mL), dried over $MgSO_4$ and concentrated under vacuum. This yielded **70** as a yellow oil (145 mg, 61% yield). Spectral data was consistent with as previously reported.[15]

4.2.2 Esterification of 4-Cyanophenylacetic Acid

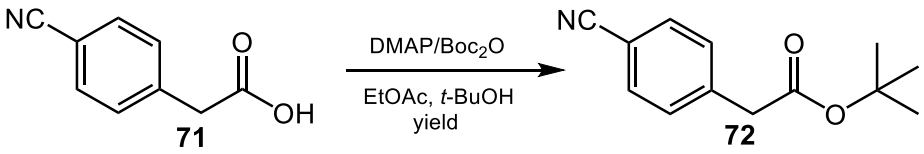

Figure 27. Esterification of 4-Cyanophenylacetic Acid **71**

4-Cyanophenylacetic acid **71** (1.07 g, 6.65 mmol) was dissolved in diethyl ether (4.6 mL), methylene chloride (4.0 mL), and *tert*-butanol (6.4 mL). 4-Dimethylaminopyridine (163 mg, 1.33 mmol) was added and the solution was stirred at room temperature for 15 min. Di-*tert*-butyl dicarbonate (2.18 g, 9.97 mmol) was warmed to rt and added via syringe to the reaction which was stirred at rt for 26 h. The reaction mixture was extracted with methylene chloride and washed twice with 1 M HCl (2 × 15 mL), then twice with saturated sodium bicarbonate (2 × 15 mL). Finally, the organic layer was washed with brine (20 mL), dried over $MgSO_4$ and concentrated under vacuum. The crude product was purified with column chromatography (10% EtOAc:Hexane) to yield **72** as a colorless powder (1.31 g, 90% yield). Spectral data consistent as previously reported.[15]

4.2.3 Esterification of Phenylacetic Acid

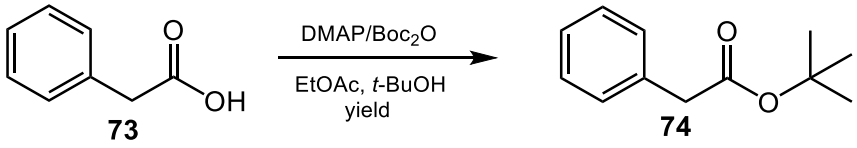

Figure 28. Esterification of Phenylacetic Acid **73**

Phenylacetic acid **73** (10.0 g, 74.0 mmol) was dissolved in ethyl acetate (74.0 mL) and *tert*-butanol (74.0 mL). 4-Dimethylaminopyridine (1.83 g, 15.0 mmol) was added and the solution was stirred at room temperature for 15 min. Di-*tert*-butyl dicarbonate (24.1 g, 110.0 mmol) was added to the reaction then stirred at rt for 23 h. The reaction mixture was extracted with ethyl acetate and washed three times with 1 M HCl (2 × 15 mL), then three times with saturated sodium bicarbonate (2 × 15 mL). Finally, the organic layer was washed with brine (20 mL), dried over $MgSO_4$ and concentrated under vacuum. This yielded **74** as a yellow oil (7.30 g, 52 % yield). Spectral data was consistent as previously reported.[15]

4.2.4 Esterification of 4-Methoxyphenylacetic Acid

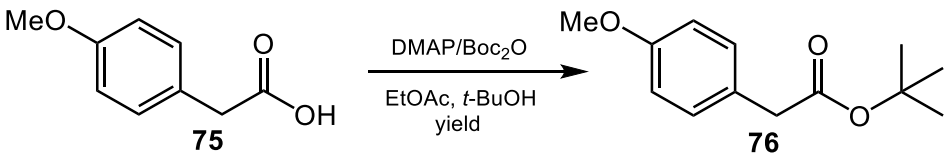

Figure 29. Esterification of 4-Methoxyphenylacetic Acid **75**

4-Methoxyphenylacetic acid **75** (5.00 g, 30.1 mmol) was dissolved in diethyl ether (23.8 mL) and *tert*-butanol (28.8 mL). 4-Dimethylaminopyridine (377.3 mg, 3.1 mmol) was added and the solution was stirred at room temperature for 15 min. Di-*tert*-butyl dicarbonate (7.22 g, 33.1 mmol) was added to the reaction then stirred at rt for 24 h. The reaction mixture was dissolved in 400 mL of 2 % EtOAc:Hexane and vacuum filtered through a silica plug. The resulting solution was dried over $MgSO_4$ and concentrated under vacuum. This yielded **76** as a yellow oil (3.47 g, 56 % yield). Spectral data was consistent as previously reported.[15]

4.2.5 Esterification of 4-Tolylphenylacetic Acid

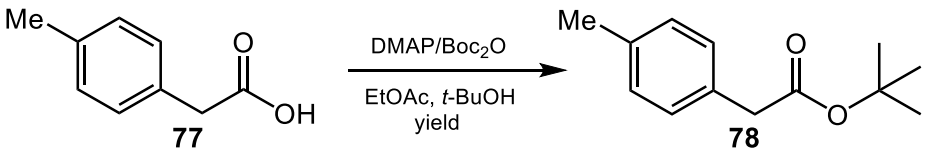

Figure 30. Esterification of 4-Tolylphenylacetic Acid **77**

4-Tolylphenylacetic acid **77** (5.00 g, 33.3 mmol) was dissolved in diethyl ether (26.3 mL) and *tert*-butanol (31.9 mL). 4-Dimethylaminopyridine (407 mg, 3.3 mmol) was added and the solution was stirred at room temperature for 15 min. Di-*tert*-butyl dicarbonate (8.00 g, 36.6 mmol) was added to the reaction then stirred at rt for 24 h. The reaction mixture was extracted in diethyl ether and washed with 15 mL of saturated sodium bicarbonate, twice with water (2 x 15 mL), dried over $MgSO_4$ and concentrated under vacuum. This yielded **78** as a yellow oil (4.61 g, 67 % yield). Spectral data was consistent as previously reported.[19]

4.2.6 Esterification of 4-Biphenylacetic Acid

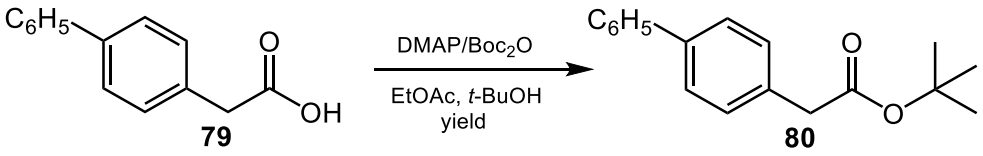

Figure 31. Esterification of 4-Biphenylacetic Acid **79**

4-Biphenylacetic acid **79** (5.00 g g, 23.6 mmol) was dissolved in diethyl ether (38.0 mL) and *tert*-butanol (3.1 mL). 4-Dimethylaminopyridine (288 mg, 2.36 mmol) was added and the solution was stirred at room temperature for 15 min. Di-*tert*-butyl Dicarbonate (5.65 mg, 25.9 mmol) was added to the reaction which was stirred at rt for 24 h. The reaction mixture was extracted with methylene chloride and washed twice with saturated sodium bicarbonate (1 $\times$ 15 mL), and water (4 x 15 mL). Finally, the organic layer was washed with brine (20 mL), dried over $MgSO_4$ and concentrated under vacuum. This yielded **80** as a yellow oil (4.30 g, 68 % yield). ^{1}H NMR (400 MHz, Chloroform-*d*) δ 7.58 (d, *J* = 7.7 Hz, 2H), 7.54 (d, *J* = 7.8 Hz, 2H), 7.42 (t, *J* = 7.5 Hz, 2H), 7.33 (d, *J* = 7.4 Hz, 3H), 3.56 (s, 2H), 1.45 (s, 9H).

4.2.7 Esterification of 4-Trifluoromethylphenylacetic Acid

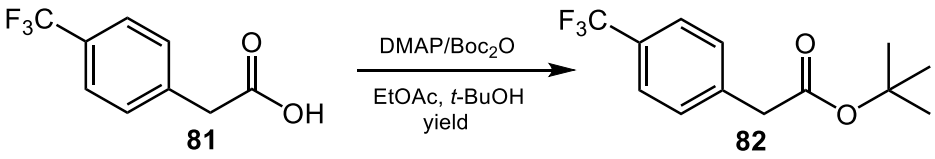

Figure 32. Esterification of 4-Trifluoromethylphenylacetic Acid **81**

4-Trifluoromethylphenylacetic acid (0.99 g, 4.89 mmol) was dissolved in ethyl acetate (4.4 mL) and *tert*-butanol (4.4 mL). 4-Dimethylaminopyridine (121.6 mg, 0.98 mmol) was added and the solution was stirred at room temperature for 15 min. Di-*tert*-butyl dicarbonate (1.39 g, 6.37 mmol) was added to the reaction then stirred at rt for 24 h. The reaction mixture was extracted with ethyl acetate and washed two times with 1M HCl (2 $\times$ 10 mL), then two times with saturated sodium bicarbonate (2 $\times$ 10 mL). Finally, the organic layer was washed with water (10 mL) and brine (20 mL), dried over $MgSO_4$ and concentrated under vacuum. This yielded **82** as a yellow oil (1.27 g, 80 % yield). Spectral data was consistent as previously reported.[20]

4.2.8 Esterification of 4-*tert*-Butylphenylacetic Acid

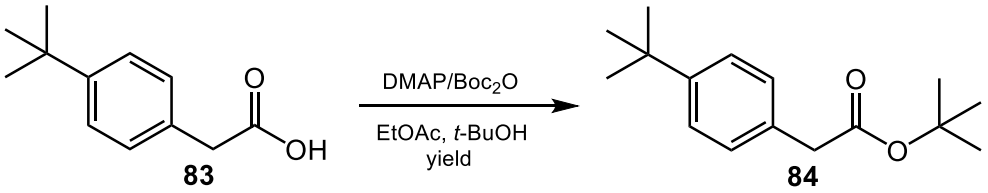

83 **84**

Figure 33. Esterification of 4-*tert*-Butylphenylacetic Acid **83**

4-tert-butylphenylacetic acid (395 mg, 2.06 mmol) was dissolved in ethyl acetate (2.0 mL) and *tert*-butanol (2.0 mL). 4-Dimethylaminopyridine (51.0 mg, 0.41 mmol) was added and the solution was stirred at room temperature for 15 min. Di-*tert*-butyl dicarbonate (672 mg, 3.08 mmol) was added to the reaction then stirred at rt for 24 h. The reaction mixture was extracted with ethyl acetate and washed two times with 1M HCl (2 $\times$ 10 mL), then two times with saturated sodium bicarbonate (2 $\times$ 10 mL). Finally, the organic layer was washed with brine (20 mL), dried over $MgSO_4$ and concentrated under vacuum. The resulting crude mixture was pushed without purification. Spectral data was consistent as previously reported.[20]

4.2.9 Esterification of 4-Isopropylphenylacetic Acid

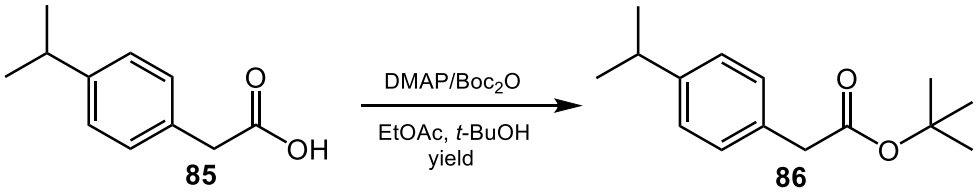

Figure 34. Esterification of 4-Isopropylphenylacetic Acid **85**

4-isopropylphenylacetic acid (1.00 g, 4.27 mmol) was dissolved in ethyl acetate (4.3 mL) and *tert*-butanol (4.3 mL). 4-Dimethylaminopyridine (104 mg, 0.85 mmol) was added and the solution was stirred at room temperature for 15 min. Di-*tert*-butyl dicarbonate (140 mg, 6.4 mmol) was added to the reaction then stirred at rt for 24 h. The reaction mixture was extracted with ethyl acetate and washed two times with 1M HCl (2 × 10 mL), then two times with saturated sodium bicarbonate (2 × 10 mL). Finally, the organic layer was washed with brine (20 mL), dried over $MgSO_4$ and concentrated under vacuum. The crude product was purified with column chromatography (5% EtOAc:Hexane) to yield **86** as a clear, colorless oil (602 mg, 46% yield). ^{1}H NMR (400 MHz, Chloroform-*d*) δ 7.17 (s, 4H), 3.49 (s, 2H), 2.87 (hept, *J* = 7.0 Hz, 1H), 1.43 (s, 9H), 1.23 (d, *J* = 6.9 Hz, 6H). ^{13}C NMR (101 MHz, Chloroform-*d*) δ 171.3, 147.4, 132.0, 129.2, 126.6, 80.8, 42.2, 33.8, 28.2, 24.1.

4.2.10 Esterification of 4-isobutylphenylacetic Acid

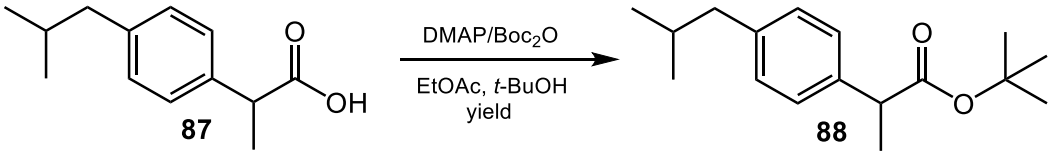

Figure 35. Esterification of 4-Isobutylphenylacetic Acid **87**

4-isobutylphenylacetic acid (0.99 mg, 4.85 mmol) was dissolved in ethyl acetate (4.9 mL) and *tert*-butanol (4.9 mL). 4-Dimethylaminopyridine (123 mg, 0.97 mmol) was added and the solution was stirred at room temperature for 15 min. Di-*tert*-butyl dicarbonate (1.59 g, 7.27 mmol) was added to the reaction then stirred at rt for 20 h. The reaction mixture was extracted with ethyl acetate and washed two times with 1M HCl (2 × 10 mL), two times with saturated sodium bicarbonate (2 × 10 mL), then two times with saturated sodium chloride (2 x 10 mL). Finally, the organic layer was washed with water (10 mL) and brine (20 mL), dried over $MgSO_4$ and concentrated under vacuum. This yielded **88** as an orange oil (1.10 g, 87 % yield). ^{1}H NMR (500 MHz, Chloroform-*d*) δ 7.18 (d, *J* = 8.0 Hz, 2H), 7.07 (d, *J* = 8.0 Hz, 2H), 3.57 (q, *J* = 7.2 Hz, 1H), 2.43 (d, *J* = 7.2 Hz, 2H), 1.84 (sept, *J* = 6.5 Hz, 1H), 1.42 (d, *J* = 7.2 Hz, 3H), 1.38 (s, 9H), 0.88 (d, *J* = 6.6 Hz, 6H).

4.3 Alkylations of Esters

4.3.1 Alkylation of Reference

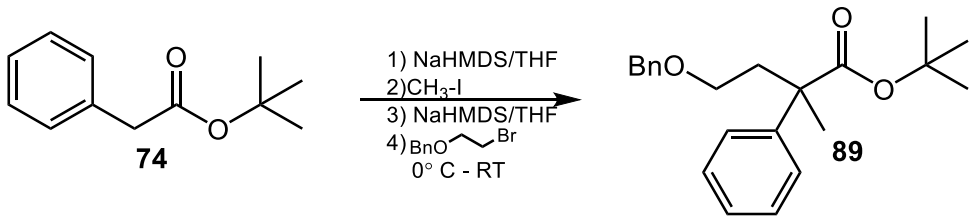

Figure 36. Alkylation of Reference **74**

To a solution of NaHMDS (10.44 g, 57.0 mmol) in THF (76 mL) was added compound **74** (7.30 g, 38.0 mmol) and the solution was stirred for 2 h at 0° C. Methyl iodide (8.10 g, 57.0 mmol) was added drop-wise and the solution was stirred and allowed to warm to room temperature overnight for 18 h. The reaction was quenched with saturated NH_4Cl (20 mL), phases were separated and the organic phase was washed three times with water (3 x 15 mL), The resulting organic layer was washed with saturated sodium chloride (15 mL), dried over $MgSO_4$, then concentrated under vacuum. The crude product was then added to a solution of NaHMDS (9.54 g, 57.0 mmol) in THF (76 mL) at 0° C and stirred for 2 h. Benzyl 2-bromoethyl ether (12.3 g, 57.0 mmol) was then added drop-wise and the reaction was stirred and allowed to warm to room temperature overnight. The reaction was quenched with saturated NH_4Cl (20 mL), phases were separated and the organic phase was washed three times with water (3 x 15 mL), The resulting organic layer was washed with saturated sodium chloride (15 mL), dried over $MgSO_4$, then concentrated under vacuum. The crude product

was purified with column chromatography (2-14% EtOAc:Hexane) to yield compound **89** as a clear, colorless oil (2.71 g, 21% yield). Spectral data was consistent as previously reported.[10]

4.3.2 Alkylation of Cyano

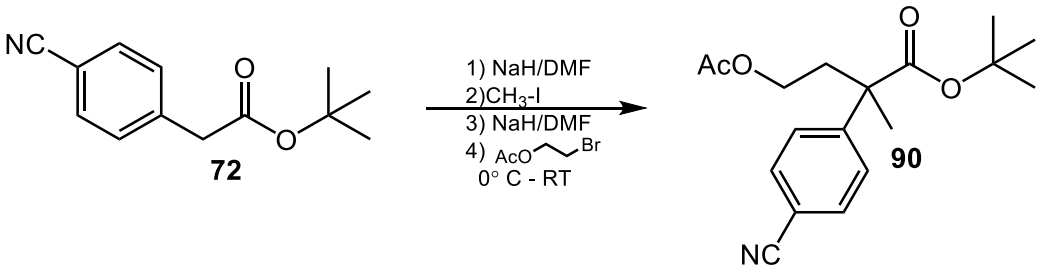

Figure 37. Alkylation of Cyano **72**

To a solution of NaH (44.0 mg, 1.83 mmol) in DMF (6.7 mL) was added compound **72** (362 mg, 1.67 mmol) and the solution was stirred for 45 min at 0° C. Methyl iodide (261 mg, 1.83 mmol) was added drop-wise and the solution was stirred and allowed to warm to room temperature overnight for 18 h. The reaction was quenched with saturated NH_4Cl (10 mL) and diluted with 30 mL of diethyl ether, phases were separated and the organic phase was washed six times with water (6 x 15 mL). The aqueous layer was extracted two times with diethyl ether (2 x 20 mL). The combined organic layers were washed with saturated sodium chloride (30 mL), dried over $MgSO_4$, then concentrated under vacuum. The crude product was then added to a solution of NaH (218 mg, 9.10 mmol) in DMF (5.2 mL) at 0° C and stirred for 45 min. 2-bromoethyl acetate (1.52 g, 9.10 mmol) was

then added drop-wise and the reaction was stirred and allowed to warm to room temperature overnight. The reaction was quenched with saturated NH_4Cl (10 mL) and diluted with 30 mL of diethyl ether, phases were separated and the organic phase was washed six times with water (6 x 15 mL). The aqueous layer was extracted two times with diethyl ether (2 x 20 mL). The combined organic layers were washed with saturated sodium chloride (30 mL), dried over $MgSO_4$, then concentrated under vacuum. The crude product was purified with column chromatography (6-15% EtOAc:Hexane) to yield compound **90** as a clear, colorless oil (412 mg, 42% yield). ^{1}H NMR (400 MHz, Chloroform-*d*) δ 7.62 (d, *J* = 8.3 Hz, 2H), 7.42 (d, *J* = 8.6 Hz, 2H), 4.07 – 3.95 (m, 2H), 2.39 – 2.28 (m, 1H), 2.28-2.17 (m, 1H), 1.94 (s, 3H), 1.56 (s, 3H), 1.37 (s, 9H). ^{13}C NMR (101 MHz, Chloroform-*d*) δ 173.5, 170.9, 148.8, 132.3, 126.9, 110.9, 81.8, 61.2, 37.4, 31.7, 27.8, 22.8, 22.6, 20.9.

4.3.3 First Alkylation of Tolyl

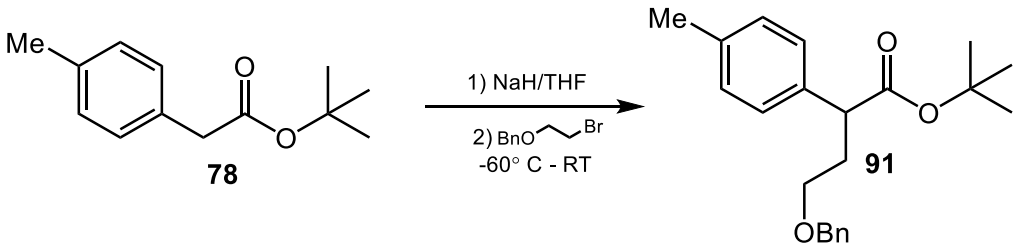

Figure 38. First Alkylation of Tolyl **78**

To a solution of NaH (906 mg, 37.8 mmol) in THF (18.9 mL) was added compound **78** (3.89 g, 18.9 mmol) and the solution was stirred for 15 min at -60° C. Benzyl 2-bromoethyl ether (5.78 g, 18.9 mmol) was added drop-wise and the solution was stirred and allowed to warm to room temperature overnight for 18 h. The reaction was quenched with saturated NH_4Cl (6 mL) and diluted with 80 mL of diethyl ether, phases were separated and the organic phase was washed with saturated sodium chloride (1 x 15 mL). The aqueous layer was extracted two times with diethyl ether (2 x 20 mL). The combined organic layers were washed with saturated sodium chloride (30 mL), dried over $MgSO_4$, then concentrated under vacuum. The crude product was purified with column chromatography (2-10% EtOAc:Hexane) to yield compound **91** as a clear, colorless oil (2.13 g, 35% yield).

4.3.4 Methylation of Tolyl

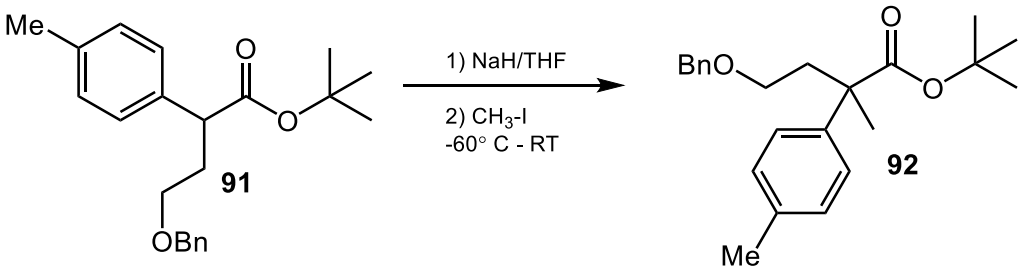

Figure 39. Methylation of Tolyl **91**

To a solution of LiHMDS (3.13 g, 18.7 mmol) in THF (23.8 mL) was added compound **91** (2.13 g, 6.23 mmol) and the solution was stirred for 15 min at -60° C. Methyl Iodide (2.65 g, 18.7 mmol) was added drop-wise and the solution was stirred and allowed to warm to room temperature overnight for 18 h. The reaction was quenched with saturated NH_4Cl (6 mL) and diluted with 50 mL of diethyl ether, phases were separated and the organic phase was washed with saturated sodium chloride (1 x 15 mL). The aqueous layer was extracted two times with diethyl ether (2 x 20 mL). The combined organic layers were washed with saturated sodium chloride (30 mL), dried over $MgSO_4$, then concentrated under vacuum. The crude product was purified with column chromatography (2-10% EtOAc:Hexane) to yield compound **92** as a clear, colorless oil (1.76 g, 80% yield). ^{1}H NMR (500 MHz, Chloroform-*d*) δ 7.30 (m, 5H), 7.20 (s, 2H), 7.11 (s, 2H), 4.52 – 4.38 (m, 2H), 3.46 (m, 2H), 2.39 (m, 1H), 2.21 (m, 1H), 1.49 (s, 3H), 1.34 (s, 9H).

4.3.5 First Alkylation of Methoxy

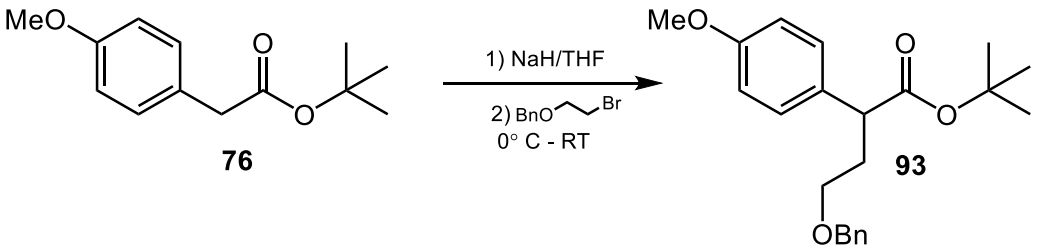

Figure 40. First Alkylation of Methoxy **76**

To a solution of NaH (689 mg, 28.7 mmol) in THF (12.1 mL) was added compound **76** (3.19 g, 14.4 mmol) and the solution was stirred for 30 min at -60° C. Benzyl 2-bromoethyl ether (3.09 g, 14.4 mmol) was added drop-wise and the solution was stirred and allowed to warm to room temperature overnight for 18 h. The reaction was quenched with saturated NH_4Cl (20 mL) and diluted with 50 mL of diethyl ether, phases were separated and the organic phase was washed with saturated sodium chloride (1 x 15 mL). The aqueous layer was extracted two times with diethyl ether (2 x 20 mL). The combined organic layers were washed with saturated sodium chloride (30 mL), dried over $MgSO_4$, then concentrated under vacuum. The crude product was purified with column chromatography (4-10% EtOAc:Hexane) to yield compound **93** as a clear, colorless oil (2.54 g, 50% yield).

4.3.6 Methylation of Methoxy

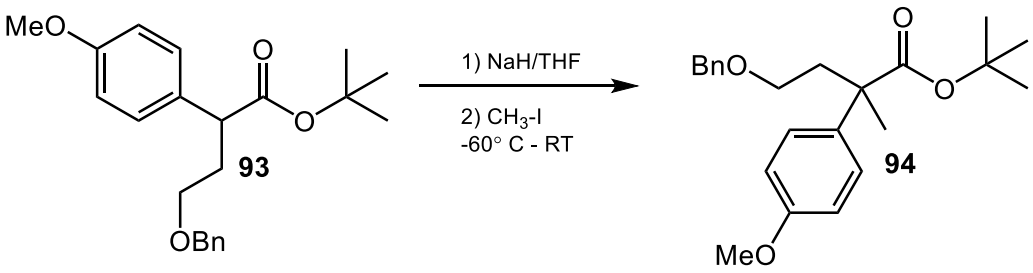

Figure 41. Methylation of Methoxy **93**

To a solution of LiHMDS (3.57 g, 21.3 mmol) in THF (27.0 mL) was added compound **93** (2.54 g, 7.11 mmol) and the solution was stirred for 15 min at -60° C. Methyl Iodide (3.03 g, 21.3 mmol) was added drop-wise and the solution was stirred and allowed to warm to room temperature overnight for 18 h. The reaction was quenched with saturated NH_4Cl (6 mL) and diluted with 50 mL of diethyl ether, phases were separated and the organic phase was washed with saturated sodium chloride (1 x 15 mL). The aqueous layer was extracted two times with diethyl ether (2 x 20 mL). The combined organic layers were washed with saturated sodium chloride (30 mL), dried over $MgSO_4$, then concentrated under vacuum. The crude product was purified with column chromatography (5-10% EtOAc:Hexane) to yield compound **94** as a clear, colorless oil (1.66 g, 63% yield). ^{1}H NMR (500 MHz, Chloroform-*d*) δ 7.29 (m, 5H), 7.23 (m, 2H), 6.86 – 6.81 (m, 2H), 4.50 – 4.37 (m, 2H), 3.79 (s, 3H), 3.49 – 3.37 (m, 2H), 2.44 – 2.32 (m, 1H), 2.27 – 2.14 (m, 1H), 1.49 (s, 3H), 1.34 (s, 9H).

4.3.7 Alkylations of Biaryl

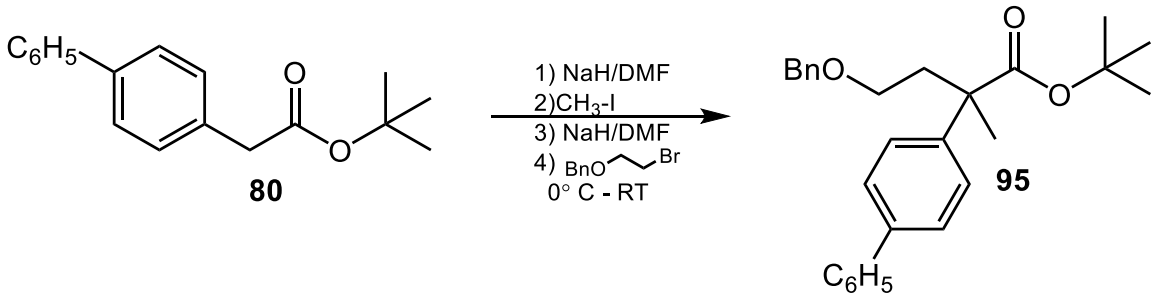

Figure 42. Alkylations of Biaryl **80**

To a solution of NaH (98.3 mg, 4.10 mmol) in DMF (15.0 mL) was added compound **80** (1.00 g, 3.73 mmol) and the solution was stirred for 45 min at 0° C. Methyl iodide (582 mg, 4.10 mmol) was added drop-wise and the solution was stirred and allowed to warm to room temperature overnight for 18 h. The reaction was quenched with saturated NH_4Cl (10 mL) and diluted with 50 mL of diethyl ether, phases were separated and the organic phase was washed six times with water (6 x 15 mL). The aqueous layer was extracted two times with diethyl ether (2 x 20 mL). The combined organic layers were washed with saturated sodium chloride (30 mL), dried over $MgSO_4$, then concentrated under vacuum. The crude product was then added to a solution of NaH (535 mg, 22.3 mmol) in DMF (12.8 mL) at 0° C and stirred for 45 min. Benzyl 2-bromoethyl ether (2.06 g, 9.56 mmol) was then added drop-wise and the reaction was stirred and allowed to warm to room temperature overnight. The reaction was quenched with saturated NH_4Cl (10 mL) and diluted with 50 mL of diethyl ether, phases were separated and the

organic phase was washed six times with water (6 x 15 mL). The aqueous layer was extracted two times with diethyl ether (2 x 20 mL). The combined organic layers were washed with saturated sodium chloride (30 mL), dried over $MgSO_4$, then concentrated under vacuum. The crude product was purified with column chromatography (5-10% EtOAc:Hexane) to yield compound **95** as a clear, colorless oil (1.55 g, 31% yield). ^{1}H NMR (500 MHz, Chloroform-*d*) δ 7.60 (d, *J* = 9.8 Hz, 2H), 7.55 (d, *J* = 9.8 Hz, 2H), 7.44 (t, *J* = 7.5 Hz, 2H), 7.39 (d, *J* = 9.8 Hz, 2H), 7.36 – 7.26 (m, 6H), 4.52 – 4.40 (m, 2H), 3.54 – 3.42 (m, 2H), 2.50 – 2.38 (m, 1H), 2.33 – 2.22 (m, 1H), 1.56 (s, 3H), 1.37 (s, 9H).

4.3.8 First Alkylation of Trifluoromethyl

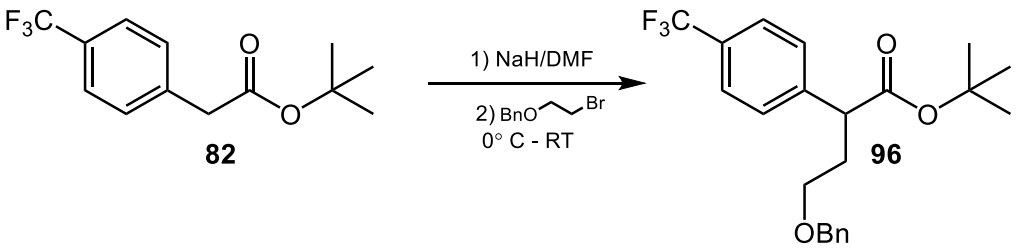

Figure 43. First Alkylation of Trifluoromethyl **82**

To a solution of NaH (121 mg, 5.03 mmol) in DMF (38.7 mL) was added compound **82** (1.01 g, 3.87 mmol) and the solution was stirred for 30 min at 0° C. Benzyl 2-bromoethyl ether (1.08 g, 5.03 mmol) was added drop-wise and the solution was stirred and allowed to warm to room temperature overnight for 18 h. The reaction was quenched with saturated NH_4Cl (10 mL) and diluted with 50 mL

of diethyl ether, phases were separated and the organic phase was washed six times with water (6 x 15 mL). The aqueous layer was extracted two times with diethyl ether (2 x 20 mL). The combined organic layers were washed with saturated sodium chloride (30 mL), dried over $MgSO_4$, then concentrated under vacuum. The crude product was purified with column chromatography (6-10% EtOAc:Hexane) to yield compound **96** as a clear, colorless oil (536 mg, 35% yield).

4.3.9 Methylation of Trifluoromethyl

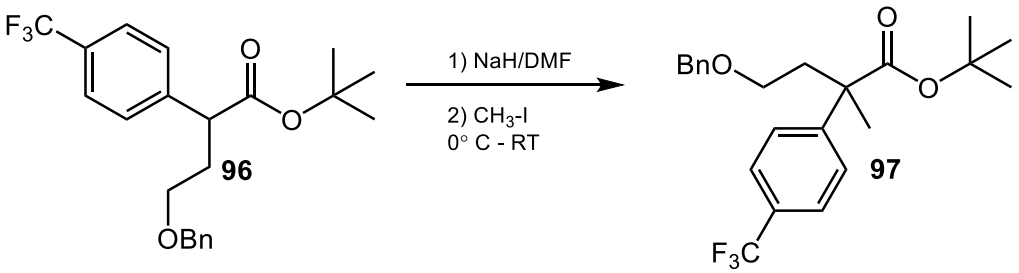

Figure 44. Methylation of Trifluoromethyl **96**

To a solution of NaH (196 mg, 1.36 mmol) in DMF (2.7 mL) was added compound **96** (536 g, 1.36 mmol) and the solution was stirred for 15 min at 0° C. Methyl Iodide (1.16 g, 8.15 mmol) was added drop-wise and the solution was stirred and allowed to warm to room temperature overnight for 24 h. The reaction was quenched with saturated NH_4Cl (10 mL) and diluted with 30 mL of diethyl ether, phases were separated and the organic phase was washed six times with water (6 x 15 mL). The aqueous layer was extracted two times with diethyl ether

(2 x 20 mL). The combined organic layers were washed with saturated sodium chloride (30 mL), dried over $MgSO_4$, then concentrated under vacuum. The crude product was purified with column chromatography (6-10% EtOAc:Hexane) to yield compound **97** as a clear, colorless oil (322 mg, 58% yield). ^{1}H NMR (400 MHz, Chloroform-*d*) δ 7.55 (d, *J* = 8.3 Hz, 2H), 7.41 (d, *J* = 8.4 Hz, 2H), 7.35 – 7.25 (m, 5H), 4.48 – 4.34 (m, 2H), 3.51 – 3.35 (m, 2H), 2.40 (m, 1H), 2.23 (m, 1H), 1.53 (s, 3H), 1.34 (s, 9H). ^{13}C NMR (101 MHz, Chloroform-*d*) δ 176.9, 138.3, 128.5, 127.7, 127.7, 126.4, 81.2, 73.1, 67.0, 49.6, 38.4, 27.8, 23.3. ^{19}F NMR (376 MHz, Chloroform-*d*) δ -62.4.

4.3.10 Esterification and Alkylations of *tert*-Butyl

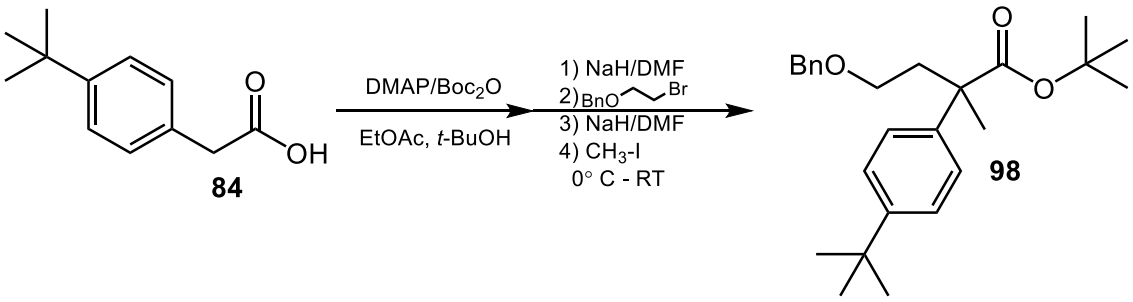

Figure 45. Esterification and Alkylations of *tert*-Butyl **84**

To a solution of NaH (73.9 mg, 3.09 mmol) in DMF (2.1 mL) was added compound **84** (506 mg, 2.06 mmol) and the solution was stirred for 15 min at 0° C. Benzyl 2-bromoethyl ether (665 mg, 3.09 mmol) was added drop-wise and the solution was stirred and allowed to warm to room temperature overnight for 24 h. The reaction was quenched with saturated NH_4Cl (10 mL) and diluted with 20 mL of diethyl ether, phases were separated and the organic phase was washed six times with water (6 x 15 mL). The aqueous layer was extracted two times with diethyl ether (2 x 20 mL). The combined organic layers were washed with saturated sodium chloride (30 mL), dried over $MgSO_4$, then concentrated under vacuum. The crude product was then dissolved in a solution of NaH (148 mg, 6.16 mmol) in DMF (2.1 mL) and the solution was stirred for 15 min at 0° C. Methyl Iodide (874 mg, 6.16 mmol) was added drop-wise and the solution was stirred and allowed to warm to room temperature overnight for 24 h. The reaction was quenched with saturated NH_4Cl (10 mL) and diluted with 30 mL of diethyl

ether, phases were separated and the organic phase was washed six times with water (6 x 15 mL). The aqueous layer was extracted two times with diethyl ether (2 x 20 mL). The combined organic layers were washed with saturated sodium chloride (30 mL), dried over $MgSO_4$, then concentrated under vacuum. The crude product was purified with column chromatography (2-4% EtOAc:Hexane) to yield compound **98** as a clear, colorless oil (54.9 mg, 7% yield). ^{1}H NMR (400 MHz, Chloroform-*d*) δ 7.36 – 7.19 (m, 9H), 4.54 – 4.38 (m, 2H), 3.53 – 3.38 (m, 2H), 2.50 – 2.32 (m, 1H), 2.29 – 2.12 (m, 1H), 1.50 (s, 3H), 1.36 (s, 9H), 1.30 (s, 9H).

4.3.11 Alkylation of Isobutyl

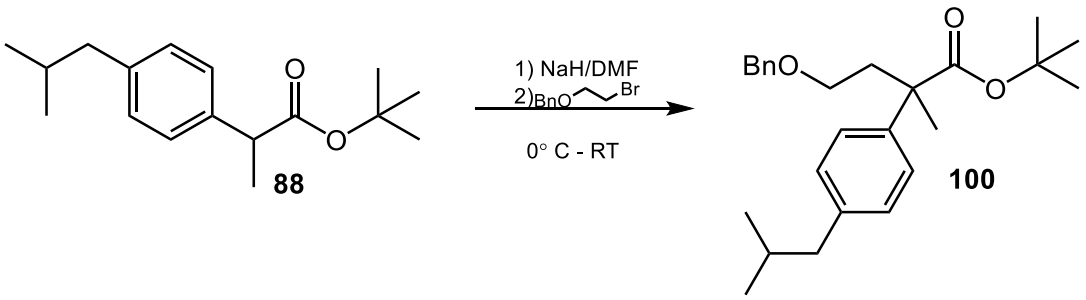

Figure 46. Alkylation of Isobutyl **88**

To a solution of NaH (290 mg, 12.1 mmol) in DMF (4.0 mL) was added compound **88** (1.06 g, 4.03 mmol) and the solution was stirred for 15 min at 0° C. Benzyl 2-bromoethyl ether (2.60 g, 12.1 mmol) was added drop-wise and the solution was stirred and allowed to warm to room temperature overnight for 24 h. The reaction was quenched with saturated NH_4Cl (10 mL) and diluted with 30 mL of diethyl ether, phases were separated and the organic phase was washed six

times with water (6 x 15 mL). The aqueous layer was extracted two times with diethyl ether (2 x 20 mL). The combined organic layers were washed with saturated sodium chloride (30 mL), dried over $MgSO_4$, then concentrated under vacuum. The crude product was purified with column chromatography (2% EtOAc:Hexane) to yield **100** as a clear, colorless oil (0.84 g, 52% yield). ^{1}H NMR (400 MHz, Chloroform-*d*) δ 7.61 – 7.22 (m, 5H), 7.20 (d, *J* = 9.0 Hz, 2H), 7.06 (d, *J* = 8.0 Hz, 2H), 4.51 – 4.35 (m, 2H), 3.53 – 3.34 (m, 2H), 2.41 (m, 3H), 2.28 – 2.14 (m, 1H), 1.83 (hept, *J* = 6.8 Hz, 1H), 1.50 (s, 3H), 1.33 (s, 9H), 0.87 (d, *J* = 6.5 Hz, 6H). ^{13}C NMR (101 MHz, Chloroform-*d*) δ 175.2, 141.3, 139.9, 138.5, 129.0, 128.4, 127.7, 127.6, 125.6, 80.6, 73.0, 67.5, 49.1, 45.0, 38.4, 30.3, 27.9, 23.42, 22.5.

4.4 Alcohol Deprotection of Hydroxy Esters

4.4.1 Hydrogenolysis of Reference

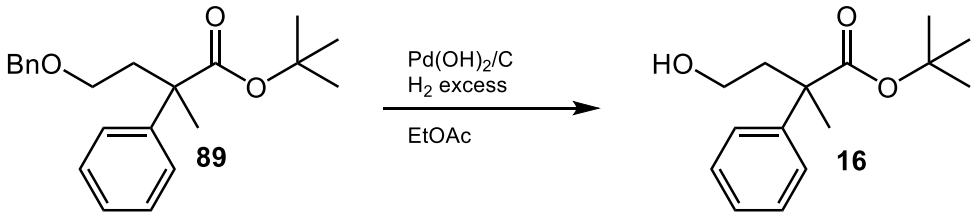

Figure 47. Hydrogenolysis of Reference **89, 16**

$Pd(OH)_2/C$ (20% on Carbon, 112 mg, 0.80 mmol) was added to ethyl acetate (16.0 mL) in a flask. Compound **89** was added to the flask and H_2 gas was flushed through with a balloon and vacuum. The reaction was stirred overnight for 24 h at room temperature. The resulting reaction mixture was filtered through a Celite® plug and concentrated under vacuum. The crude mixture was purified by column chromatography (15% EtOAc:Hexane) to yield **16** as a clear, colorless oil (1.99 g, 94% yield). Spectral data was consistent as previously reported.[10]

4.4.2 Deprotection of Cyano

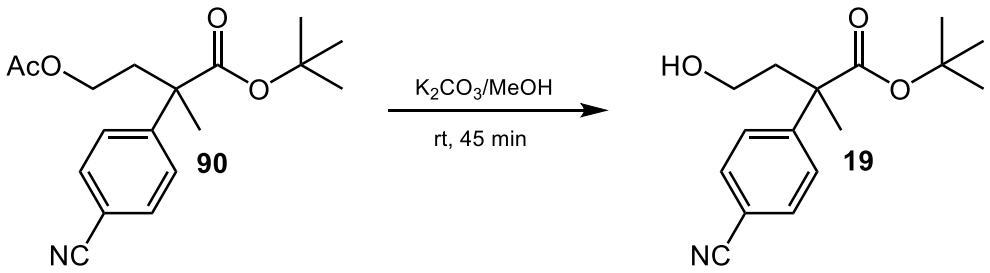

Figure 48. Deprotection of Cyano **90, 19**

K_2CO_3 (300 mg, 2.17 mmol) was added to a solution of compound **90** (172 mg, 0.54) dissolved in methanol (4.0 mL). The reaction was stirred at room temperature for 45 min. The reaction mixture was diluted with methylene chloride (20 mL) and washed with water (1 x 20 mL). The organic layer was washed with saturated sodium chloride (1 x 15 mL), dried over $MgSO_4$, and concentrated under vacuum. The crude mixture was purified with column chromatography (20-50% EtOAc:Hexane) to yield **19** as a clear, colorless oil (130 mg, 87% yield). ^{1}H NMR (500 MHz, Chloroform-*d*) δ 7.63 (d, *J* = 8.7 Hz, 2H), 7.43 (d, *J* = 8.7 Hz, 2H), 3.70 – 3.57 (m, 2H), 2.36 – 2.28 (m, 1H), 2.12 – 2.05 (m, 1H), 1.58 (s, 3H), 1.38 (s, 9H).

4.4.3 Hydrogenolysis of Methoxy

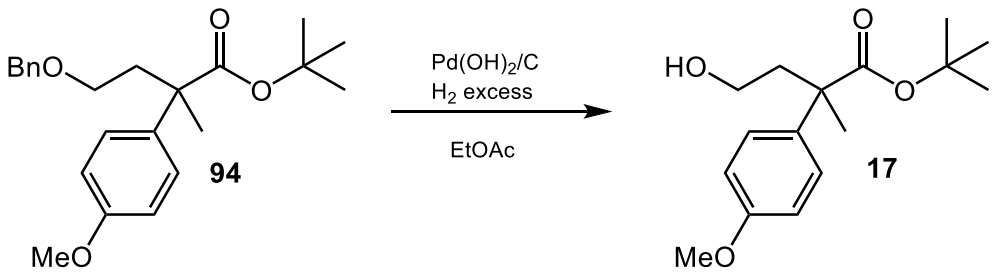

Figure 49. Hydrogenolysis of Methoxy **94, 17**

$Pd(OH)_2/C$ (20% on Carbon, 62.9 mg, 0.45 mmol) was added to ethyl acetate (64.0 mL) in a flask. Compound **94** (1.66 g, 4.48 mmol) was added to the flask and H_2 gas was flushed through with a balloon and vacuum. The reaction was stirred overnight for 24 h at room temperature. The resulting reaction mixture was filtered through a Celite® plug and concentrated under vacuum to yield **17** as a clear, colorless oil in quantitative yield. ^{1}H NMR (400 MHz, Chloroform-*d*) δ 7.22 (d, *J* = 8.5 Hz, 2H), 6.84 (d, *J* = 8.4 Hz, 2H), 3.78 (s, 3H), 3.61 (m, 2H), 2.26 (m, 1H), 2.08 (m, 1H), 1.80 (s, 1H), 1.53 (s, 3H), 1.37 (s, 9H).

4.4.4 Hydrogenolysis of Tolyl

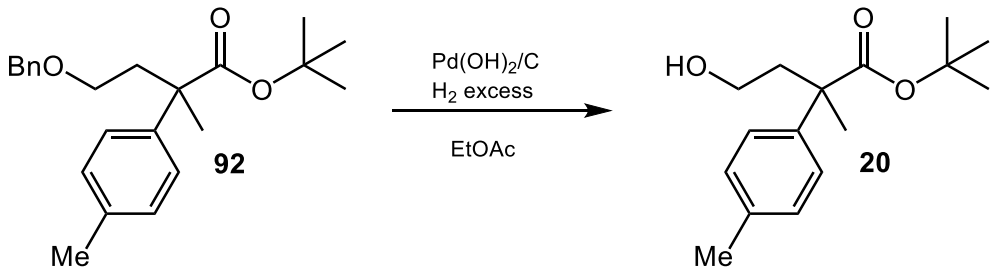

Figure 50. Hydrogenolysis of Tolyl **92, 20**

$Pd(OH)_2/C$ (20% on Carbon, 72.6 mg, 0.52 mmol) was added to ethyl acetate (73.9 mL) in a flask. Compound **92** (1.76 g, 4.97 mmol) was added to the flask and H_2 gas was flushed through with a balloon and vacuum. The reaction was stirred overnight for 24 h at room temperature. The resulting reaction mixture was filtered through a Celite® plug and concentrated under vacuum to yield **20** as a clear, colorless oil in quantitative yield. ^{1}H NMR (500 MHz, Chloroform-*d*) δ 7.18 (d, *J* = 8.3 Hz 2H), 7.12 (d, *J* = 8.3 Hz, 2H), 3.70 – 3.53 (m, 2H), 2.32 (s, 3H), 2.27 (m, 1H), 2.09 (m, 1H), 1.54 (s, 3H), 1.39 (s, 9H). ^{13}C NMR (126 MHz, Chloroform-*d*) δ 176.1, 141.1, 136.3, 129.2, 125.7, 81.1, 59.9, 49.5, 42.3, 27.9, 23.4, 21.0.

4.4.5 Hydrogenolysis of Biaryl

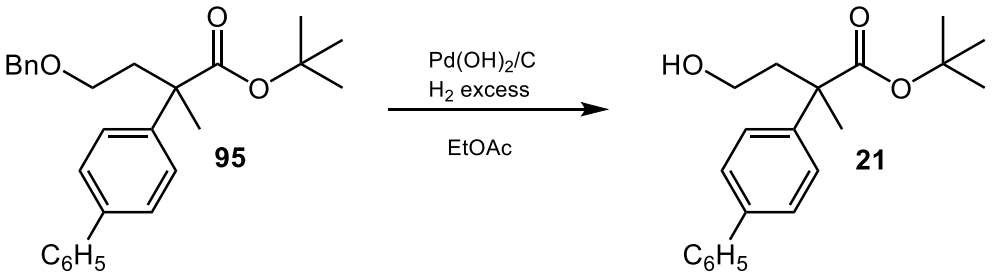

Figure 51. Hydrogenolysis of Biaryl **95, 21**

$Pd(OH)_2/C$ (20% on Carbon, 16.4 mg, 0.12 mmol) was added to ethyl acetate (11.7 mL) in a flask. Compound **95** (486 mg, 1.17 mmol) was added to the flask and H_2 gas was flushed through with a balloon and vacuum. The reaction was stirred overnight for 24 h at room temperature. The resulting reaction mixture was filtered through a Celite® plug and concentrated under vacuum. The crude mixture was purified with column chromatography (30% EtOAc:Hexane) to yield **21** as a clear, colorless oil in quantitative yield. ^{1}H NMR (500 MHz, Chloroform-*d*) δ 7.59 (d, *J* = 8.4 Hz, 2H), 7.56 (d, *J* = 8.5 Hz, 2H), 7.43 (t, *J* = 7.3 Hz, 2H), 7.38 (d, *J* = 8.6 Hz, 2H), 7.34 (t, *J* = 7.3, 1.2 Hz, 1H), 3.77 – 3.58 (m, 2H), 2.42 – 2.28 (m, 1H), 2.21 – 2.08 (m, 1H), 1.84 (s, 1H), 1.60 (s, 3H), 1.42 (s, 9H).

4.4.6 Hydrogenolysis of Trifluoromethyl

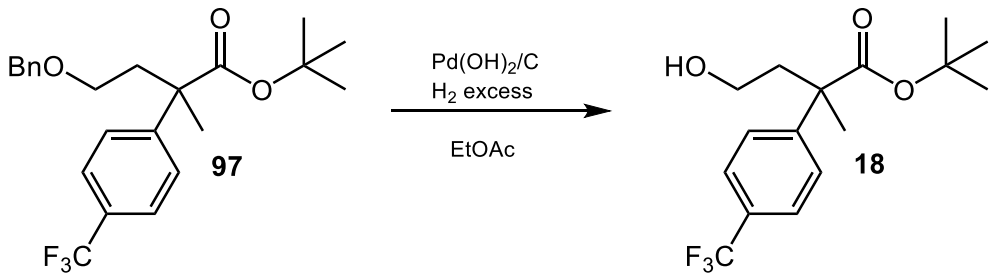

Figure 52. Hydrogenolysis of Trifluoromethyl **97, 18**

$Pd(OH)_2/C$ (20% on Carbon, 10.6 mg, 0.08 mmol) was added to ethyl acetate (1.5 mL) in a flask. Compound **97** (309 mg, 0.76 mmol) was added to the flask and H_2 gas was flushed through with a balloon and vacuum. The reaction was stirred overnight for 24 h at room temperature. The resulting reaction mixture was filtered through a Celite® plug and concentrated under vacuum. The crude mixture was purified with column chromatography (15-20% EtOAc:Hexane) to yield **18** as a clear, colorless oil (228 mg, 95% yield). ^{1}H NMR (400 MHz, Chloroform-*d*) δ 7.57 (d, *J* = 8.4 Hz, 2H), 7.42 (d, *J* = 8.2 Hz, 2H), 3.63 (m, 2H), 2.32 (m, 1H), 2.09 (m, 1H), 1.75 (t, *J* = 5.4, 1H), 1.58 (s, 3H), 1.38 (s, 9H). ^{13}C NMR (101 MHz, Chloroform-*d*) δ 175.2, 126.3, 125.4, 125.4, 81.6, 59.6, 49.9, 41.9, 27.9, 23.2. ^{19}F NMR (376 MHz, Chloroform-*d*) δ -62.4.

4.4.7 Hydrogenolysis of *tert*-Butyl

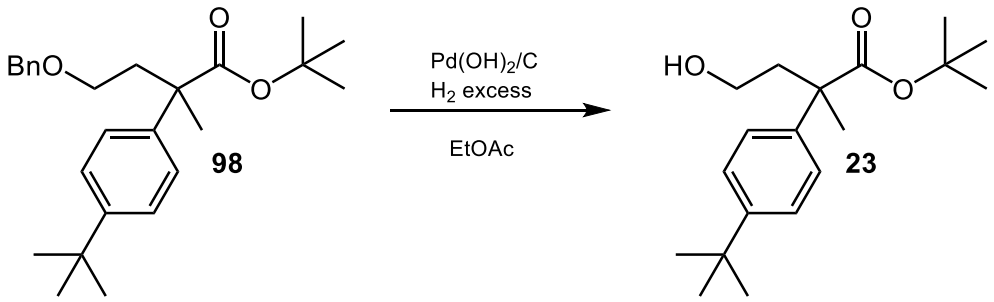

Figure 53. Hydrogenolysis to *tert*-Butyl **98, 23**

$Pd(OH)_2/C$ (20% on Carbon, 2.0 mg, 0.014 mmol) was added to ethyl acetate (0.28 mL) in a flask. Compound **98** (54.9 mg, 0.14 mmol) was added to the flask and H_2 gas was flushed through with a balloon and vacuum. The reaction was stirred overnight for 24 h at room temperature. The resulting reaction mixture was filtered through a Celite® plug and concentrated under vacuum to yield **23** as a clear, colorless oil in quantitative yield. ^{1}H NMR (500 MHz, Chloroform-*d*) δ 7.32 (d, *J* = 8.6 Hz, 2H), 7.22 (d, *J* = 8.6 Hz, 2H), 3.70 – 3.55 (m, 2H), 2.34 – 2.22 (m, 1H), 2.13 – 2.04 (m, 1H), 1.54 (s, 3H), 1.41 (s, 9H), 1.30 (s, 9H).

4.4.8 Hydrogenolysis of Isobutyl

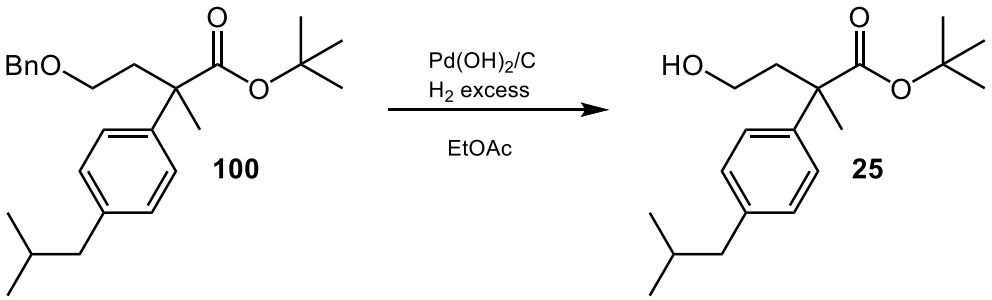

Figure 54. Hydrogenolysis of Isobutyl **100, 25**

$Pd(OH)_2/C$ (20% on Carbon, 28.0 mg, 0.20 mmol) was added to ethyl acetate (4.0 mL) in a flask. Compound **100** (784 mg, 1.98 mmol) was added to the flask and H_2 gas was flushed through with a balloon and vacuum. The reaction was stirred overnight for 24 h at room temperature. The resulting reaction mixture was filtered through a Celite® plug and concentrated under vacuum. The crude mixture was purified with column chromatography (15-100% EtOAc:Hexane) to yield **25** as a clear, colorless oil in quantitative yield. ^{1}H NMR (400 MHz, Chloroform-*d*) δ 7.19 (d, *J* = 8.3 Hz, 2H), 7.07 (d, *J* = 8.2 Hz, 2H), 3.69 – 3.55 (m, 2H), 2.43 (d, *J* = 7.1 Hz, 2H), 2.31 – 2.21 (m, 1H), 2.16 – 2.05 (m, 1H), 1.91 – 1.75 (m, 2H), 1.54 (s, 3H), 1.38 (s, 9H), 0.87 (d, *J* = 6.6 Hz, 6H). ^{13}C NMR (101 MHz, Chloroform-*d*) δ 176.1, 141.2, 140.1, 129.2, 125.5, 81.0, 59.9, 49.5, 44.9, 42.3, 30.3, 27.9, 23.3, 22.5.

4.5 General Procedure for Kinetic Resolutions

Hydroxyester starting material was dissolved in a stock solution of 0.1002 M 1,2,4,5-tetrachloro-3-nitrobenzene in $CDCl_3$ to a 0.1 M concentration. *R*-TRIP was added to the solution and stirred. There were 600 µL of reaction mixture transferred to a NMR tube and sealed with parafilm. An initial scan was taken before the addition of *R*-TRIP to determine initial substrate concentration. There were 16 ^1H NMR scans taken every 10 min for 12 h at 18° C to determine reaction rate and conversion. Chiral HPLC was utilized to determine enantiomeric excess at given time points.

CHAPTER V

DI-TERTBUTYL DI-CARBONATE COUPLED ESTERIFICATION

5.1 Introduction

The esterification of carboxylic acids is a commonly used transformation in the field of organic chemistry. Two common methods employed by synthetic chemists are the Mitsunobu and Steglich coupling reactions (Figure 56).[21] These reactions, while effective, produce byproducts that can often be difficult to remove.[23]

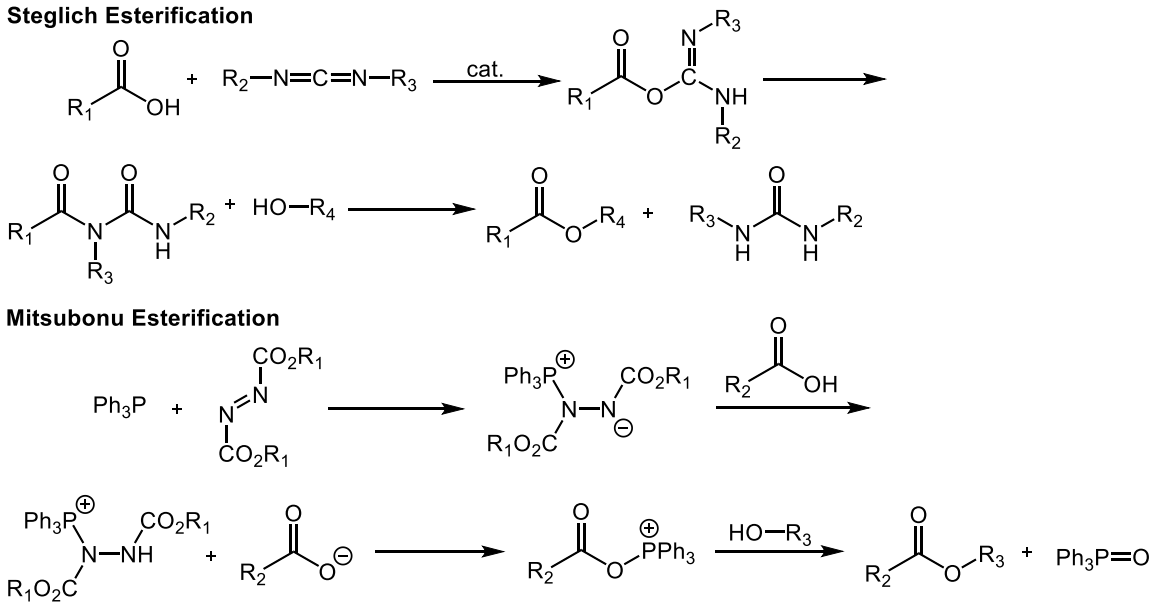

Figure 55. Mitsunobu and Steglich Esterifications

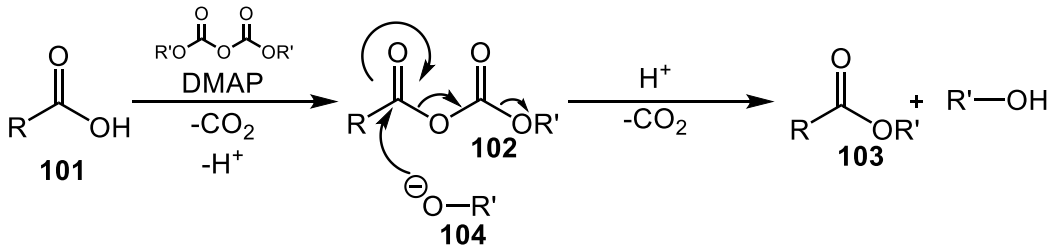

Figure 56. Dicarbonate Coupled Esterification

The use of di-*tert*-butyl dicarbonate (*Boc*$_2$O) as a coupling reagent for these types of transformations has shown to be effective for a variety of both carboxylic acids and alcohols and is convenient for molecules that may be sensitive to acidic conditions. In 1994, Takada et. Al. published this reaction with the use of dimethylamino pyridine (DMAP) as a catalyst, several *N*-protected amino acids as their carboxylic acids, and a variety of dicarbonates as coupling reagents: dimethyl dicarbonate (Moc$_2$O), diethyl dicarbonate (Eoc$_2$O), di-*tert*-butyl dicarbonate (Boc$_2$), and diallyl dicarbonate (Bnoc$_2$O).[22] These dicarbonates are all commercially available making them convenient for this method of esterification. They showed that catalytic amounts of DMAP (10-30%) in THF as a solvent could be used to transform carboxylic acids to their corresponding esters. The dimethyl dicarbonate results in the methyl ester, diethyl produces the ethyl ester, and so on. This transformation was made possible by the production of an alkoxide **104** as a mixed anhydride **102** forms during the addition of the carboxylic acid **101** to the dicarbonate. This alkoxide then attacks the carbonyl of the mixed anhydride **102** and forms the corresponding ester.[22]

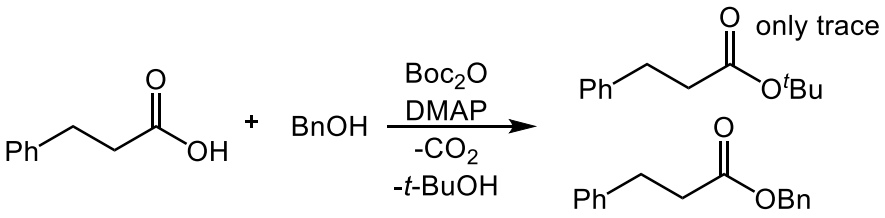

Figure 57. Esterification with Alternative Alcohols

Gooben et Al. realized that when di-*tert*-butyl dicarbonates were used as the coupling reagent, the reaction was slow enough, due to steric bulk, to allow for the addition of virtually any alcohol that they wanted.[23] The biggest benefit of this reaction was that all of the byproducts produced were very volatile and the catalyst could be removed in an aqueous work-up. The substrate scope of alcohols done gave yields of 88-99% for 12 different alcohols. A carboxylic acid substrate scope was done as well, with benzyl alcohol, and produced yields from 91-99%, except when 2-fluoro benzoic acid and 3-nitro benzoic acids were used. The benzoic acids both produced yields less than 5 %.[23]

5.2 Results and Discussion

With this reaction in mind, it was attempted to produce a version of this methodology that used more environmentally friendly reaction conditions. *N*-methylimidazole (NMI) was employed in the place of DMAP. Both catalysts are capable of being removed in an aqueous media, but NMI, LD50: 1130 mg/kg [Rat], is significantly less toxic than DMAP, LD50: 190 mg/kg [Rat].[24,25] For the solvent, in place of THF or nitromethane as used in the previously discussed papers,[22,23] ethyl acetate was chosen. In a paper on green solvents, Capello et.

Al. use an EHS (environmental, health, and safety) tool and LCA (life-cycle assessment) to evaluate how green organic solvents are.[26] The EHS tool screens for chemical hazards, while the LCA method can give an assessment of environmental emissions and the full life-cycle of the solvent. In the EHS method, ethyl acetate scores under 3, while THF is almost 4. Ethyl acetate scores much better in the LCA method than THF.[26] Nitromethane is not reported in this paper. It can be noted that diethyl ether scores very high in the LCA method, this suggests it would be considered a relatively green solvent. This method has not yet been employed for the use of ionic liquids, which may be a potential green solvent for this transformation.[26]

With mildly “greener” solvents in hand, an optimization study was done with 4-nitrophenylacetic acid and phenylacetic acid. Di-*tert*-butyl dicarbonate was used as the coupling reagent with ethyl acetate as a solvent and *t*-butanol as the alcohol (Table 4). All reactions were run at 0.1 M. Phenylacetic acid showed highest yields with 5 mol% of catalyst, 1.1 equivalents of Boc_2O and 10 equivalents of *tert*-butanol at 50°C. The yield under those conditions was 52%. When drying phenylacetic acid, product was being lost during concentration due to its volatility. Therefore, it was decided to use 4-nitrophenylacetic acid as the optimization substrate. Initial reaction conditions with 10 mol% catalyst loading, 1.1 equivalents of Boc_2O, and 10 equivalents of *tert*-butanol, gave a yield of 94%. Reducing catalyst loading to 5 mol% resulted in a drop of yield to 30%. Increasing temperature to 50°C resulted in a slight increase of yield to 96%, but

this was not considered a significant enough change in yield to warrant increasing the temperature of all substrates.

Table 4. Esterification Optimization

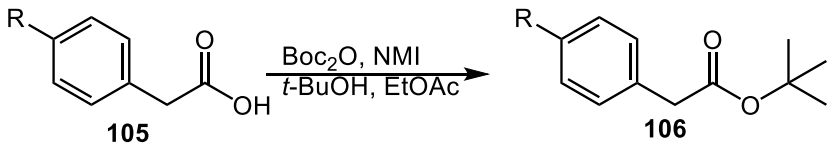

105 **106**

R =	NMI eq.	Boc_2O eq.	*t*-BuOH eq	Temp. °C	yield (%)
-H	0.05	1.1	10	RT	16
-H	0.01	1.1	10	RT	NR
-H	0.00	1.1	10	RT	NR
-H	1.00	1.1	10	RT	18
-H	0.10	1.1	10	RT	31
-H	0.05	1.1	10	50	52
$-NO_2$	0.10	1.1	10	RT	94
$-NO_2$	0.10[a]	1.1	10	RT	61
$-NO_2$	0.05	1.1	10	RT	30
$-NO_2$	0.10	1.1	10	50	96
$-NO_2$	0.10	1.1	2	RT	23
$-NO_2$	0.10	1.1	1	RT	18

[a]Catalyst used was DMAP.

However, it is important to note that the increase in temperature for phenylacetic acid in the table did result in a significant increase in yield from 16 to 52%. When

using these same conditions, DMAP resulted in a lower yield, 61%. Optimization of the *tert*-butanol showed that a decrease in the equivalents results in a much slower reaction. With the optimized conditions of 10 mol% catalyst, 1.1 equivalents of Boc_2O, 10 equivalents of *tert*-butanol and room temperature in hand, the substrate scope was evaluated. It was discovered that other than phenylacetic acids tested, the reaction was unsuccessful for all other substrates with very low yields or no desired product at all.

The substrates that were tested are shown in Figure 59. It was observed that for most of these substrates, there was a problem with insolubility. It is possible that most of these substrates are simply not very soluble in the ethyl acetate/*t*-BuOH solvent system for this reaction. Due to this, plans for future study to test the viability of a newer class of solvents for this reaction, ionic liquids, are being discussed.

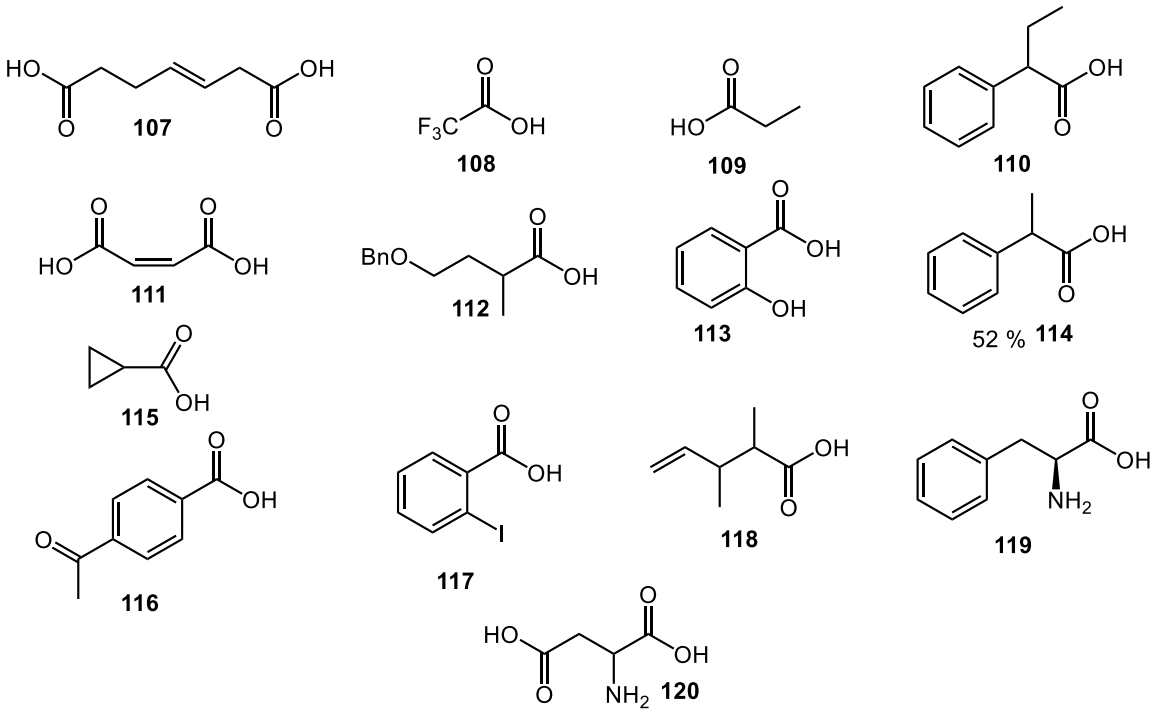

Figure 58. Substrate Scope for Esterification

5.3 Future Work

Ionic liquids are liquids that have very low melting points, many are liquid at room temperature, and they have shown to be useful solvents in many organic reactions. Ionic liquids also have the ability to be removed in an aqueous workup and by nature are very polar which may prove useful with the insolubility problem. They have already shown to be useful solvents and even catalysts in a wide variety of organic reactions.[27] Plans to purchase a variety of these solvents to screen for their effectiveness in the esterification reaction and to evaluate their ability to work as solvents for a wider substrate scope, are being explored.

5.4 Conclusion

Di-*tert*-butyl dicarbonate coupled esterification is an effective means of converting acids to esters. A greener approach to this method, utilizing ethyl acetate as a solvent and *N*-methylimidazole as a catalyst has proven ineffective in producing a wide range of esters, while being very efficient at converting phenylacetic acids to their esters. Solubility was an issue in this transformation and will be addressed through the use of Ionic liquids.

REFERENCES

1. Nguyen, L. A.; He, H.; Pham-Huy, C. Chiral Drugs: An Overview. *J. Biomed. Sci.,* **2006**, *2*, 85-100.

2. Pasteur, M. L. *C. R. Hebd. Seances Acad. Sci.,* **1858**, *46*, 615-618.

3. Martin, V. S.; Woodard, S. S.; Katsuki, T.; Yamada, Y.; Ikada, M.; Sharpless, K. B. Kinetic Resolution of Racemic Alcohols by Enantioselective Epoxidation. A Route to Substances of Absolute Enantiomeric Purity. *J. Am. Chem. Soc.,* **1981,** *103*, 6237-6240.

4. Kagan, H. B.; Fiaud, J. C. *In Topics in Stereochemistry*; Eliel, E. L., Ed.; Wiley & Sons: New York, **1988**, 18, 249-330.

5. Edwin, V.; Jure, M. Efficiency in Nonenymatic Kinetic Resolution. *Ang. Chem. Int. Ed.,* **2005**, *44*, 3974-4001.

6. Ovchinnikov, M. Y.; Yangirov, T. A.; Lobov, A. N.; Sultanova, R. M.; Khursan, S. L. 1,3-Dipolar Cycloaddition of Diazo Compounds to Electron-Deficient Alkenes: Kinetics and Mechanism of Formation of Dimethyl-4,5-dihydro-1H-pyrazol-3,5-dicarboxylate. *Int. J. Chem. Kin.,* **2013**, *45*, 499-507.

7. (a) Petersen, K. S. Nonenymatic Enantioselective Synthesis of All-Carbon Quaternary Centers through Desymmetrization.*Tetrahedron Lett.* **2015**. *56*, 6523-6535. (b) Bertelsen, S.; Jørgensen, K. A. Organocatalysis—After the Gold Rush. *Chem. Soc. Rev.,* **2009**, *38*, 2178-2189.

8. (a) Etzenbach-Effers, K.; Berkessel, A. Noncovalent Organocatalysis Based on Hydrogen Bonding: Elucidation of Reaction Paths by Computational Methods. *Top. Curr. Chem.* **2010**, *291*, 1-27.; (b) Kampen, D.; Reisinger, C. M.; List, B. Chiral Brønsted Acids for Asymmetric Organocatalysis. *Top. Curr. Chem*., **2010**, *291*, 395-456.

9. Ruepuing, M.; Kuenkel, A.; Atodiresei, I. Chiral Brønsted acids in enantioselective carbonylactivations – activation modes and applications. *Chem. Soc. Rev.,* **2011**, *40*, 4539-4549.

10. Qabaja, G.; Wilent, J. E.; Benavides, A. R.; Bullard, G. E.; Petersen, K.S. Facile Synthesis of Versatile Enantioenriched α-Substituted Hydroxy Esters through a Brønsted Acid Catalyzed Kinetic Resolution. *Org. Lett.,* **2013**, *15*, 1266-1269.

11. (a) Hansch, C.; Leo, A.; Taft, R. W. A Survey of Hammett Substituent Constants and Resonance and Field Parameters. *Chem. Rev.,* **1991**, *91*, 165-195. (b) Hansch, C.; Leo, A. Substituent Constants for Correlation Analysis in Chemistry and Biology; John Wiley & Sons: New York, **1979**.

12. Swain, C. G.; Lupton, E. C., Jr. Field and Resonance Components of Substituent Effects. *J. Am. Chem. Soc.,* **1968**, *90*, 4328-4337.

13. Akhani, R. K.; Moore, M. I.; Pribyl J. G.; Wiskur, S. L. Linear Free-Energy Relationship and Rate Study on a Silylation-Based Kinetic Resolution: Mechanistic Insights. *J. Org. Chem.,* **2014**, *79*, 2384-2396.

14. Hama, T. Ge, S., Hartwig, J. F. Palladium-Catalyzed α-Arylation of Zinc Enolates of Esters: Reaction Conditions and Substrate Scope. *J. Org. Chem.*, **2013**, *78*, 8250-8266.

15. Hama, T.; Hartwig, J. F. Palladium-Catalyzed α-Arylation of Esters with Chloroarenes. *Org. Lett.,* **2008**, *10*, 1549-1552.

16. Breining, S. R.; Melvin, M. Bhatti, B. S.; Byrd, G. D.; Kiser, M. N.; Hepler, C. D.; Hooker, D. N.; Zhang, J.; Reynolds, L. A.; Benson, L. R.; Fedorov, N. B.; Sidach, S. S.; Mitchener, J. P.; Lucero, L. M.; Lukas, R. J.; Whiteaker, P.; Yohannes, D. Structure-Activity Studies of 7-Heteroaryl-3azabicyclo[3.3.1]non-6-enes: A Novel Class of Highly Potent Nicotinic Receptor Ligands. *J. Med. Chem.*, **2012**, *55*, 9929-9945.

17. Changotra, A.; Sunoj, R. B. Origin of Kinetic Resolution of Hydroxy Esters through Catalytic Enantioselective Lactonization by Chiral Phosphoric Acids. *Org. Lett.,* **2016**, *18*, 3730-3733.

18. Dunitz, J. D.; Taylor, R. Organic Fluorine Hardly Ever Accepts Hydrogen Bonds. *Chem. Eur. J.,* **1997**, *3*, 89-98.

19. Biscoe, M. R.; Buchwald, S. L.; Selective Monoarylation of Acetate Esters and Aryl Methyl Ketones using Aryl Chlorides. *Org. Lett.* **2009**, *11*, 1773-1775.

20. Hama, T.;, Hartwig, J. F. α-Arylation of Esters Catalyzed by the Pd(I) Dimer {[P(*t*-Bu)$_3$]PdBr}$_2$. *Org. Lett.*, **2008**, *10*, 1545-1548.

21. Tsakos, M.; Schaffert, E. S.; Clement, L. L.; Villadsen, N. L.; Poulsen, T. B. Ester coupling reactions – an enduring challenge in the chemical synthesis of bioactive natural products. *Nat. Prod. Rep.*, **2015**, *32*, 605-632.

22. Takeda, K.; Akiyama, A.; Nakamura, H.; Takizawa, S.; Mizuno, Y.; Takayanagi, H.; Harigaya, Y. Dicarbonates: Convenient 4-Dimethylaminopyridine Catalyzed Esterification Reagents. *Synthesis*, **1994**, 1063-1066.

23. GooBen, L. J.; Dohrin, A. A. Convenient Protocol for the Esterification of Carboxylic Acids with Alcohols in the Presence of di-*tert*-Butyl Dicarbonate. *Synlett.*, **2004**, *2*, 263-266.

24. *4-Dimethylaminopyridine;* MSDS No. SLD1903 [Online]; Sciencelab.com, Inc.: Houston, Tx, May 21, 2013. http://www.sciencelab.com/msds.php?msdsId=9927157.

25. *1-Methylimidazole;* MSDS No. SLM 1756 [Online]; Sciencelab.com, Inc.: Houston, Tx, May 21, 2013. http://www.sciencelab.com/msds.php?msdsId=9926068.

26. Capello C.; Fisher, U.; Hungerbuhler, K. What is a green solvent? A comprehensive framework for the environmental assessment of solvents. *Green Chem.*, **2007**, *9*, 927-934.

27. Qureshi, Z. S.; Deshmukh, K. M.; Bhanage, B. M. Applications of ionic liquids in organic synthesis and catalysis. *Clean Techn. Environ. Policy.* **2014**. *16*, 1487-1513.

APPENDIX A

NMR SPECTRA

^{1}H, ^{13}C, and ^{19}F NMR spectra were taken on JEOL 400 and 500, and Agilent 400 MHz spectrometers with $CDCl_3$ as the solvent at 25° C. The NMR chemical shifts (δ) are reported in ppm.

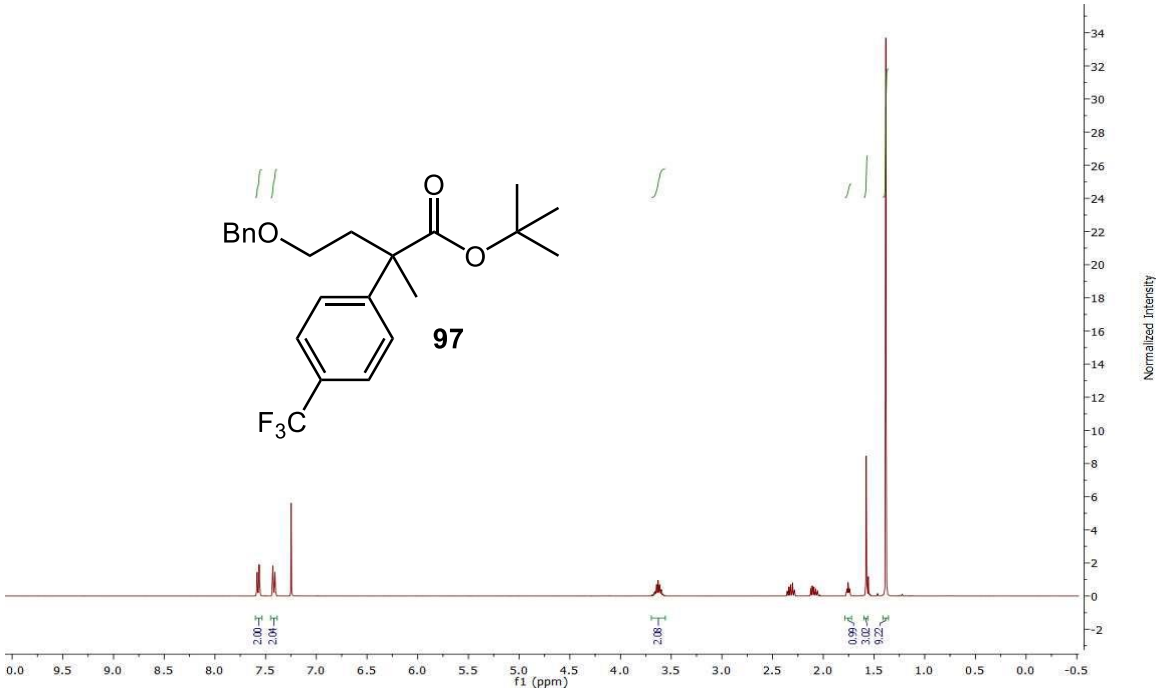
BnO
O
O
97
F3C
2.00
2.04
2.08
0.99
3.02
9.22
f1 (ppm)
Normalized Intensity

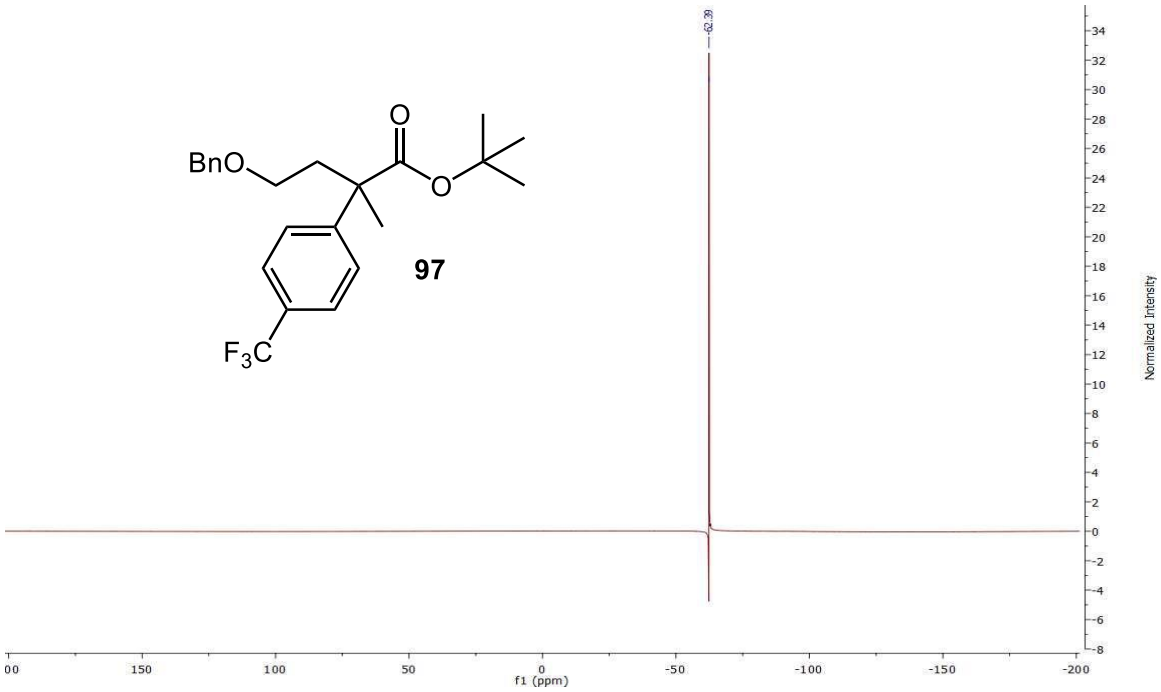
-62.39
BnO
O
O
97
F3C
f1 (ppm)
Normalized Intensity

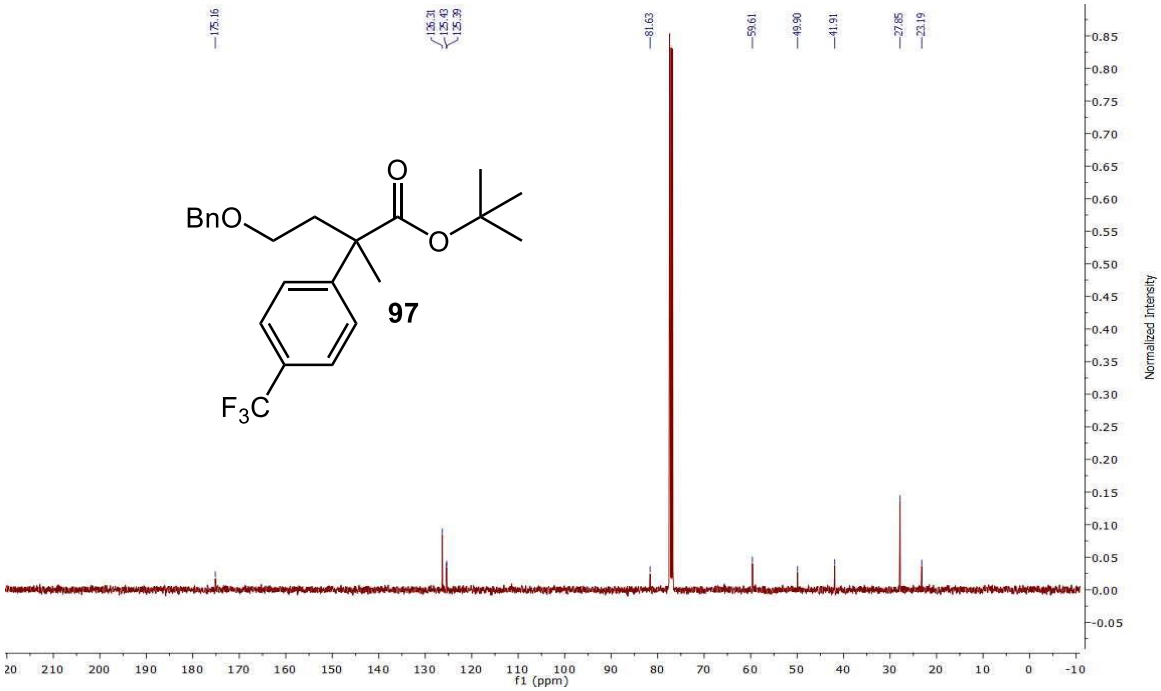
175.16
126.31
125.43
125.39
81.63
59.61
49.90
41.91
27.85
23.19
BnO
O
O
97
F3C
f1 (ppm)
Normalized Intensity

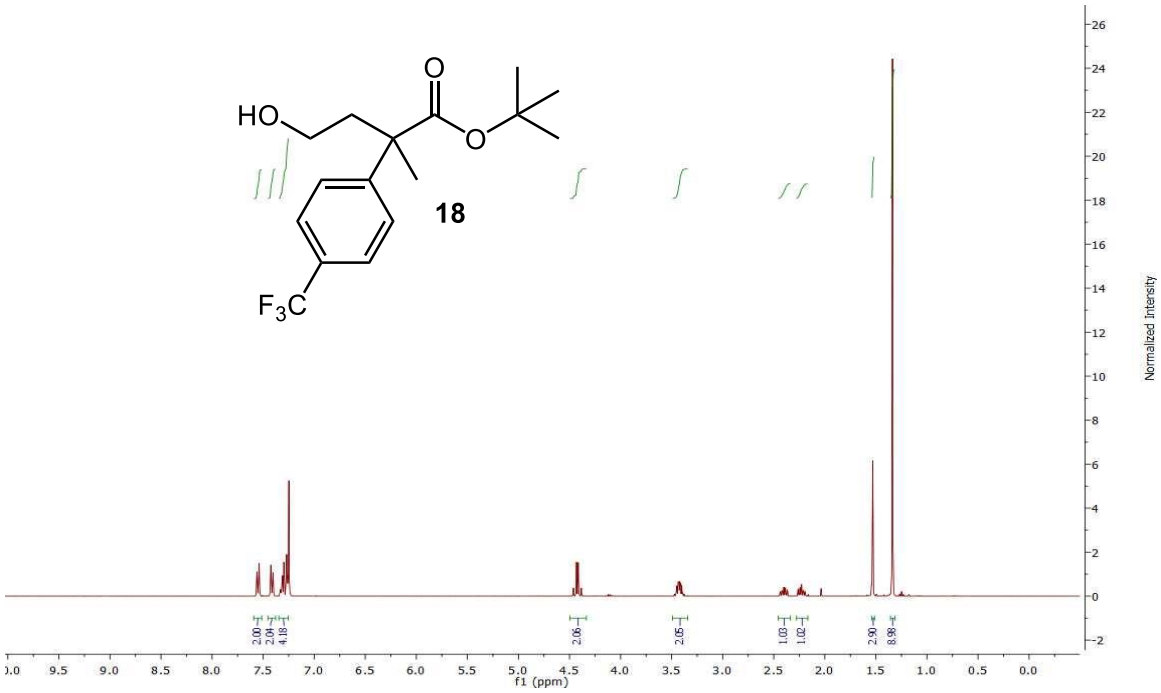
HO
O
O
18
F3C
2.00
2.04
4.18
2.06
2.05
1.03
1.02
2.90
8.99
f1 (ppm)
Normalized Intensity

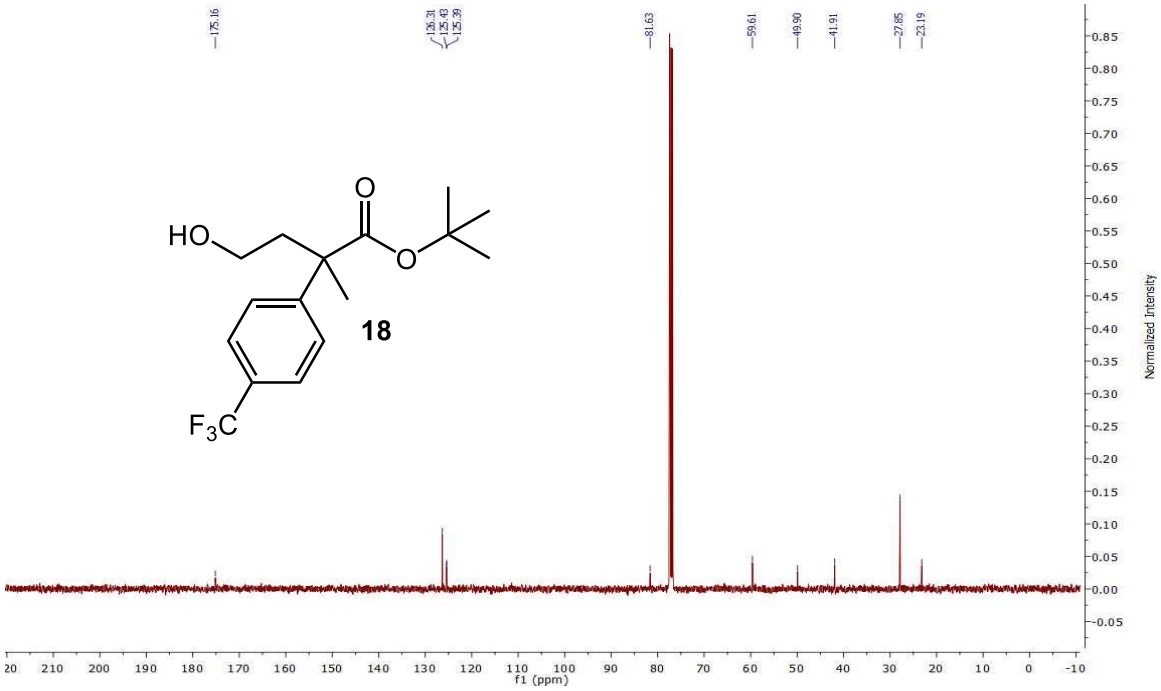
175.16
136.31
135.49
135.39
81.63
59.61
49.90
41.91
27.85
23.19
HO
O
O
18
F3C
Normalized Intensity
f1 (ppm)

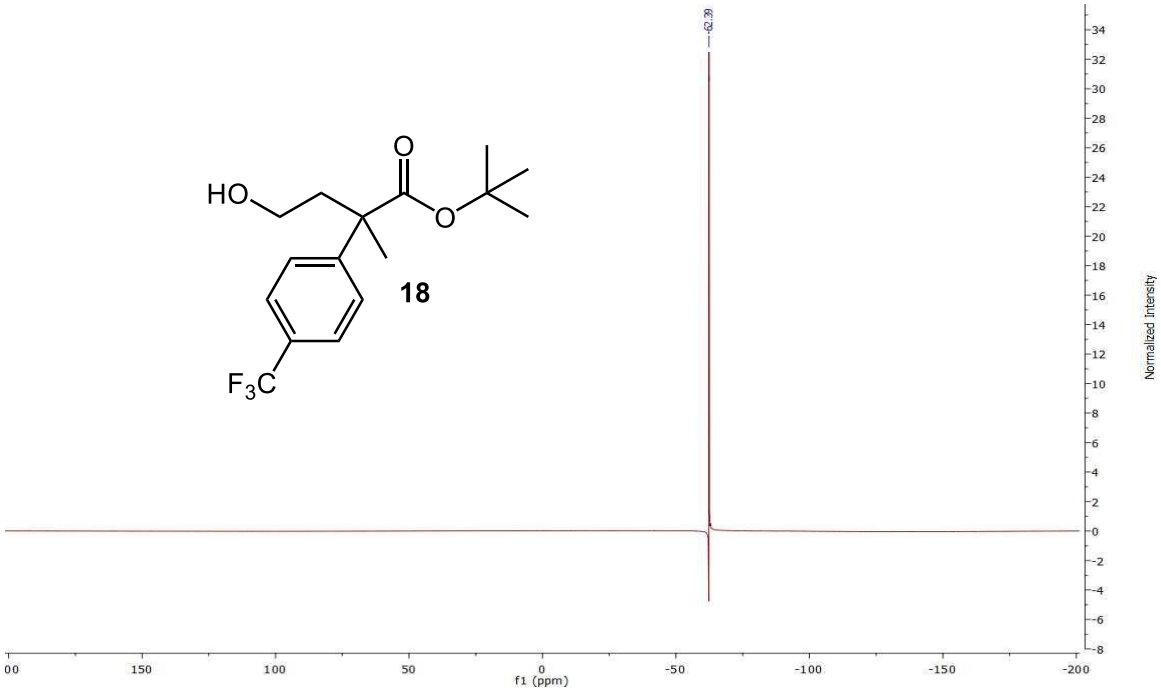
62.39
HO
O
O
18
F3C
Normalized Intensity
f1 (ppm)

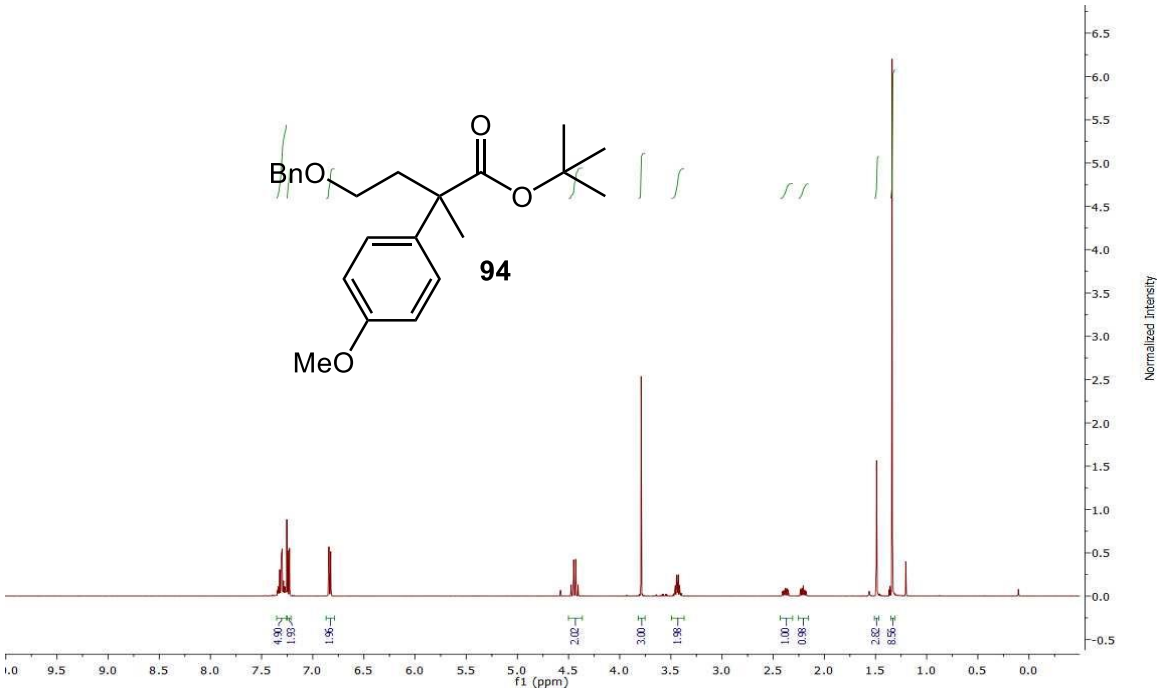
BnO
O
O
MeO
94
Normalized Intensity
f1 (ppm)

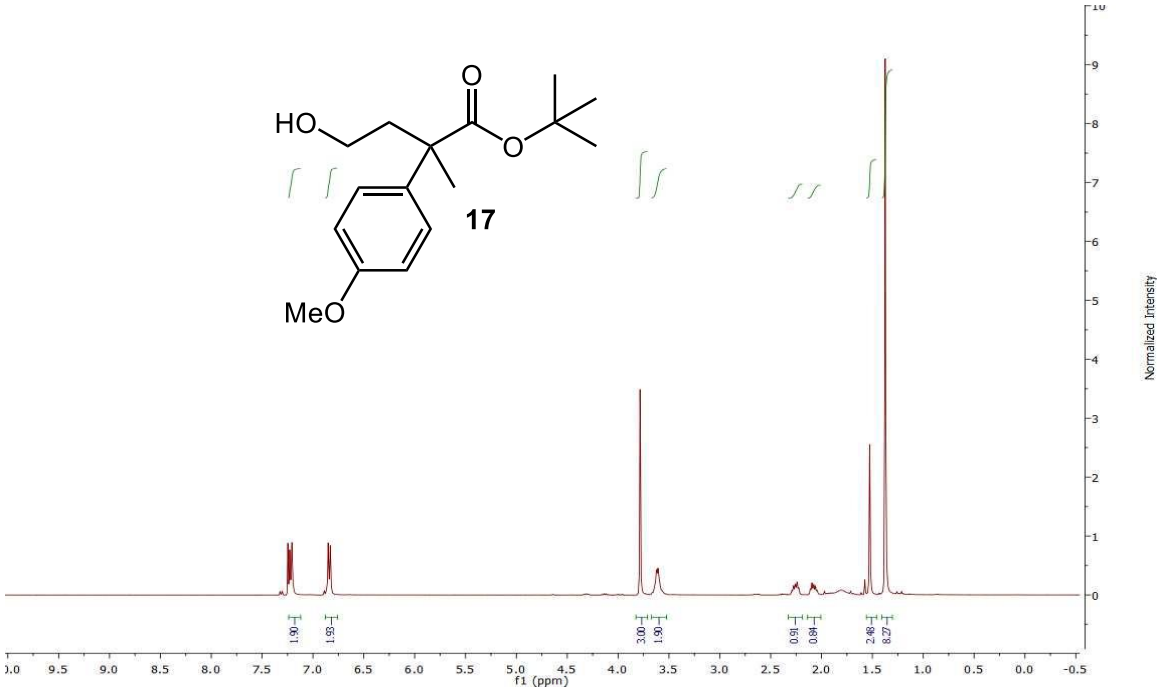
HO
O
O
MeO
17
Normalized Intensity
f1 (ppm)

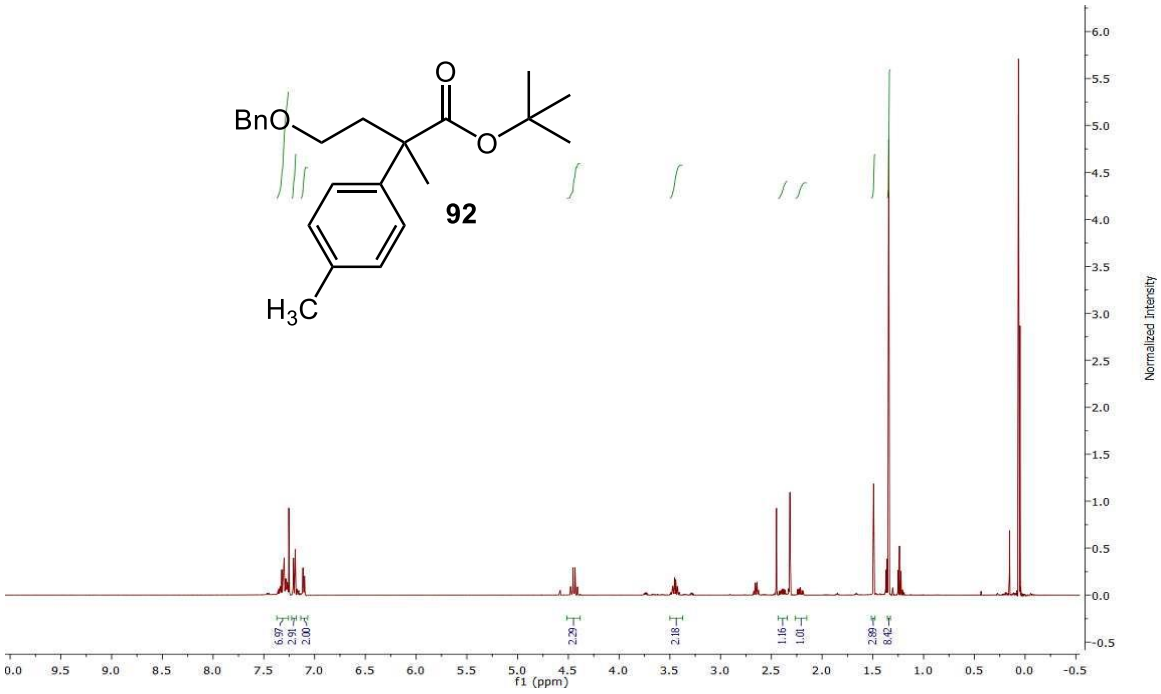
BnO
O
O
92
H_3C
Normalized Intensity
f1 (ppm)

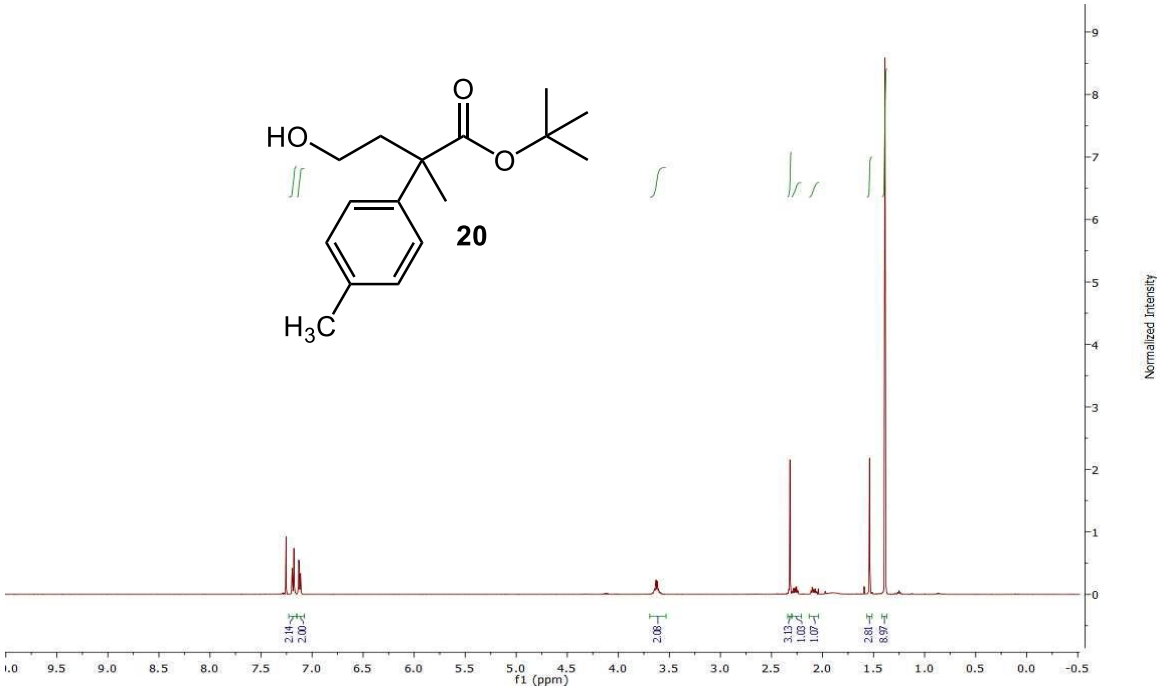
HO
O
O
20
H_3C
Normalized Intensity
f1 (ppm)

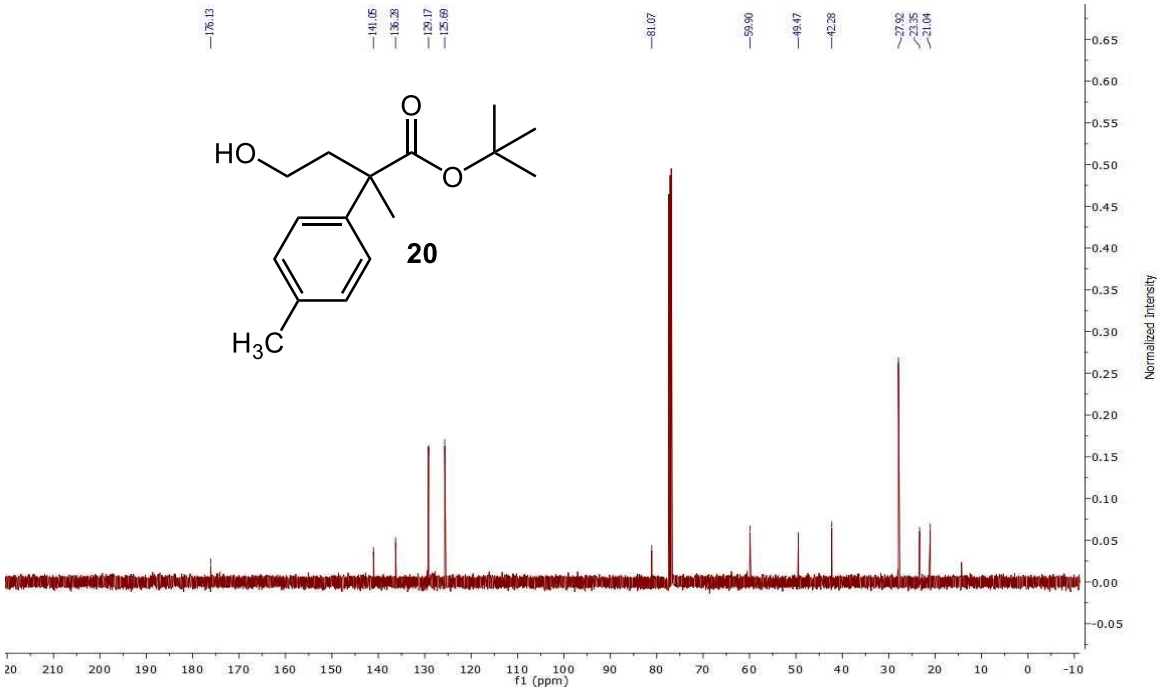
176.13
141.05
136.28
129.17
125.69
81.07
59.90
49.47
42.28
27.92
23.35
21.04
HO
O
O
20
H3C
Normalized Intensity
f1 (ppm)

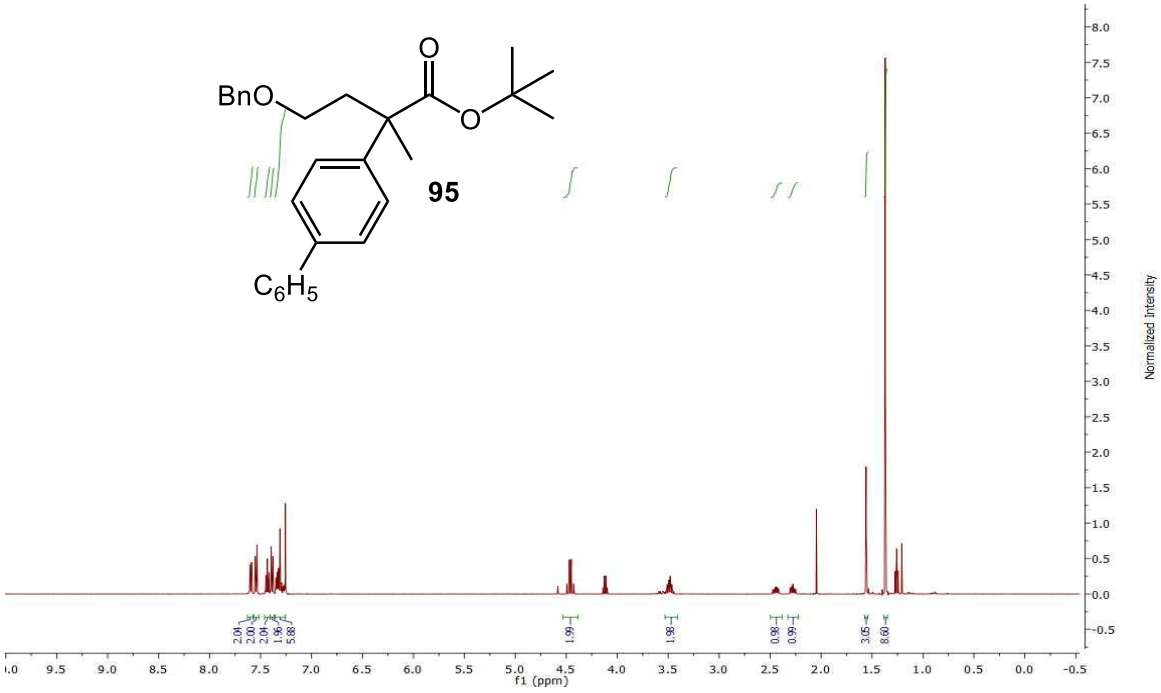
BnO
O
O
95
C6H5
2.04
2.00
2.04
1.96
5.88
1.99
1.98
0.98
0.99
3.05
8.60
Normalized Intensity
f1 (ppm)

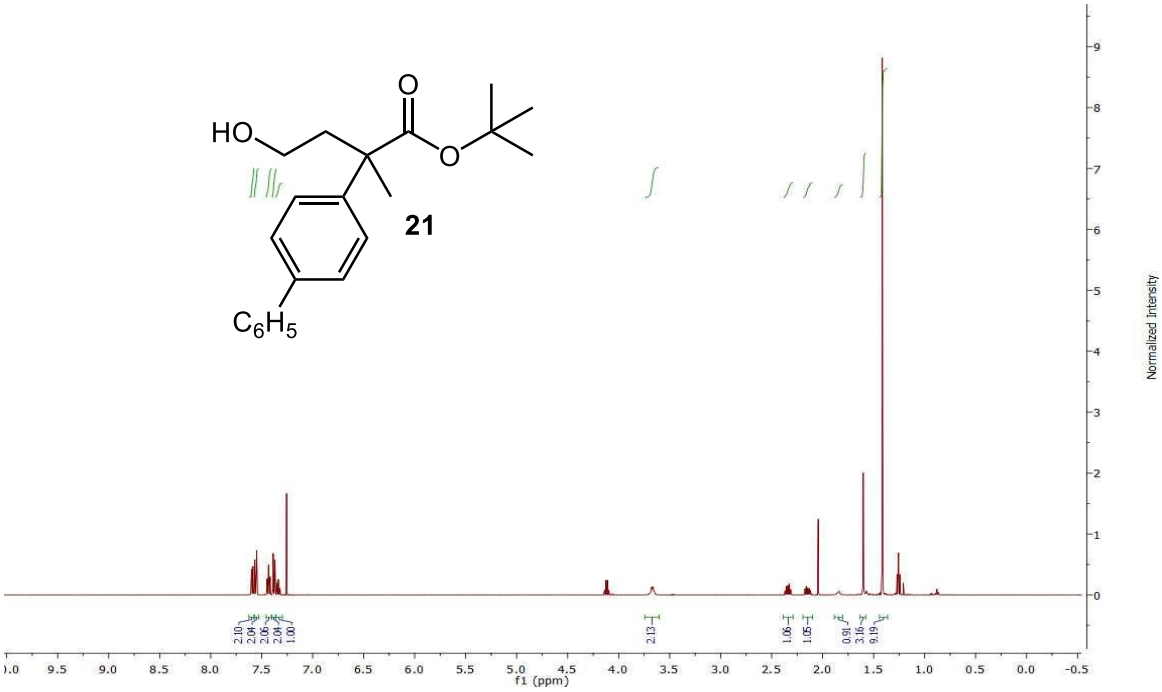
HO
O
O
21
C6H5
f1 (ppm)
Normalized Intensity

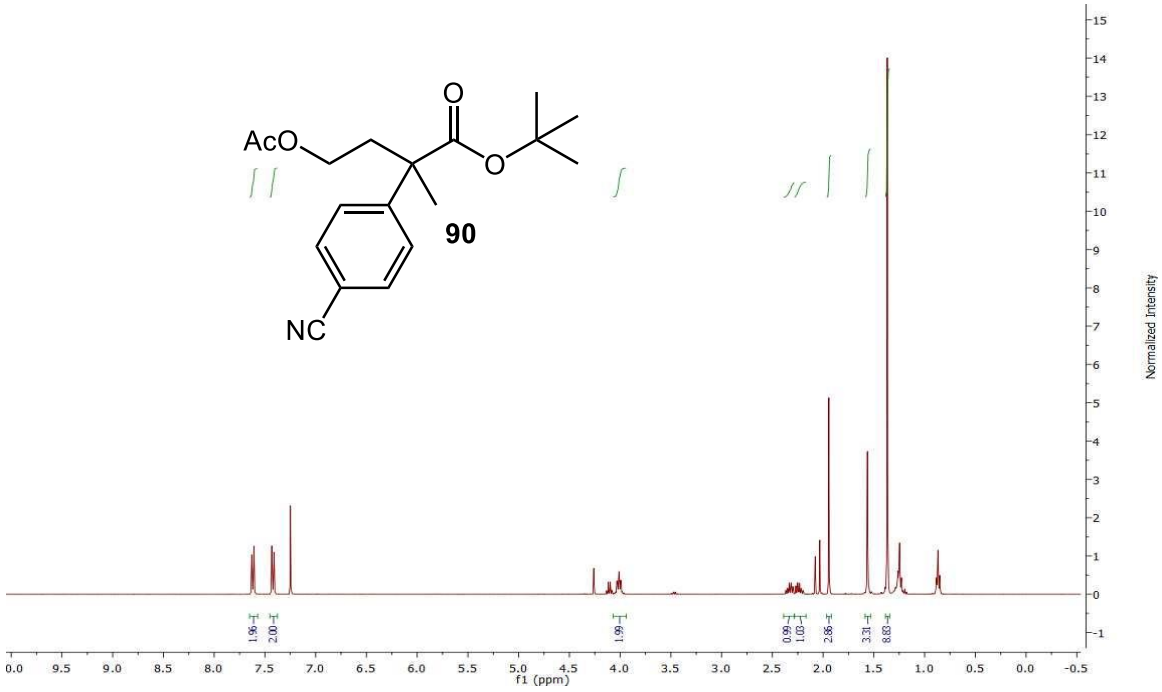
AcO
O
O
90
NC
f1 (ppm)
Normalized Intensity

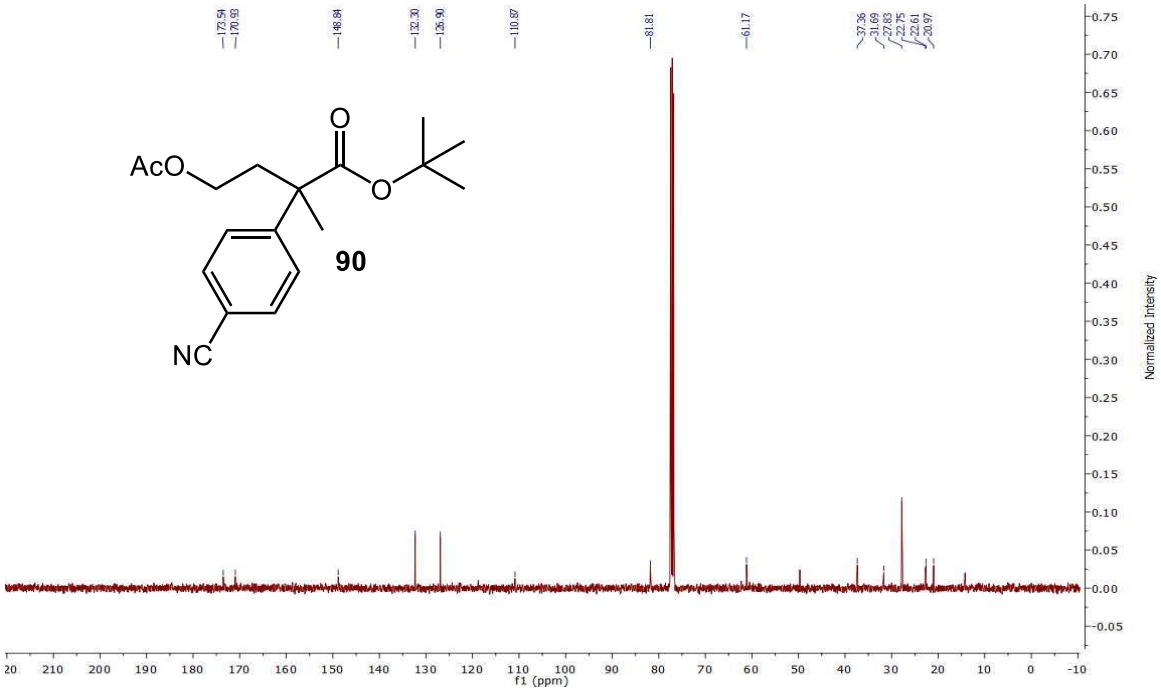
AcO
O
O
NC
90
f1 (ppm)
Normalized Intensity

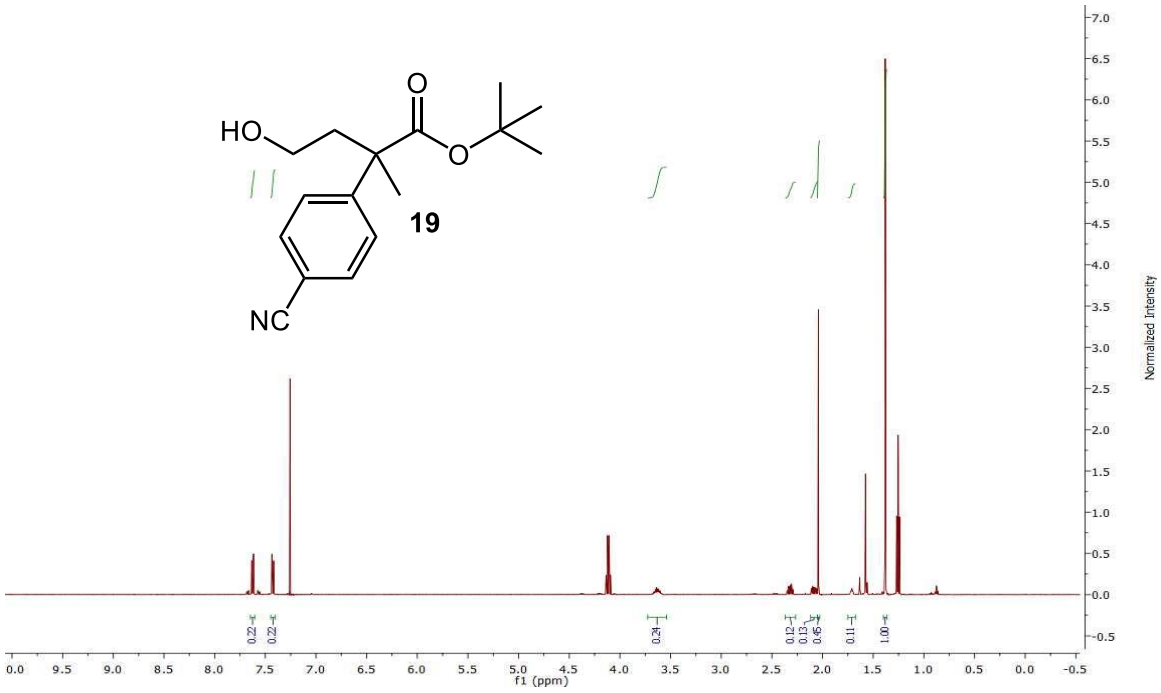
HO
O
O
NC
19
f1 (ppm)
Normalized Intensity

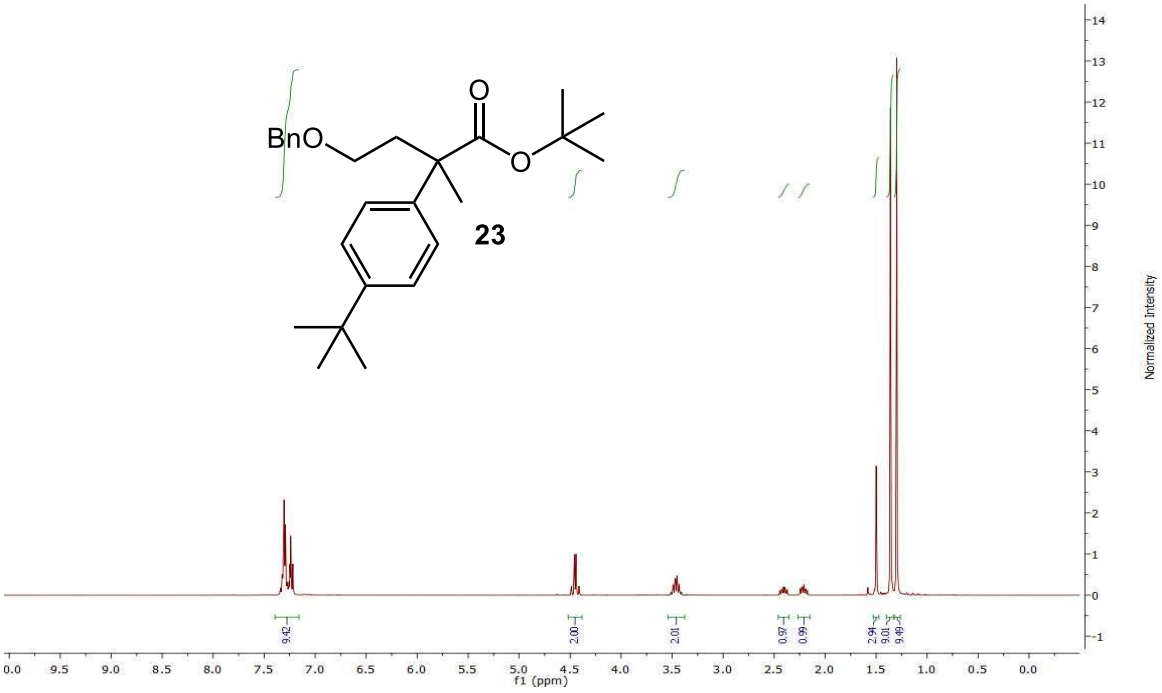
BnO
O
O
23
f1 (ppm)
Normalized Intensity

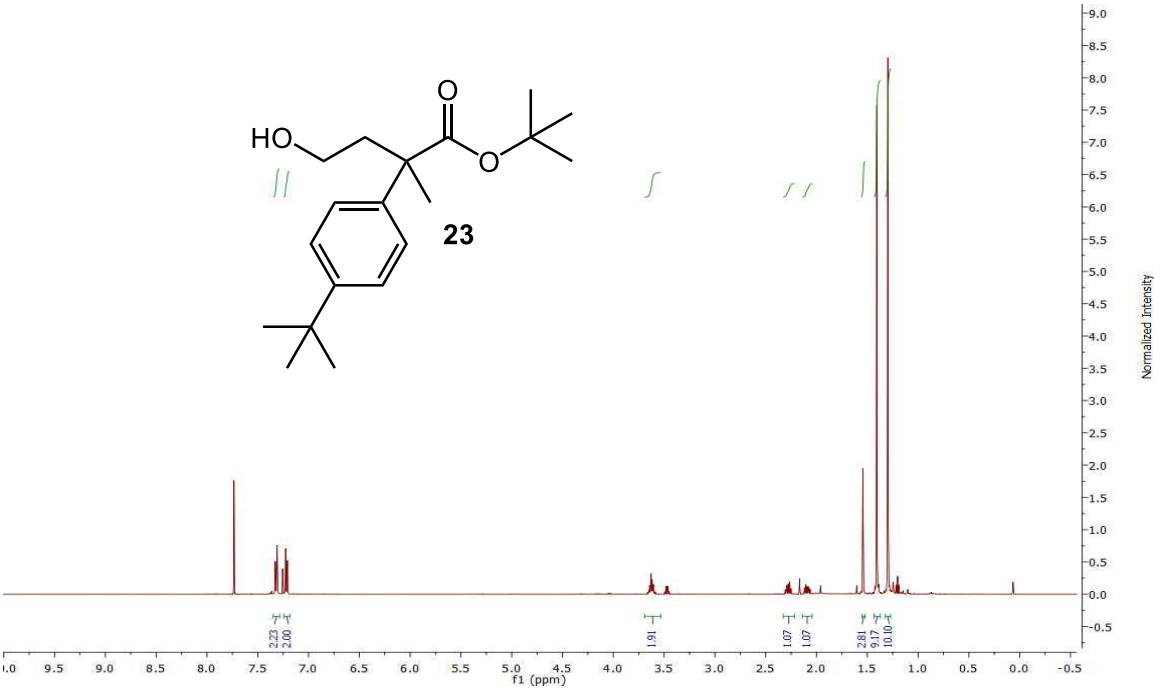
HO
O
O
23
f1 (ppm)
Normalized Intensity

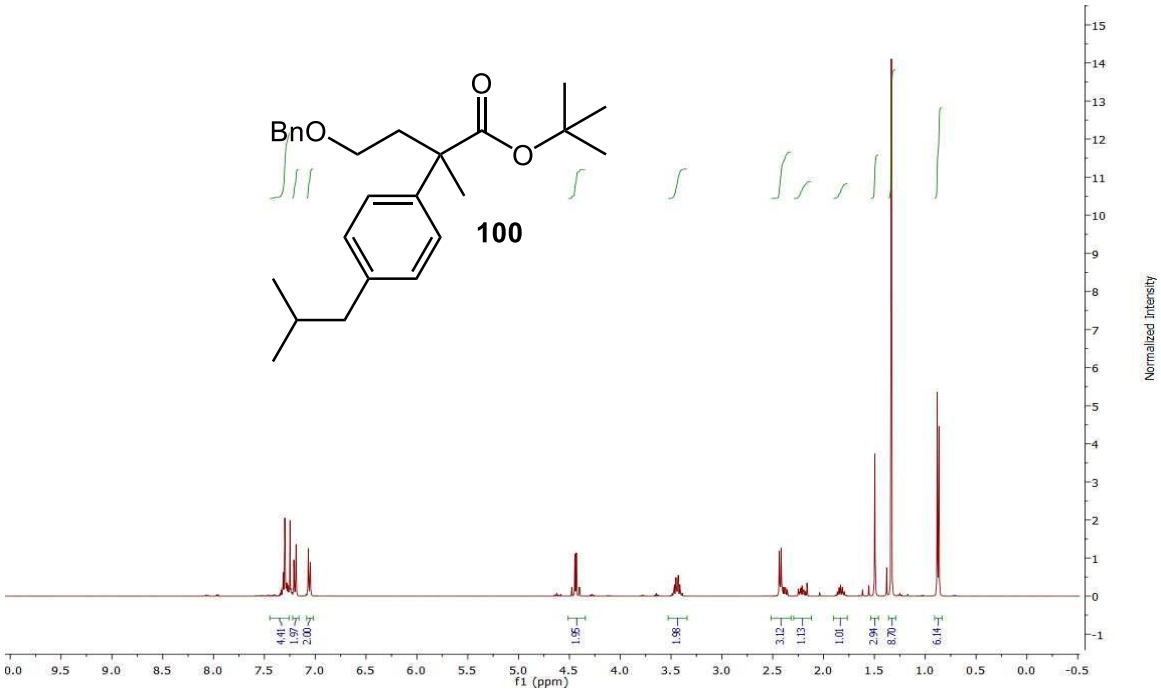
BnO
O
O
100
Normalized Intensity
f1 (ppm)

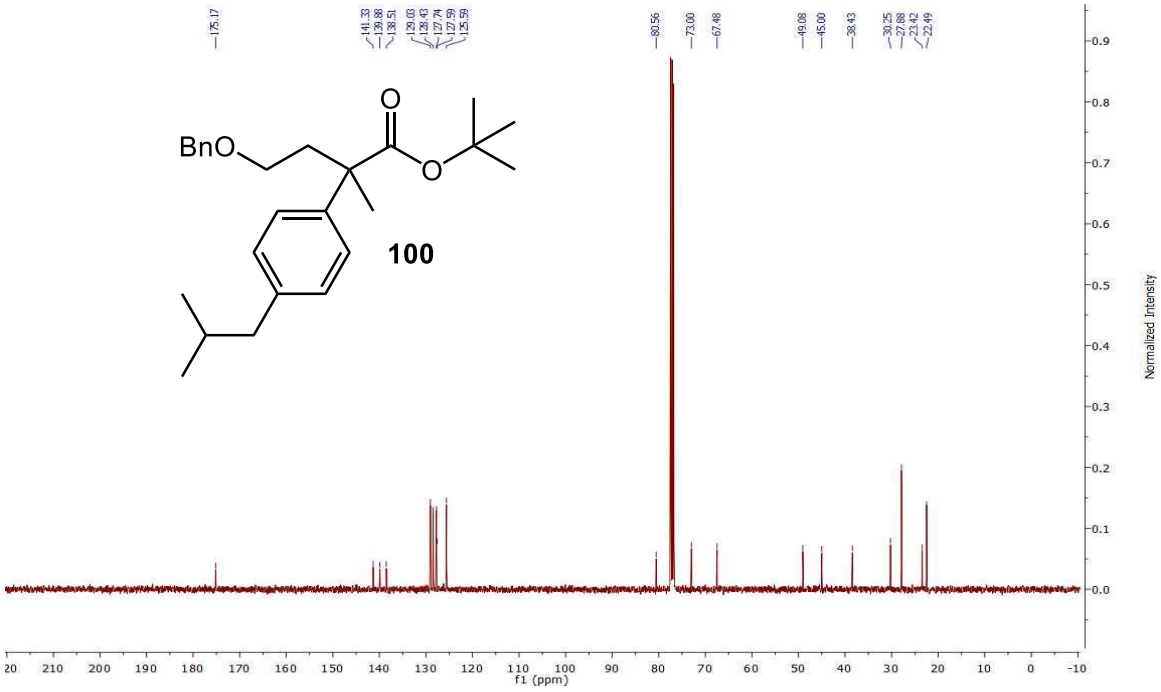
BnO
O
O
100
Normalized Intensity
f1 (ppm)

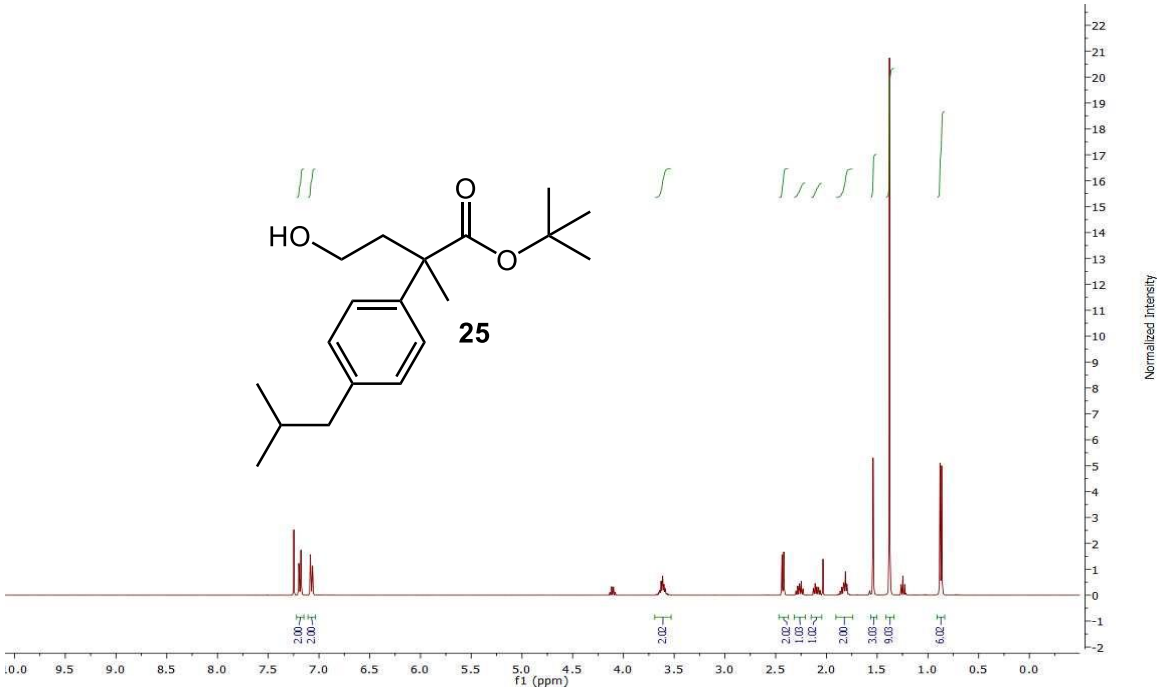
HO
O
O
25
f1 (ppm)
Normalized Intensity

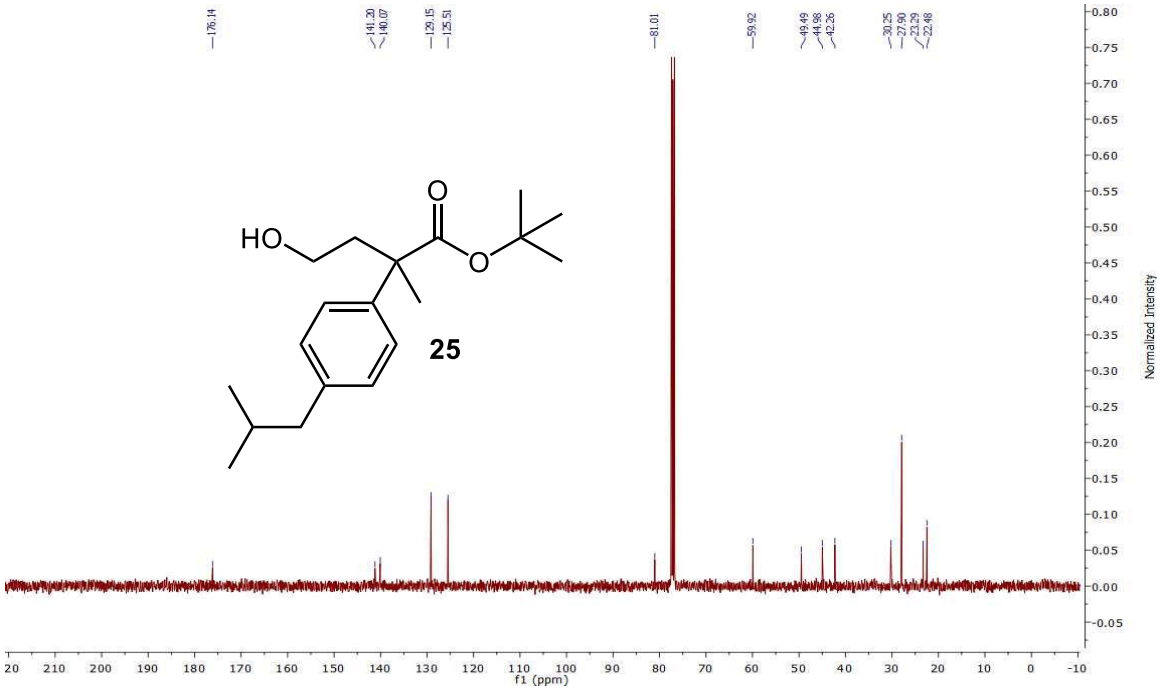
176.14
141.20
140.07
129.15
125.51
81.01
59.92
49.49
44.98
42.26
30.25
27.90
23.29
22.48
HO
O
O
25
f1 (ppm)
Normalized Intensity

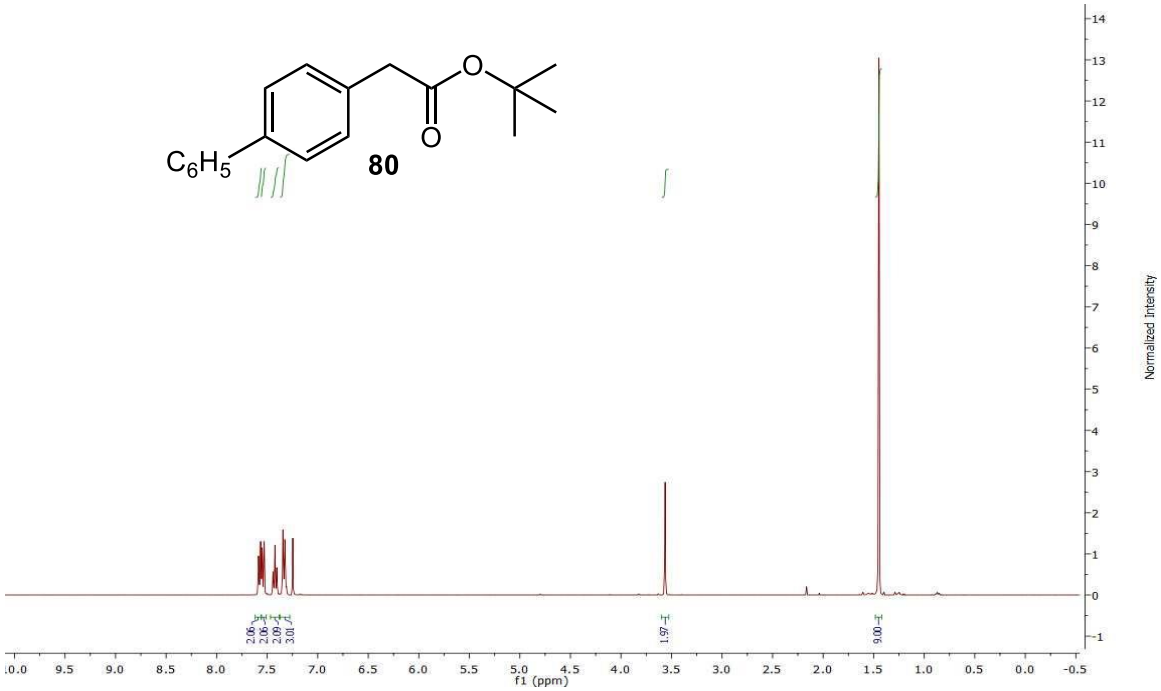
C6H5
80
f1 (ppm)
Normalized Intensity

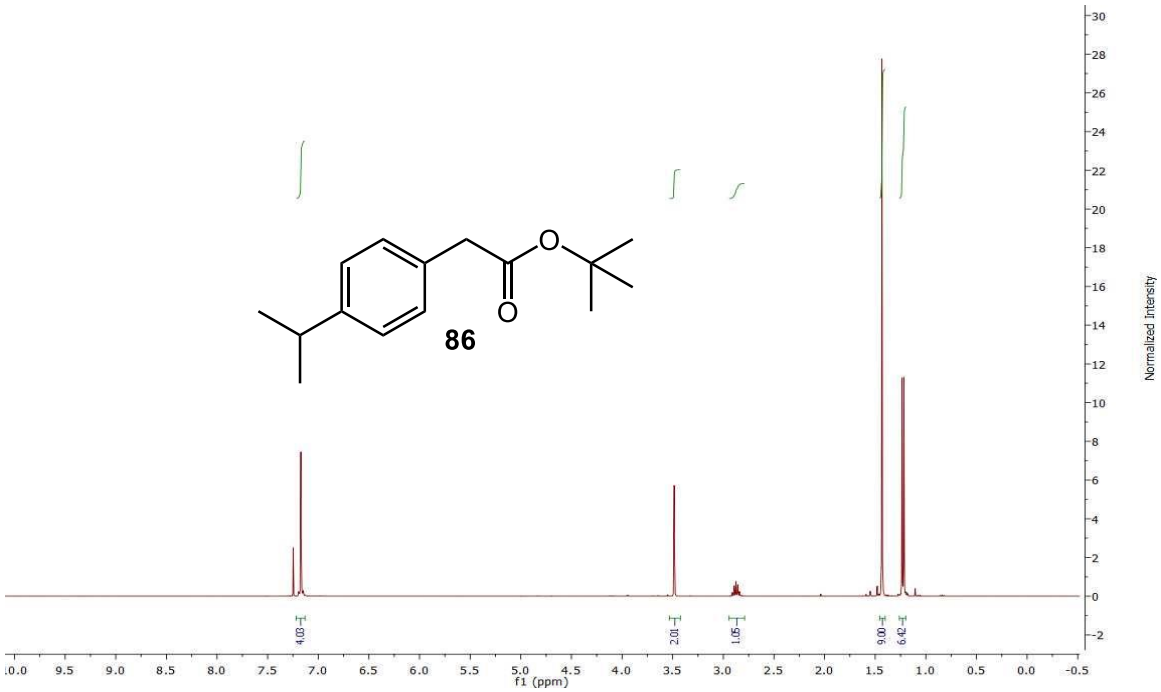
86
f1 (ppm)
Normalized Intensity

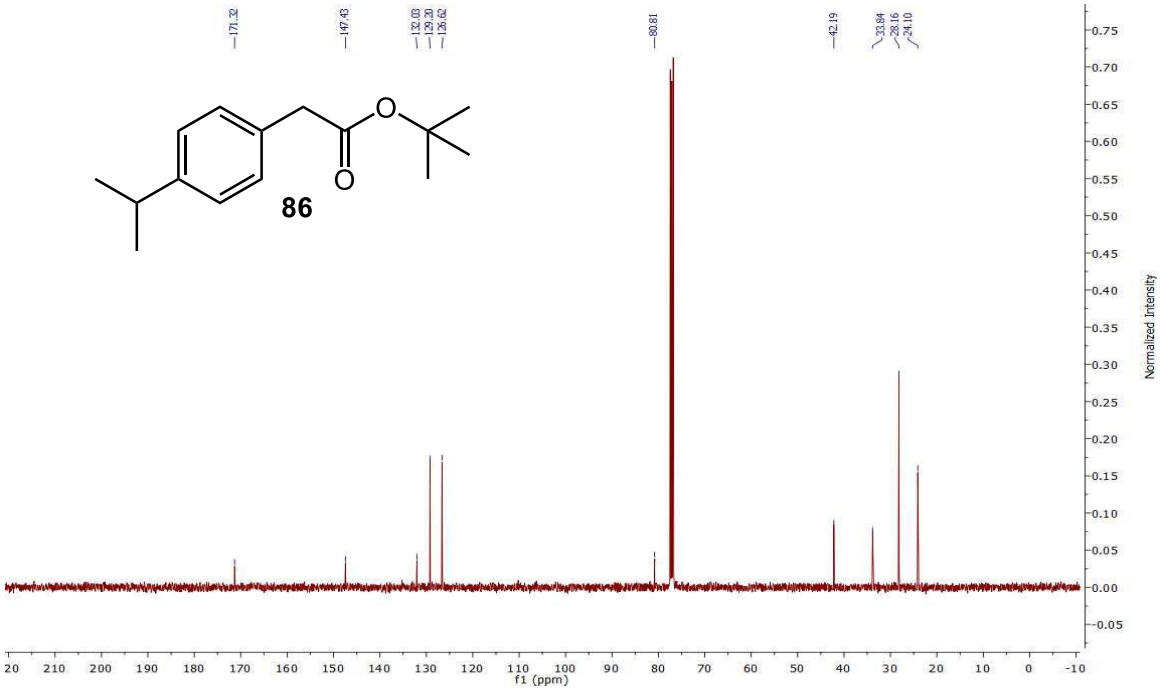
171.32
147.43
132.03
129.20
126.62
80.81
42.19
33.64
28.16
24.10
86
Normalized Intensity
f1 (ppm)

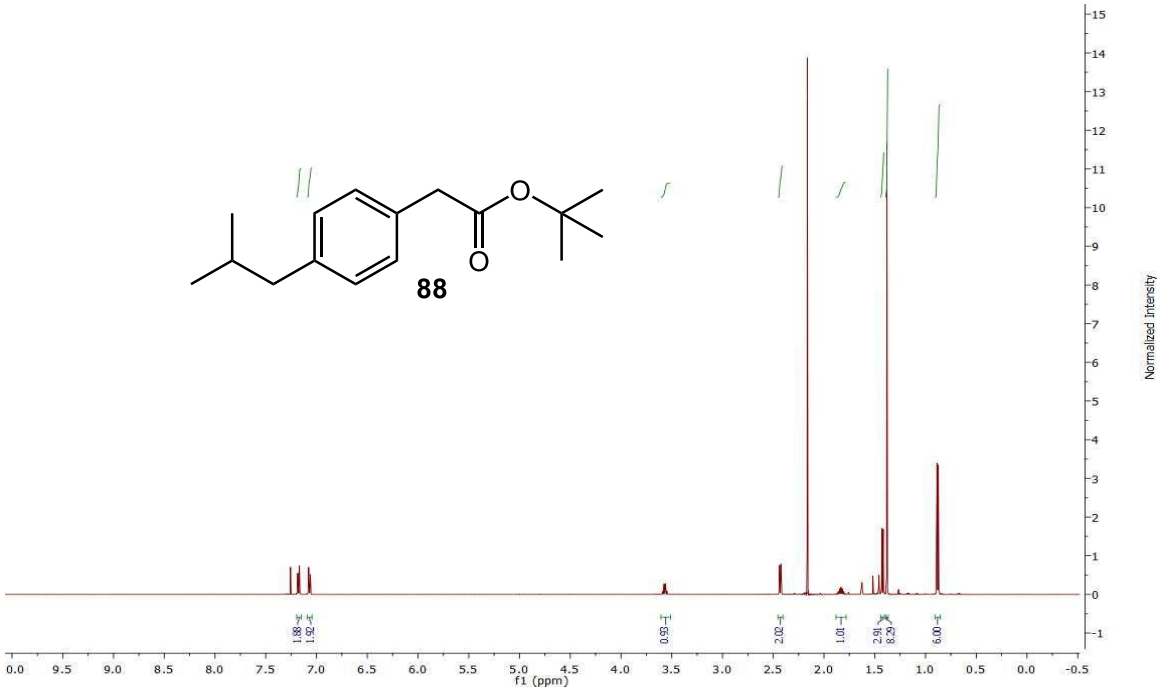
88
1.88
1.92
0.93
2.02
1.01
2.91
8.29
6.00
Normalized Intensity
f1 (ppm)

Kinetic NMR experiments were run for all substrates to determine the overall reaction rate as well as to track conversion for each substrate. The following plots were made by calculating conversion by using a stock solution of the internal standard, 2,3,5,6-tetrachloro 4-nitrobenzene at 0.1002 M. A kinetic experiment was ran for each substrate, taking 16 scans every 10 minutes for 12 hours. The integration of a peak for product, starting material, and internal standard was tracked for the entirety of the reaction. This allowed for the calculation of the concentration of both starting material and product in the reaction.

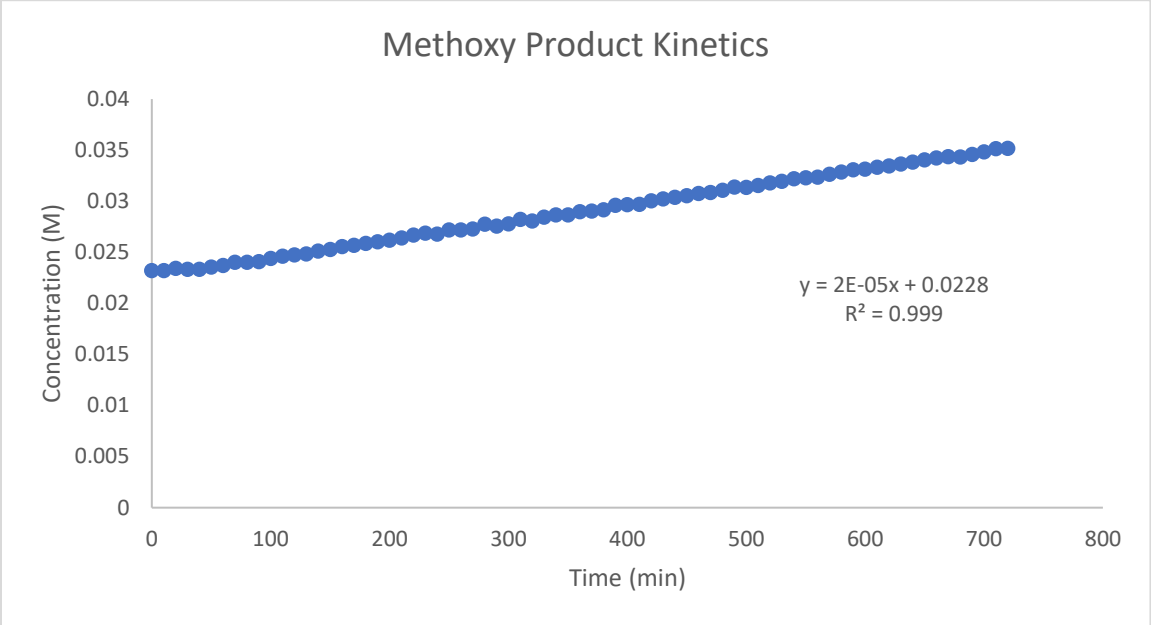
Methoxy Product Kinetics
Concentration (M)
0.04
0.035
0.03
0.025
0.02
0.015
0.01
0.005
0
0
100
200
300
400
500
600
700
800
Time (min)
y = 2E-05x + 0.0228
R² = 0.999

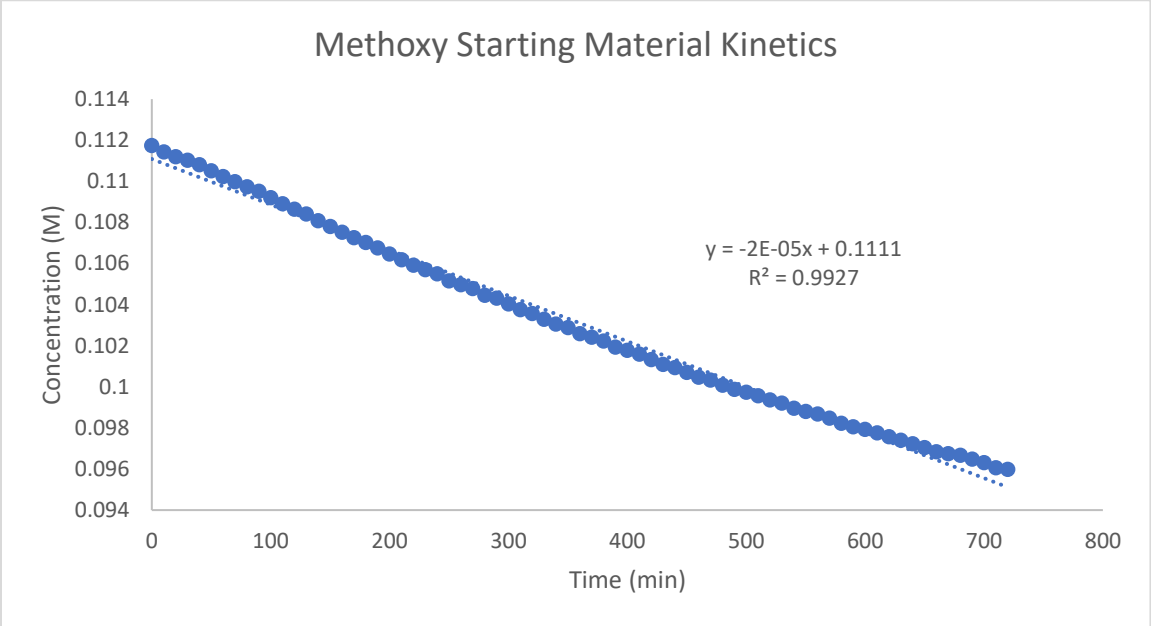
Methoxy Starting Material Kinetics
Concentration (M)
0.114
0.112
0.11
0.108
0.106
0.104
0.102
0.1
0.098
0.096
0.094
0
100
200
300
400
500
600
700
800
Time (min)
y = -2E-05x + 0.1111
R² = 0.9927

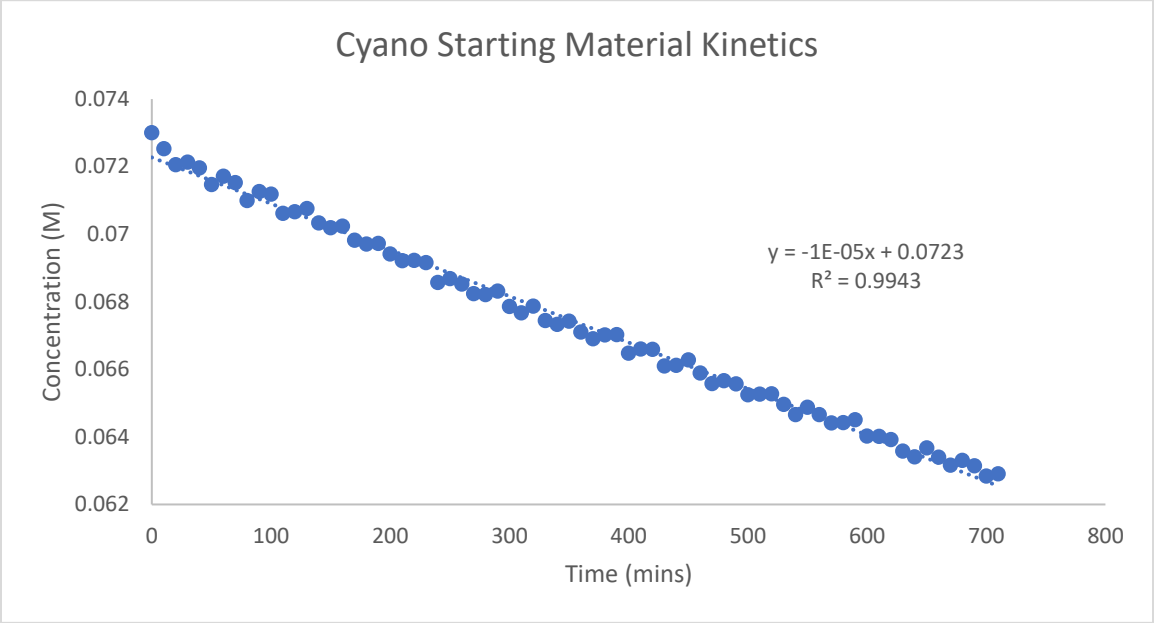
Cyano Starting Material Kinetics
Concentration (M)
0.074
0.072
0.07
0.068
0.066
0.064
0.062
0
100
200
300
400
500
600
700
800
Time (mins)
y = -1E-05x + 0.0723
R² = 0.9943

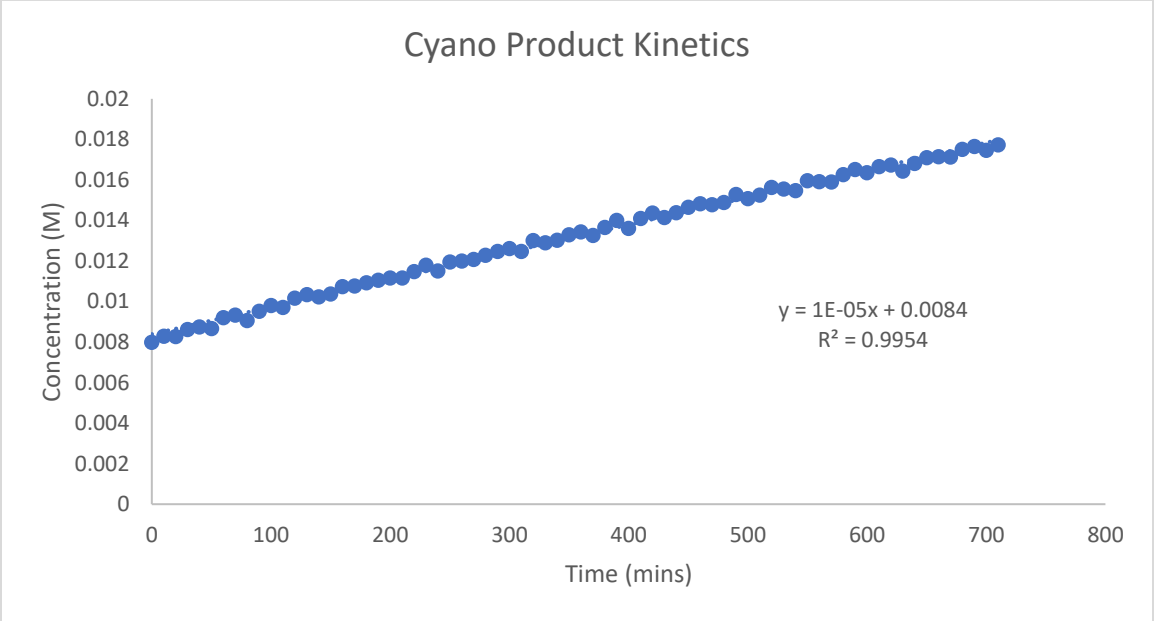
Cyano Product Kinetics
Concentration (M)
0.02
0.018
0.016
0.014
0.012
0.01
0.008
0.006
0.004
0.002
0
0
100
200
300
400
500
600
700
800
Time (mins)
y = 1E-05x + 0.0084
R² = 0.9954

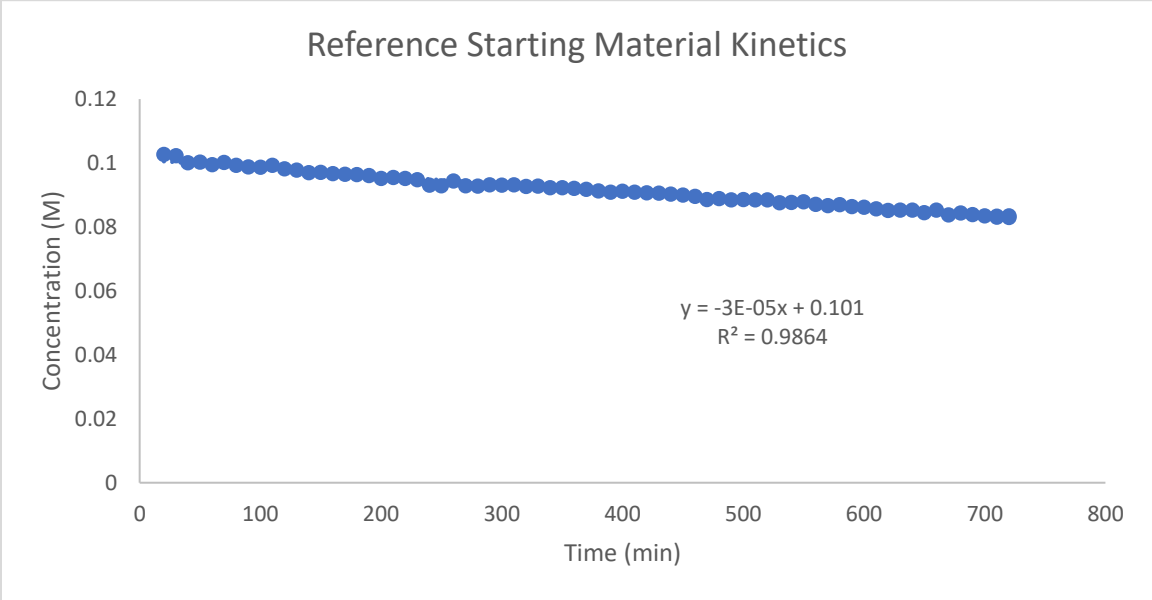
Reference Starting Material Kinetics
Concentration (M)
0.12
0.1
0.08
0.06
0.04
0.02
0
0
100
200
300
400
500
600
700
800
Time (min)
y = -3E-05x + 0.101
R² = 0.9864

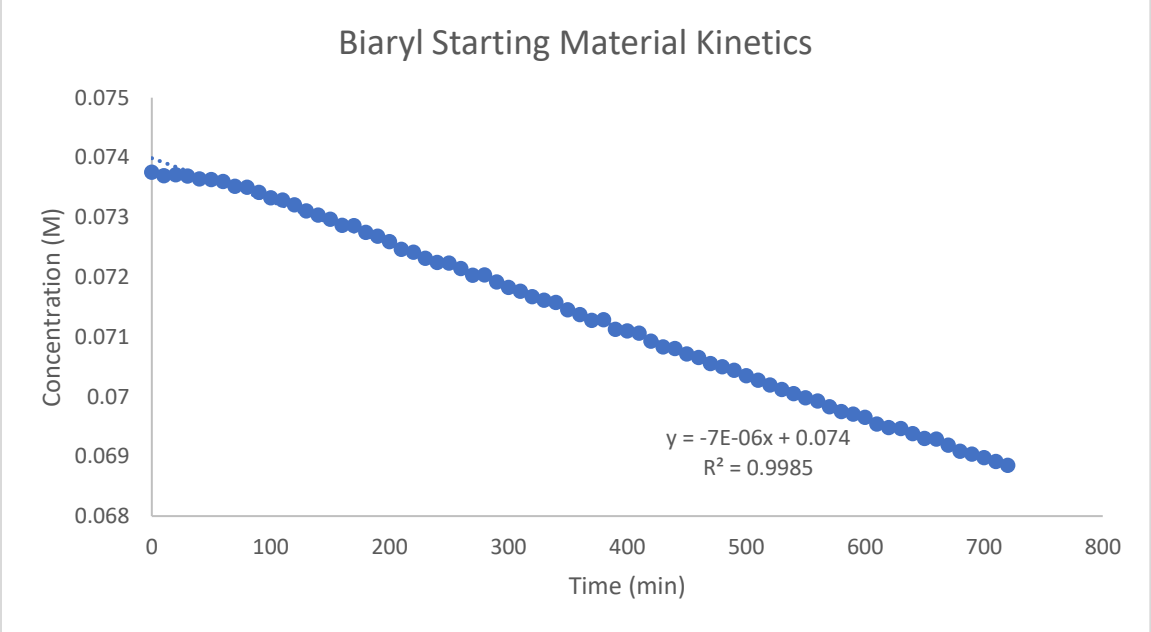
Biaryl Starting Material Kinetics
Concentration (M)
0.075
0.074
0.073
0.072
0.071
0.07
0.069
0.068
0
100
200
300
400
500
600
700
800
Time (min)
y = -7E-06x + 0.074
R² = 0.9985

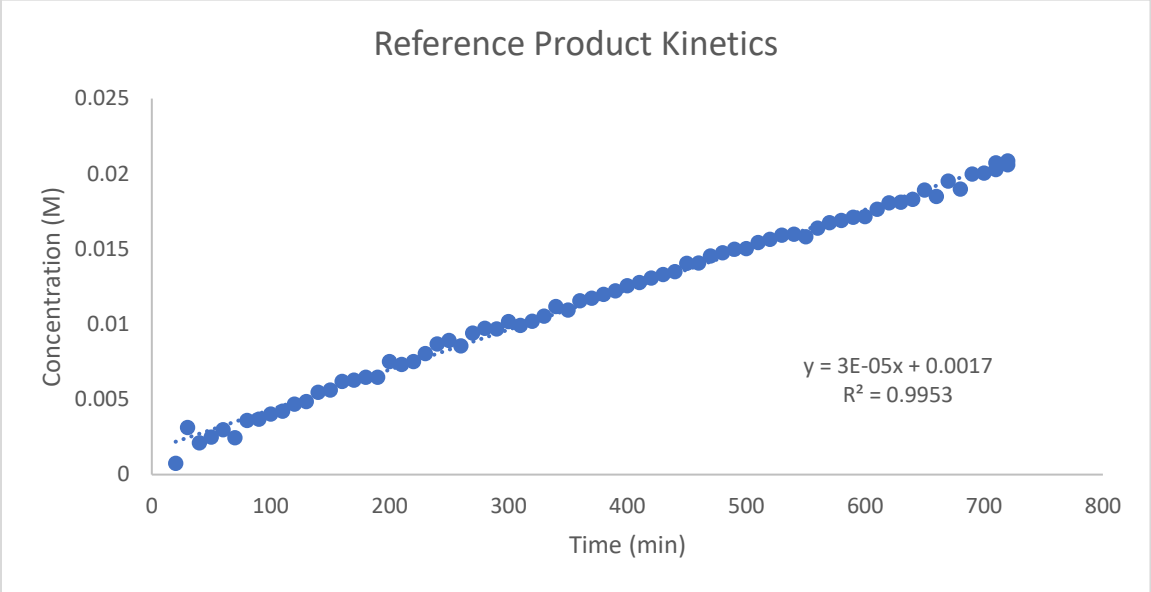
Reference Product Kinetics
Concentration (M)
0.025
0.02
0.015
0.01
0.005
0
0
100
200
300
400
500
600
700
800
Time (min)
y = 3E-05x + 0.0017
R² = 0.9953

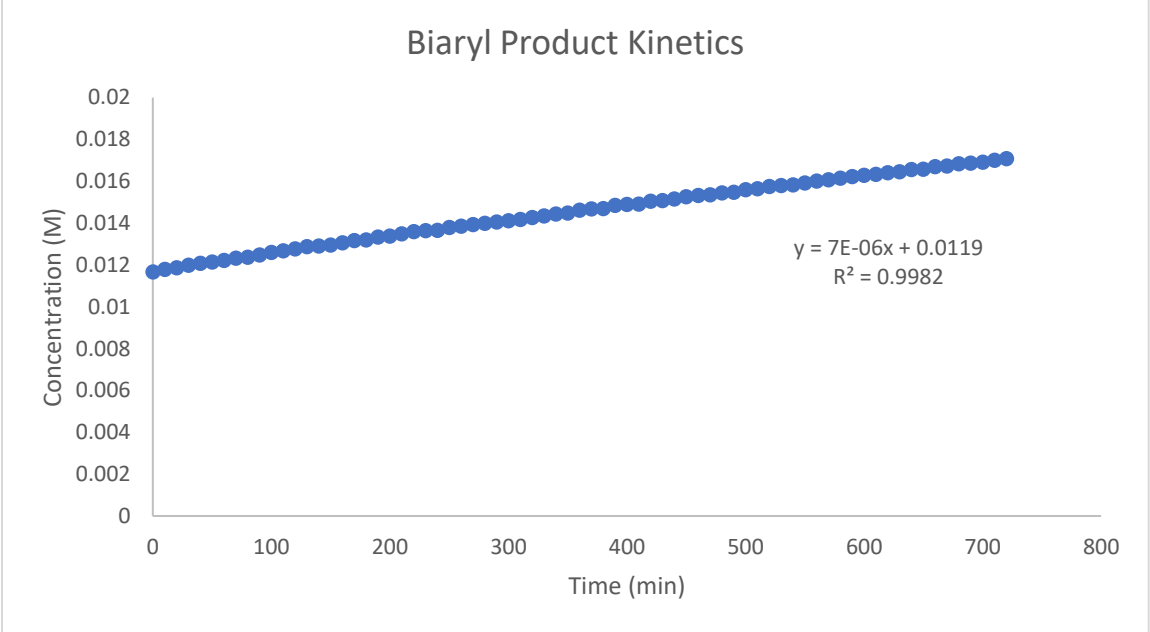
Biaryl Product Kinetics
Concentration (M)
0.02
0.018
0.016
0.014
0.012
0.01
0.008
0.006
0.004
0.002
0
0
100
200
300
400
500
600
700
800
Time (min)
y = 7E-06x + 0.0119
R² = 0.9982

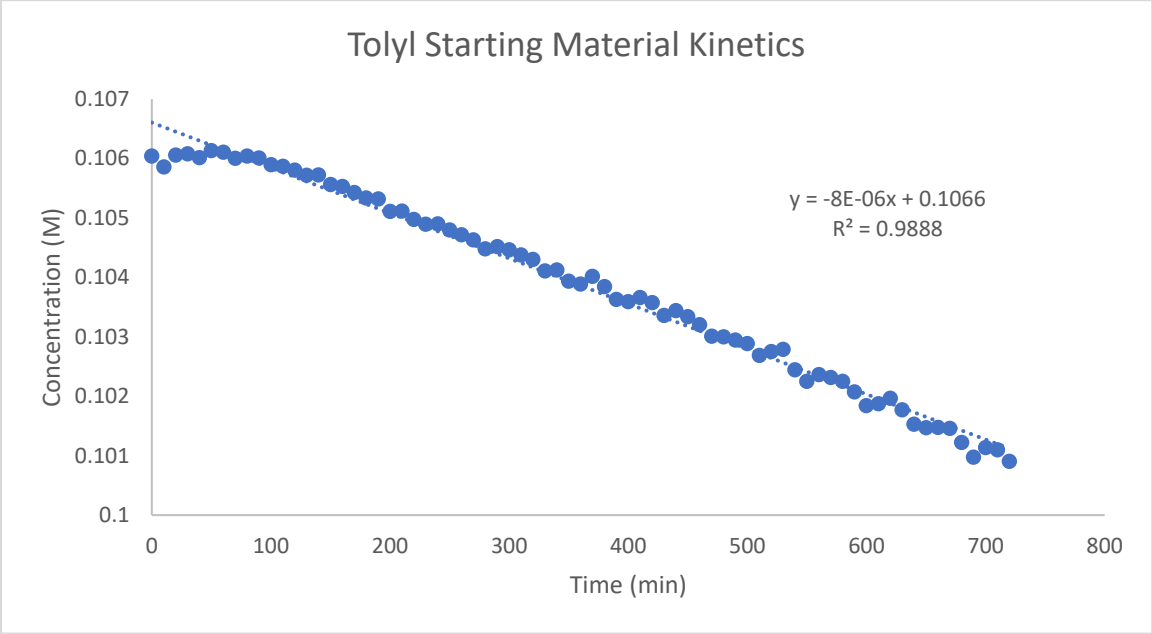
Tolyl Starting Material Kinetics
0.107
0.106
0.105
0.104
0.103
0.102
0.101
0.1
Concentration (M)
y = -8E-06x + 0.1066
R² = 0.9888
0
100
200
300
400
500
600
700
800
Time (min)

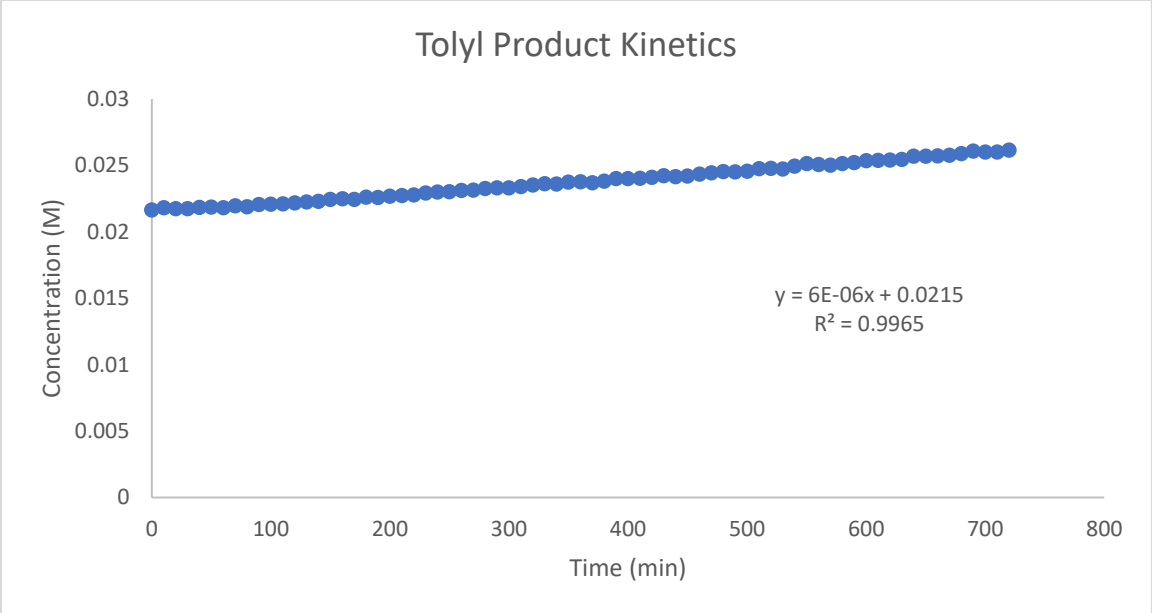
Tolyl Product Kinetics
0.03
0.025
0.02
0.015
0.01
0.005
0
Concentration (M)
y = 6E-06x + 0.0215
R² = 0.9965
0
100
200
300
400
500
600
700
800
Time (min)

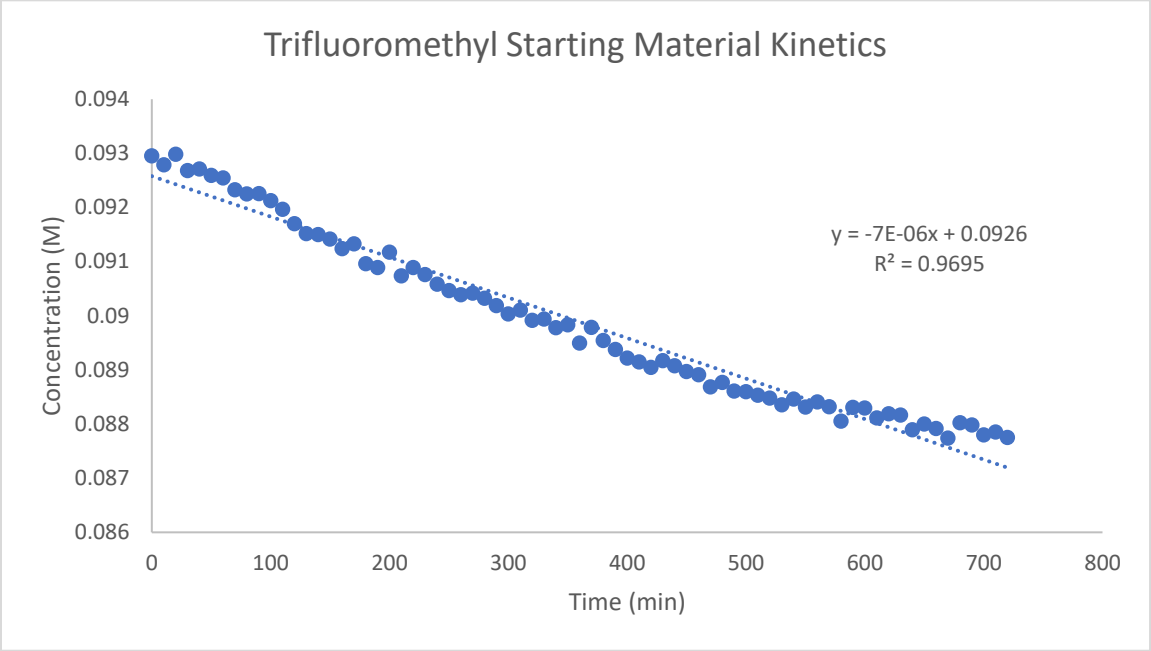
Trifluoromethyl Starting Material Kinetics
Concentration (M)
0.094
0.093
0.092
0.091
0.09
0.089
0.088
0.087
0.086
0
100
200
300
400
500
600
700
800
Time (min)
y = -7E-06x + 0.0926
R² = 0.9695

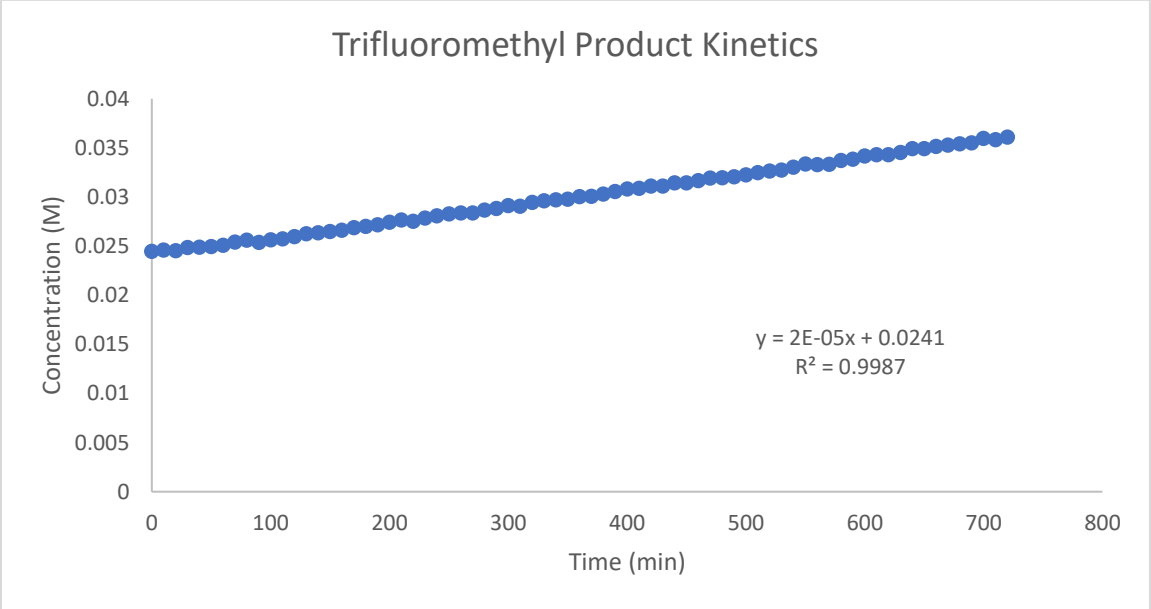
Trifluoromethyl Product Kinetics
Concentration (M)
0.04
0.035
0.03
0.025
0.02
0.015
0.01
0.005
0
0
100
200
300
400
500
600
700
800
Time (min)
y = 2E-05x + 0.0241
R² = 0.9987

APPENDIX B

CHROMATOGRAMS

HPLC chromatograms were obtained using an Agilent 1260 Infinity. The chiral columns used were CHIRALCEL OJ-H (4.6 mm x 250 mm x 5 μm) and CHIRALCEL OD-H (4.6 mm x 250 mm x 5 μm). Analysis details are given with each respective chromatogram.

Table 5. Biaryl Compound **21**

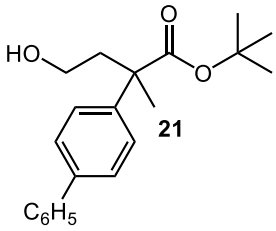

HPLC Conditions: Column: HPLC OD-H 4.6 mm x 250 mm x 5 μm; Eluent Rate: 1 mL/min; Eluent: 6% IPA/hexane; Monitoring wave: 254 nm

Enantiomeric

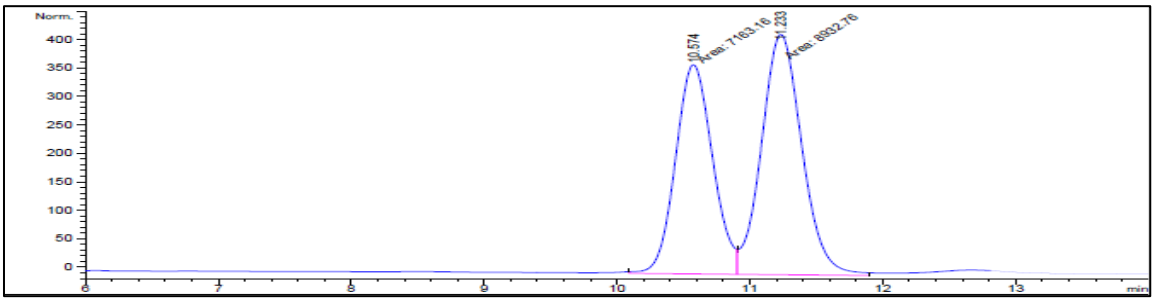

Peak #	RetTime [min]	Sig	Type	Area [mAU*s]	Height [mAU]	Area %
1	10.574	1	MF	7163.16406	367.70163	44.5030
2	11.233	1	FM	8932.76367	422.28632	55.4970
Totals :				1.60959e4	789.98795	

Racemic

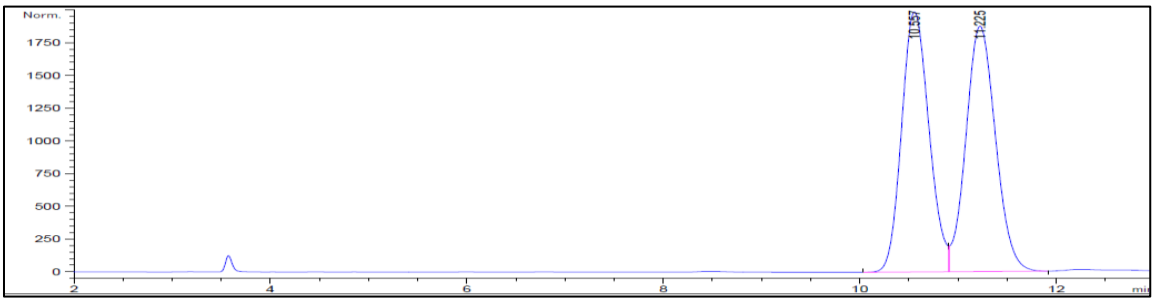

Peak #	RetTime [min]	Sig	Type	Area [mAU*s]	Height [mAU]	Area %
1	10.557	1	BV	3.85174e4	1986.59961	49.4580
2	11.225	1	VB	3.93617e4	1875.22180	50.5420
Totals :				7.78791e4	3861.82141	

Table 6. Cyano Compound **19**

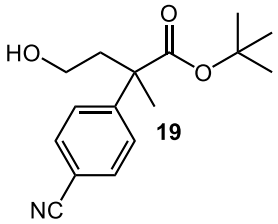

HPLC Conditions: Column: HPLC OD-H 4.6 mm x 250 mm x 5 μm; Eluent Rate: 1 mL/min; Eluent: 6% IPA/hexane; Monitoring wave: 210 nm

Enantiomeric

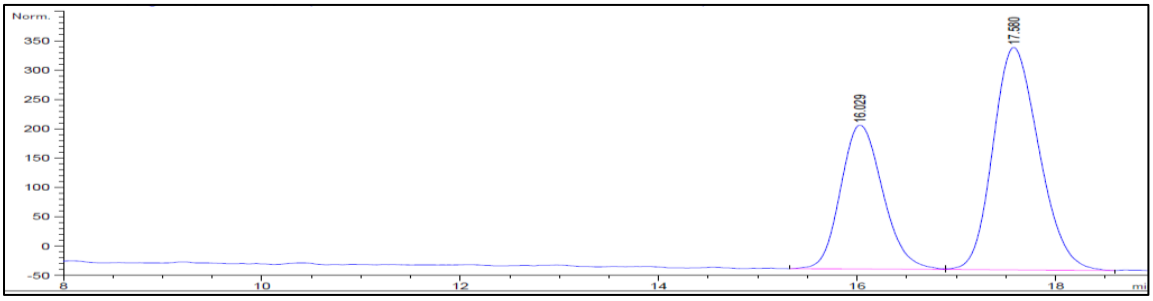

Peak #	RetTime [min]	Sig	Type	Area [mAU*s]	Height [mAU]	Area %
1	16.029	1	BV	7238.46826	245.16664	37.2676
2	17.580	1	VB	1.21845e4	378.91058	62.7324
Totals :				1.94229e4	624.07722	

Racemic

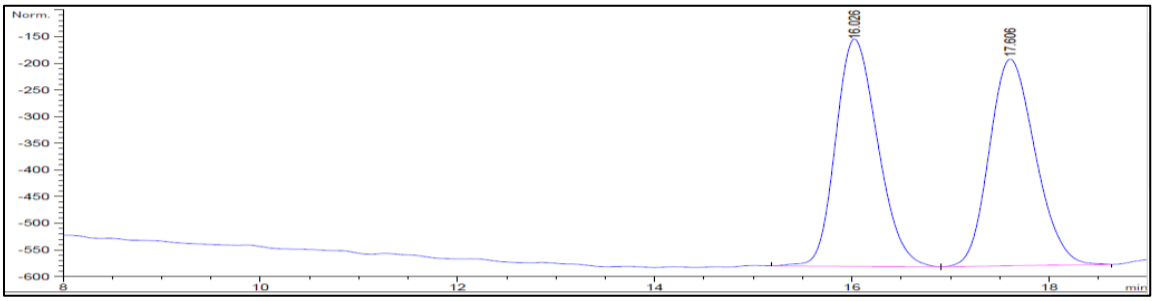

Peak #	RetTime [min]	Sig	Type	Area [mAU*s]	Height [mAU]	Area %
1	16.026	1	BB	1.26235e4	426.29886	50.1394
2	17.606	1	BB	1.25532e4	387.46277	49.8606
Totals :				2.51767e4	813.76163	

Table 7. Reference Compound **16**

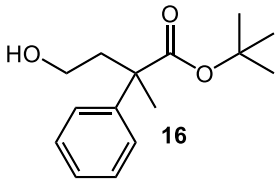

HPLC Conditions: Column: HPLC OJ-H 4.6 mm x 250 mm x 5 μm; Eluent Rate: 1 mL/min; Eluent: 4% IPA/hexane; Monitoring wave: 210 nm

Enantiomeric

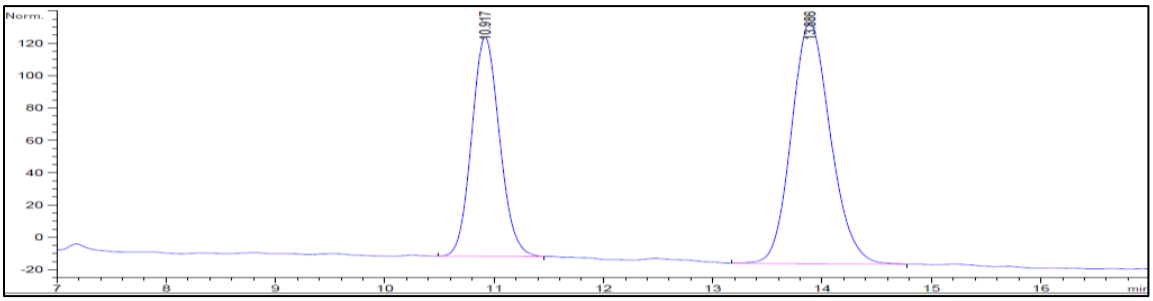

Peak #	RetTime [min]	Sig	Type	Area [mAU*s]	Height [mAU]	Area %
1	10.917	1	BB	2407.03711	135.58955	39.4273
2	13.886	1	BB	3697.96216	148.94417	60.5727
Totals :				6104.99927	284.53372	

Racemic

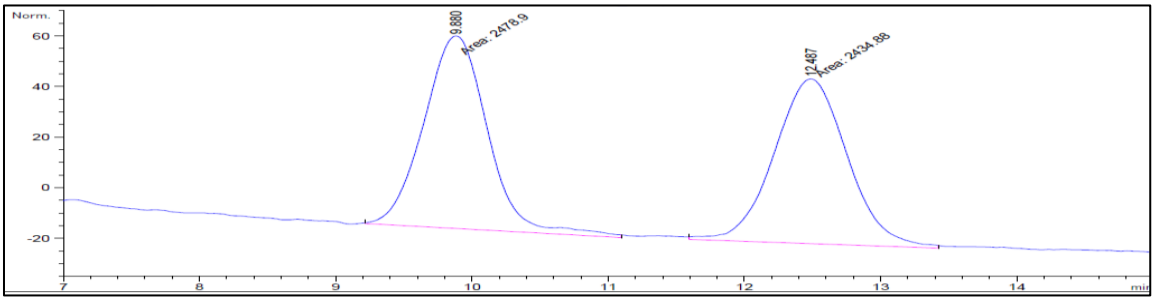

Peak #	RetTime [min]	Sig	Type	Area [mAU*s]	Height [mAU]	Area %
1	9.880	1	MM	2478.90356	76.08099	50.4479
2	12.487	1	MM	2434.88354	65.08986	49.5521
Totals :				4913.78711	141.17085	

Table 8. Trifluoromethyl Compound **18**

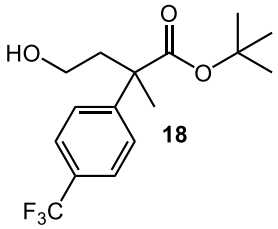

HPLC Conditions: Column: HPLC OD-H 4.6 mm x 250 mm x 5 µm; Eluent Rate: 1 mL/min; Eluent: 6% IPA/hexane; Monitoring wave: 254 nm

Enantiomeric

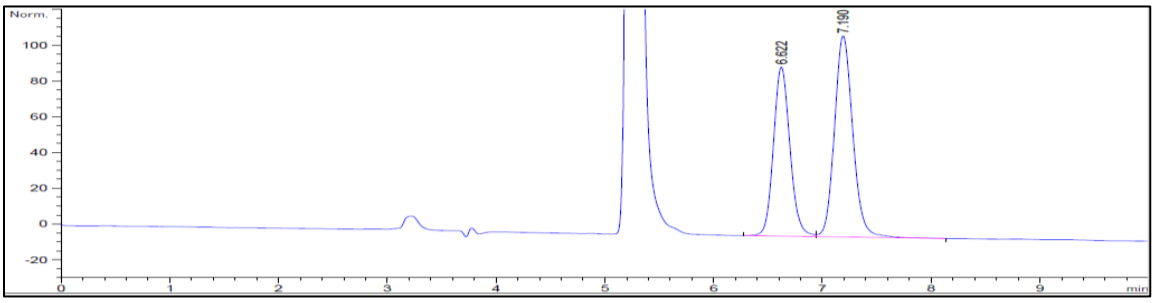

Peak #	RetTime [min]	Sig	Type	Area [mAU*s]	Height [mAU]	Area %
1	6.622	1	BV	1000.56653	94.56516	43.1680
2	7.190	1	VB	1317.27686	112.51299	56.8320
Totals :				2317.84338	207.07815	

Racemic

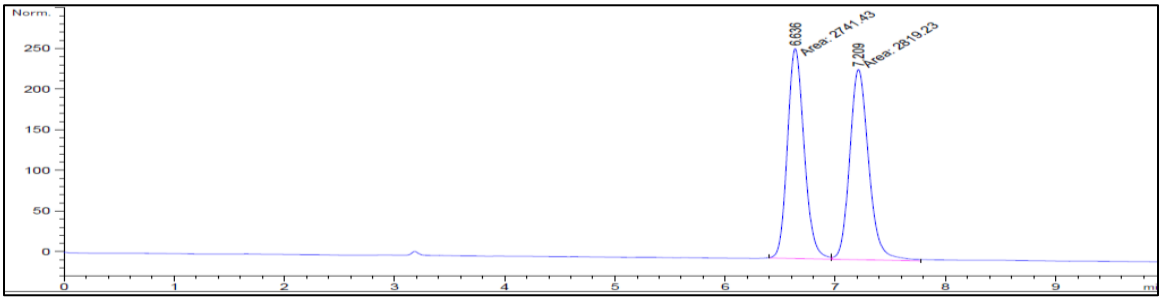

Peak #	RetTime [min]	Sig	Type	Area [mAU*s]	Height [mAU]	Area %
1	6.636	1	MF	2741.43066	258.48044	49.3004
2	7.209	1	FM	2819.23145	234.25401	50.6996
Totals :				5560.66211	492.73445	

Table 9. Tolyl Compound **20**

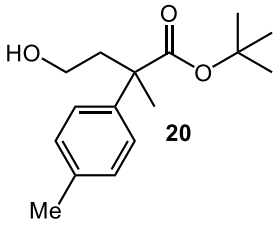

20

HPLC Conditions: Column: HPLC OD-H 4.6 mm x 250 mm x 5 µm; Eluent Rate: 1 mL/min; Eluent: 6% IPA/hexane; Monitoring wave: 254 nm

Enantiomeric

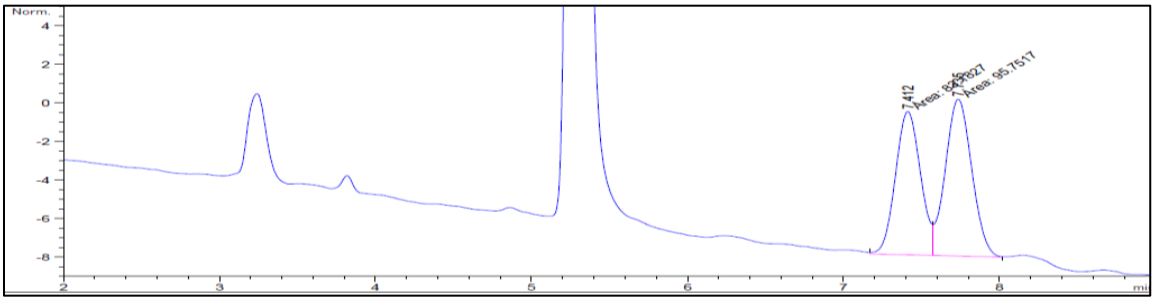

Peak #	RetTime [min]	Sig	Type	Area [mAU*s]	Height [mAU]	Area %
1	7.412	1	MF	83.18270	7.44350	46.4878
2	7.735	1	FM	95.75167	8.14643	53.5122
Totals :				178.93437	15.58993	

Racemic

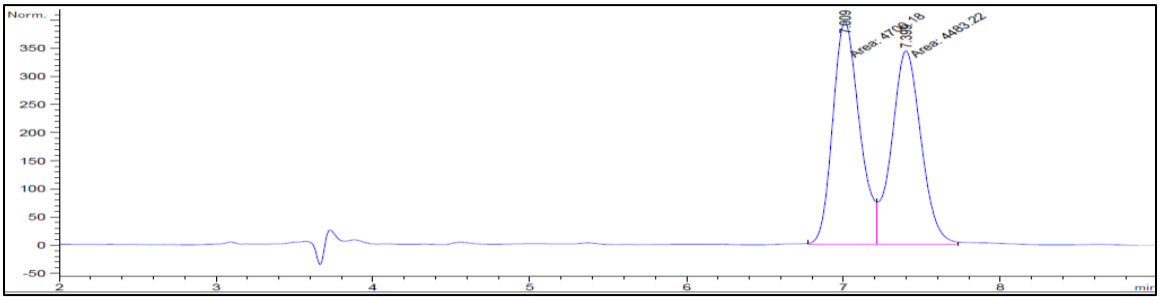

Peak #	RetTime [min]	Sig	Type	Area [mAU*s]	Height [mAU]	Area %
1	7.009	1	MF	4700.17578	395.43542	51.1812
2	7.399	1	FM	4483.22119	344.04022	48.8188
Totals :				9183.39697	739.47565	

Table 10. Methoxy Compound **17**

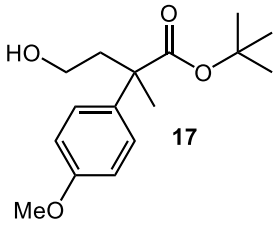

17

HPLC Conditions: Column: HPLC OD-H 4.6 mm x 250 mm x 5 µm; Eluent Rate: 1 mL/min; Eluent: 6% IPA/hexane; Monitoring wave: 254 nm

Enantiomeric

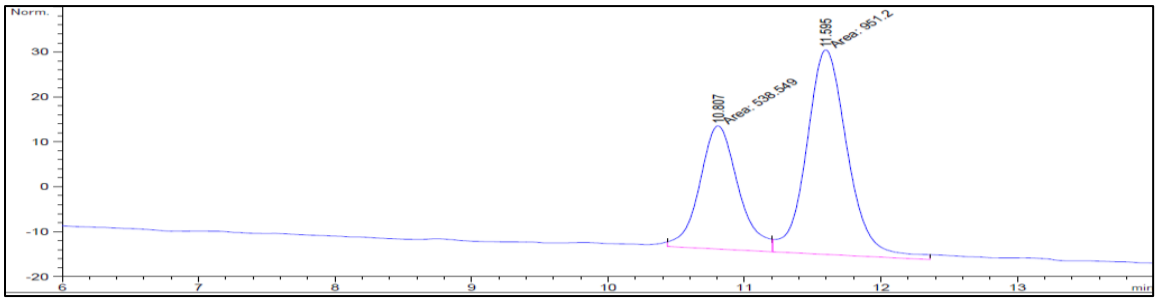

Peak #	RetTime [min]	Sig	Type	Area [mAU*s]	Height [mAU]	Area %
1	10.807	1	MF	538.54901	27.41853	36.1503
2	11.595	1	FM	951.19983	45.50496	63.8497
Totals :				1489.74884	72.92349	

Table 11. *tert*-Butyl Compound **23**

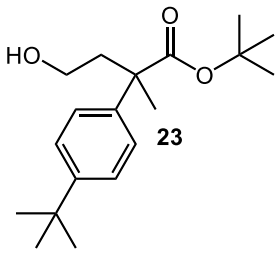

HPLC Conditions: Column: HPLC OD-H 4.6 mm x 250 mm x 5 μm; Eluent Rate: 1 mL/min; Eluent: 1% IPA/hexane; Monitoring wave: 210 nm

Enantiomeric

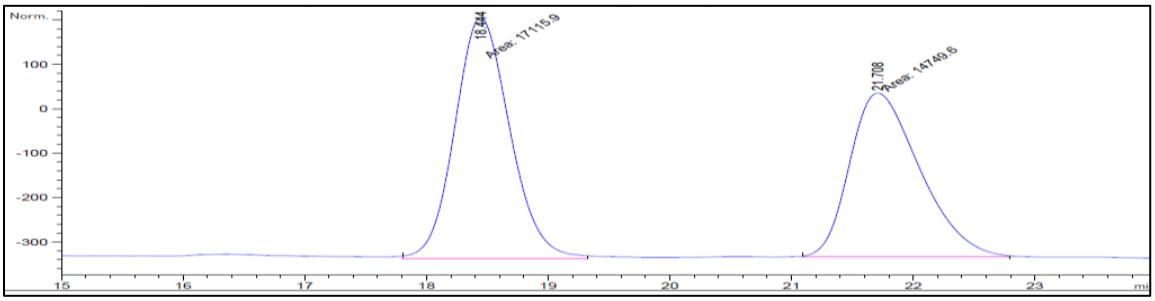

Peak #	RetTime [min]	Sig	Type	Area [mAU*s]	Height [mAU]	Area %
1	18.444	1	MM	1.71159e4	543.46283	53.7129
2	21.708	1	MM	1.47496e4	369.00775	46.2871
Totals :				3.18655e4	912.47058	